PB 211 481

EPA-R2-72-041
July 1972

Report No. SRIC 71-15

SULFUR BEHAVIOR AND SEQUESTERING OF SULFUR COMPOUNDS DURING COAL CARBONIZATION, GASIFICATION, AND COMBUSTION

Marvin L. Vestal, Alan G. Day, III, J.S. Snyderman, Gordon J. Fergusson, F.W. Lampe, R.H. Essenhigh, J.E. Hudson, G.E. Lerner, D.W. Kennedy, R. Chase, A.L. Yergey, and Wm. H. Johnston

Final Report May 1971

Contract No. CPA 70-50

SRI

Reproduced by
NATIONAL TECHNICAL
INFORMATION SERVICE
U.S. Department of Commerce
Springfield VA 22151

Report No. SRIC 71-15

SULFUR BEHAVIOR AND SEQUESTERING OF SULFUR COMPOUNDS DURING COAL CARBONIZATION, GASIFICATION, AND COMBUSTION

Marvin L. Vestal, Alan G. Day, III, J.S. Snyderman, Gordon J. Fergusson, F.W. Lampe, R.H. Essenhigh, J.E. Hudson, G.E. Lerner, D.W. Kennedy, R. Chase, A.L. Yergey, and Wm. H. Johnston

Final Report May 1971

Contract No. CPA 70-50

with the

ENVIRONMENTAL PROTECTION AGENCY

OFFICE OF AIR PROGRAMS

Leon Stankus, Contract Project Officer

Details of illustrations in this document may be better studied on microfiche

Scientific Research Instruments Corporation
Baltimore, Maryland

BIBLIOGRAPHIC DATA SHEET	1. Report No. EPA-R2-72-041	2.	3. Recipient's Accession No.

4. Title and Subtitle
Sulfur Behavior and Sequestering of Sulfur Compounds During Coal Carbonization, Gasification, and Combustion

5. Report Date
May 1971

6.

7. Author(s)
Marvin L. Vestal, Alan G. Day, III, et al

8. Performing Organization Rept. No. SRIC 71-15

9. Performing Organization Name and Address
Scientific Research Instruments Corporation
6707 Whitestone Road
Baltimore, Maryland 21207

10. Project/Task/Work Unit No.

11. Contract/Grant No.
CPA 70-50

12. Sponsoring Organization Name and Address
ENVIRONMENTAL PROTECTION AGENCY
Office of Air Programs
Research Triangle Park, N. C. 27711

13. Type of Report & Period Covered
Final

14.

15. Supplementary Notes

16. Abstracts
A description is presented of studies on coal desulfurization and related investigations. This work has emphasized the application of non-isothermal kinetic studies to the theoretical, experimental, and practical problems associated with the removal of sulfur from coal. To increase the efficiency and precision of data acquisition and interpretation, a computerized non-isothermal kinetic laboratory has been designed, built, and put into operation. Detailed non-isothermal kinetic studies of the desulfurization and gasification of five bituminous coals, lignite, anthracite, and pyrite, under reducing and oxidizing atmospheres have been conducted, leading to further clarification and understanding of the sequence of reactions that are dominant in the coal desulfurization and gasification processes. An attempt has been made to identify the types of sulfur bonding associated with the removal of sulfur from Organic I, Organic II, and Organic III sites, by application of the method to the impregnation of coal chars with a number of sulfur-containing model compounds and to their subsequent desulfurization. Non-isothermal kinetic measurements of the removal of hydrogen sulfide produced in the desulfurization under both reducing and oxidizing condition by calcium oxide and dolomite have been carried out. Reactions of hydrogen sulfide with iron, iron sulfide, and various coal chars have also been investigated. Application of the kinetic parameters obtained to the desulfurization performance of a simple experimental reactor has been made, and further development and conformance studies of the dual channel cascade reactor were initiated.

17. Key Words and Document Analysis. 17a. Descriptors

Air pollution
Sulfur
Hydrogen sulfide
Pyrite
Sulfur oxides
Bituminous coal
Lignite
Anthracite
Gasification
Carbonization
Combustion
Chelation
Desulfurization
Kinetic theory
Chemical reactors

17b. Identifiers/Open-Ended Terms

Dual Channel Cascade Reactor

17c. COSATI Field/Group 13B, 7D

18. Availability Statement	19. Security Class (This Report)	21. No. of Pages
Unlimited	UNCLASSIFIED	134
	20. Security Class (This Page) UNCLASSIFIED	22. Price

1b

TABLE OF CONTENTS

	Page
TABLE OF CONTENTS	i
LIST OF FIGURES	iii
LIST OF TABLES	vi
SUMMARY	1
INTRODUCTION	5
EXPERIMENTAL FACILITY: THE COMPUTERIZED NON-ISOTHERMAL KINETIC LABORATORY	7
REACTOR AND CONTROLLER	8
THE CHEMICAL IONIZATION QUADRUPOLE MASS SPECTROMETER	10
DIGITIZER AND MASS SELECTOR	12
DATA STORAGE AND HANDLING	13
COMPUTER SYSTEM	14
KINETIC PROGRAMS	18
THEORETICAL SUMMARY OF THE NON-ISOTHERMAL KINETIC METHOD	42
RESULTS OF DESULFURIZATION STUDIES	44
REDUCING ATMOSPHERE	44
Pyrite Hydrodesulfurization	49
Hydrodesulfurization of Organic III	50

	Page
OXIDIZING ATMOSPHERE	51
Pyrite	52
Bituminous Coal SRI Nos. 1-5	64
Anthracite and Lignite	74
MODEL COMPOUNDS	81
REMOVAL OF H_2S FROM PRODUCT GASES	82
Calcination of Dolomite	82
Adsorption of H_2S	86
EXPERIMENTAL DESULFURIZATION REACTORS	88
CONFORMANCE STUDIES ON EXPERIMENTAL REACTORS	88
Intra Layer Trapping of H_2S by CaO	92
EVALUATION OF THE DUAL CHANNEL CASCADE REACTOR FOR THE HYDRODESULFURIZATION OF COAL	101
INTRODUCTION	101
DESCRIPTION OF THE DESULFURIZATION PROCESS	104
Design and Evaluation of a Laboratory Scale Model Cascade Reactor	107
Results	110
ANALYSIS OF CROSS-MIXING BEHAVIOR OF THE DUAL CHANNEL CASCADE REACTOR	116
Analysis	116
Evaluation	121
Conclusions	124
BIBLIOGRAPHY	126
APPENDIX A	127

LIST OF FIGURES

		Page
Figure 1-	Block Diagram of the Non-Isothermal Kinetic Laboratory	9
Figure 2-	Block Diagram of the Computer System	15
Figure 3-	Block Diagram of the Program LINFIT	20
Figure 4-	Computer Program LINFIT calculating V_0 for m=10°C/min for Three Hypothetical Reactions	22
Figure 5-	Block Diagram of the Program MDATA	23
Figure 6-	Computer Program MDATA creating artifical data files SR244·ENV and SR244·IND,m=10°C/min	24
Figure 7-	Output of LINFIT and MDATA for m=10°C/min. Overall Envelope	25
Figure 8-	Output of LINFIT and MDATA for m=10°C/min. Resolution of Three reactions	26
Figure 9-	Output of LINFIT and MDATA for m=4°C/min. Overall Envelope	27
Figure 10-	Output of LINFIT and MDATA for m=4°C/min. Three reactions resolved	28
Figure 11-	Block Diagram of the Program MTM	29
Figure 12-	Computer Program MTM calculating E and k_0 for the reaction of Iron Pyrite	30
Figure 13-	Φcrit vs E for Pyrite reaction	32
Figure 14-	Best fit for T_m Data form MTM Program and Φcrit Plot - Pyrite reaction	33
Figure 15-	Φcrit vs E for Sulfide reaction	34
Figure 16-	Best fit for T_m Data from MTM Program and Φcrit Plot - Sulfide reaction	35
Figure 17-	Φcrit vs E for Organic III reaction	36

Page

Figure 18- Best fit for T_m Data from MTM Program and Φcrit Plot - Organic III reaction 37

Figure 19- Block diagram of the Program CURVE 38

Figure 20- Graphical Determination of Reaction order for the desulfurization of Pyrite 39

Figure 21- Graphical Determination of Reaction order for the desulfurization of Sulfide (Pyrite II) 40

Figure 22- Graphical Determination of Reaction order for the desulfurization of Organic III 41

Figure 23- Typical Evolution Curve for H_2S in treatment of bituminous coal with H_2 47

Figure 24- Non-isothermal Run of O_2 Adsorption onto Pyrite 56

Figure 25- Non-isothermal Run of SO_2 Evolution from Pyrite 57

Figure 26- Non-isothermal Run of SO_2 Evolution from Pyrite. O_2 Feed Stopped at 670°K 58

Figure 27- Non-isothermal Run of H_2S Evolution from Pryite 59

Figure 28- Non-isothermal Run of O_2 Adsorption onto Pyrite. Re-run of Pyrite of Figure 26 60

Figure 29- Non-isothermal Run of SO_2 Evolution from Pyrite. Re-run of Pyrite of Figure 26 61

Figure 30- Non-isothermal Run of Illinois 2.5% Coal 65

Figure 31- Non-isothermal Run of Illinois 1% Coal-SO_2 Evolution 68

Figure 32- Non-isothermal Run of Illinois 4.5% Coal-H_2S Evolution 70

Figure 33- Non-isothermal Run of Illinois 4.5% Coal-CO Evolution 72

Figure 34- Non-isothermal Run of Illinois 4.5% Coal-CO_2 Evolution 73

Figure 35- Non-isothermal Run of Anthracite-SO_2 Evolution 75

Page

Figure 36- Non-isothermal Run of Anthracite-O_2 Adsorption 76

Figure 37- Non-isothermal Run of Lignite-SO_2 Evolution 77

Figure 38- Non-isothermal Run of Lignite-O_2 Adsorption 78

Figure 39- Non-isothermal Run of CO_2 evolution from Dolomite 83

Figure 40- Non-isothermal Run of H_2O evolution from Calcined Dolomite 84

Figure 41- Non-isothermal Run of H_2S Adsorption onto Calcined Dolomite 85

Figure 42- (a) Schematic diagram of the reactor used in equation derivation and experimental measurements 89
(b) Schematic diagram of experiment showing heating curve 89

Figure 43- Plot of fraction of Organic III remaining for m=30°/min and the probability of H_2S trapping by CaO for SRI No. 4 and SRI No. 5 coals 96

Figure 44- Schematic Diagram of a Short Section of the Proposed Dual Channel Baffled Cascade Desulfurization Reactor 102

Figure 45- Simplified Block Diagram of Complete Conceptual Desulfurization System 103

Figure 46- Velocity of Fall Based on Obersvation of Leading Edge(Batch Measurements) 111

Figure 47- Variation of CO_2 Tracer Concentration Above Injection Point Under Steady State Conditions 113

Figure 48- Determination of T, the Mixing Half Time for the Dual Cascade Reactor 115

Figure 49- Schematic Diagram of the Dual Channel Cascade Reactor 118

LIST OF TABLES

		Page
I.	Kinetic Parameters Chosen for the Three H_2S Evolution Peaks Used in This Example	18
II.	Summary of KineticsPrograms	19
III.	Kinetic Data for Desulfurization of Coal	49
IV.	Oxidizing Atmosphere Experiments	53
V.	Kinetic Parameters for Desulfurization	64
VI.	Specific Activated Adsorption Processes in SRI No. 3 Coal	66
VII.	Estimated Kinetic Parameters for SO_2 Evolution from Coals in an Oxidizing Atmosphere	69
VIII.	Sulfur Analysis of Anthracite and Lignite	80
IX.	Data from Figure 38 for SRI Coal No. 4	98
X.	Data from Figure 38 for SRI Coal No. 5	99

SUMMARY

The work performed during the past year has led to significant progress in the design of an efficient gas-solid reactor for the desulfurization of coal. Application of the Juntgen non-isothermal kinetics treatment to both experimental techniques and computer programs has led to increased understanding of the complex inter-relationships between the reactions of the various coal sulfur compounds. Based upon results of the kinetics studies, both experimental reactors as well as a dual channel cascade reactor concept with potential for technological importance have been evolved and tested in the laboratory.

The powerful tool offered by the Juntgen kinetics approach, in combination with the capacity of a computer to reduce large volumes of data, have been major factors in the increased understanding of the coal desulfurization reactions. Material for a non-isothermal run is placed into a furnace which is heated at a well controlled rate. Gases are flowed over the material in the furnace during the heating period, and up to nine of the effluent mass peaks are monitored by a quadrupole mass spectrometer. Data obtained on punched paper tape from the mass spectrometer in a typical non-isothermal kinetics run are processed by a remote time-sharing digital computer reached through telephone line connections from a laboratory teletype station. As a first step, the computer is programmed to operate upon the raw data to produce temperature/intensity profiles for each of the gaseous species monitored by the mass spectrometer. These profiles are stored as data files for future reference and are also reproduced as curves printed out by the teletype.

Analysis of the stored data in terms of the non-isothermal kinetic equations is possible by extensive manipulation of such data using a library of computer programs which permit extensive manipulations of the data. Programs have been written to permit mathematical modeling of the reactions in the non-isothermal system. Other programs calculate reaction parameters and obtain statistical best fits of the data to the theoretical equations. Calculations for the kinetic parameters of activation energy, frequency factor and reaction order are based upon analysis of the experimental variables of heating rate, the temperature at the maxima of peaks in the profiles, the full-width-at-half-maximum of these peaks, and the total volume of gas evolved for a particular peak. Artificial data files which may be used to project and predict the results of non-isothermal runs can be created by selecting suitable values of the three kinetic parameters and the total volume of gas evolved for a particular mass.

Kinetic parameters and a better delination of reaction mechanism have resulted from the computer assisted analysis of the experiments that were conducted on the system of reactions for desulfurizing coals and related materials. On the basis of a number of runs in a reducing atmosphere using chars from the various coals so that interference from other sulfur sources is minimized, values of E and k_0, and activation energy and frequency factor respectively, have been obtained for the reactions of Organic III sulfur. With the revision of earlier E and k_0 values for the reactions of pyrite and sulfide with hydrogen, the description of hydrodesulfurization reactions in coals appears to be adequate. Characterization of the oxidative reactions of coals has been begun. Values for the kinetics of oxygen adsorption onto pyrites and coals have been obtained. Kinetic parameters of SO_2 and H_2S production from pyrite in an oxidizing atmosphere have resulted from these studies.

Parameters for SO_2 produced in the reactions of oxygen with the forms of sulfur in coal have also been calculated and some disagreement between these values for the SO_2 production from pyrite in coals and in pure FeS_2 has been observed.

A series of experiments in which an attempt was made to develop a model for the forms of sulfur in coal was performed. The results of these experiments indicated that low molecular weight organic compounds, even when heterocyclic in sulfur, are adequate models for the Organic III form of sulfur only. Other experiments designed to study the behavior of adsorbents for H_2S and SO_2 liberated in desulfurization reactions were performed with dolomite. The liberation of CO_2 in the pyrolysis of dolomite was monitored and the adsorption of H_2S on to calcined dolomite with the expected liberation of water was studied. In both cases experimental complications prevented the calculation of kinetic parameters.

With non-isothermal kinetics studies of coal as a basis, design, and initial testing of both a fixed-bed and a cascade reactor have been completed in the course of this program. The fixed bed reactor was designed to test equations which were used to predict the amounts of sulfur remaining in chars after a coking operation. The mathematical treatment of the reactor considered the trapping efficiency of CaO for hydrogen sulfide and the unavoidable retention of some H_2S due to the natural occurrence of calcium in coals. The agreement between the predictions of the equations and tests of the reactor were quite good.

The concept of the dual channel cascade reactor design for ultimate use in coal desulfurization at a commercial level was evolved. The reactor is the principle component of processing equipment for the desulfurization of coal. The reactions which occur are the hydrodesulfurization

of coal, followed by the adsorption of H_2S on calcined limestone and finally the regeneration of the limestone. Treatment of the thermodynamics has shown that energetically this overall process is acceptable. The reactor itself utilizes the principle of gas-solid hydrodesulfurization reactions being carried out efficiently if the extent of gas cross-mixing between two separate but simultaneously flowing streams of solids is sufficiently high. Laboratory measurements have shown that particle flow rates and gas flow patterns support the original estimates for these variables. The possibility exists for even more rapid gas mixing than was originally achieved, and the first tests lend encouragement to the scaling up of the model to an operable pilot reactor.

INTRODUCTION

This final report describes our studies on coal desulfurization and related investigations which have been conducted under Contract CPA 70-50. Our work has emphasized the application of non-isothermal kinetic studies to the theoretical, experimental, and practical problems associated with the removal of sulfur from coal. The effectiveness of the non-isothermal kinetic investigation method, developed originally by Juntgen, was demonstrated conclusively in our earlier work in this field[1,2]. To increase the efficiency and precision of our data acquisition and interpretation, we have designed, built, and put into operation a computerized non-isothermal kinetic laboratory. While our use of this laboratory, to date, has been specifically in applications of the non-isothermal kinetic method to coal desulfurization processes, the laboratory has a great potential for application to numerous practical problems involving heterogenous reactions of gases and solids.

Detailed non-isothermal kinetic studies of the desulfurization and gasification of five bituminous coals, lignite, anthracite, and pyrite, under reducing and oxidizing atmospheres have been conducted. Analysis of the results has led us to further clarification and understanding of the sequence of reactions that are dominant in the coal desulfurization and gasification processes.

We have attempted to identify the types of sulfur bonding associated with the removal of sulfur from what we have called[2] Organic I, Organic II, and Organic III sites, by application of the method to the impregnation of

coal chars with a number of sulfur-containing model compounds and to their subsequent desulfurization.

Non-isothermal kinetic measurements of the removal of hydrogen sulfide produced in the desulfurization under both reducing and oxidizing condition by calcium oxide and dolomite have been carried out. In addition, reactions of hydrogen sulfide with iron, iron sulfide, and various coal chars have been investigated in order to facilitate a quantitative understanding of the back reactions of coal desulfurization that reduce the overall efficiency of the desulfurization process.

Application of the kinetic parameters obtained to the desulfurization performance of a simple experimental reactor has been made. While the present state of the method of application is very crude and approximate, the approach used appears to have potential for further development.

Further development and conformance studies of the dual channel cascade reactor, which we believe has promise in practical coal desulfurization process, were initiated.

EXPERIMENTAL FACILITY: THE COMPUTERIZED NON-ISOTHERMAL KINETIC LABORATORY

The computerized non-isothermal kinetic laboratory was designed and built in order to characterize more rapidly and effectively the chemistry and kinetics of sulfur behavior and sequestering of sulfur compounds during coal carbonization, gasification, and combustion. The use of this laboratory, in conducting non-isothermal kinetics investigations on coal desulfurization is summarized at the end of this report. This laboratory has high potential for application to many practical process systems where reactions are occurring between solids and gases, such as regeneration of sorbents, desulfurization of oils and chemicals from coal.

Several new miniature reactors were developed to allow greater flexibility in heating rate and also to allow smaller samples to be used. With the smaller reactors, cool-down time is shorter allowing more experiments per day. A new and more sophisticated linear temperature programmer was designed and built to control the heating rate of the reactor. A new mass spectrometer was built and adapted to the system, incorporating the flexibility of the quadrupole mass spectrometer with the high sensitivity and specificity of chemical ionization. Data acquisitions were accomplished through design and construction of a solid state analog to frequency converter, an electronic counter and clock system coupled to a paper tape punch to store the data digitally.

Data handling is accomplished efficiently through use of a time sharing computer with a local plotting teletype terminal. This computer was used with programs especially written at SRIC to yield kinetic parameters from the non-isothermal experiments.

A block diagram of the non-isothermal laboratory is shown in Figure 1. The reactor is heated by the power supply which in turn is governed by the linear temperature programmer. The reactor contains the reaction tube in which the sample under study (coal, coke, pyrite, etc.) is located. The sample when heated in the reactor produces reaction products which are then monitored by the chemical ionization quadrupole mass spectrometer before being vented through a hood to the atmosphere. The analog information from the mass spectrometer is digitized by the digitizer and mass selector. The digitized data are then punched on a paper tape punch. This paper tape is then fed into a time sharing computer through a plotting teletype data terminal and the data are analyzed by proper application of stored computer programs.

REACTOR AND CONTROLLER

The Linear Temperature Programmer consists of a ramp generator, a thermocouple amplifier and a comparator. The ramp generator simulates a thermocouple signal or voltage. This voltage is made to increase linearly as a function of time. The rate of increase of this temperature ramp is continuously variable from 2 to 100^0 C/min. The thermocouple amplifier amplifies the signal from a chromel-alumel thermocouple located in the furnace. This amplified thermocouple signal is then compared with the simulated thermocouple signal from the ramp generator. The comparator output is then fed to the reactor controller.

The reactor controller controls the amount of power applied to the reactor by detecting the temperature of the reactor and comparing this to a preset temperature. In this case it uses the comparator output from the linear temperature programmer. The reactor controller functions to keep the difference signal from the comparator at a minimum (as near to zero as possible). By so doing, the furnace temperature rises linearly, as a function of time.

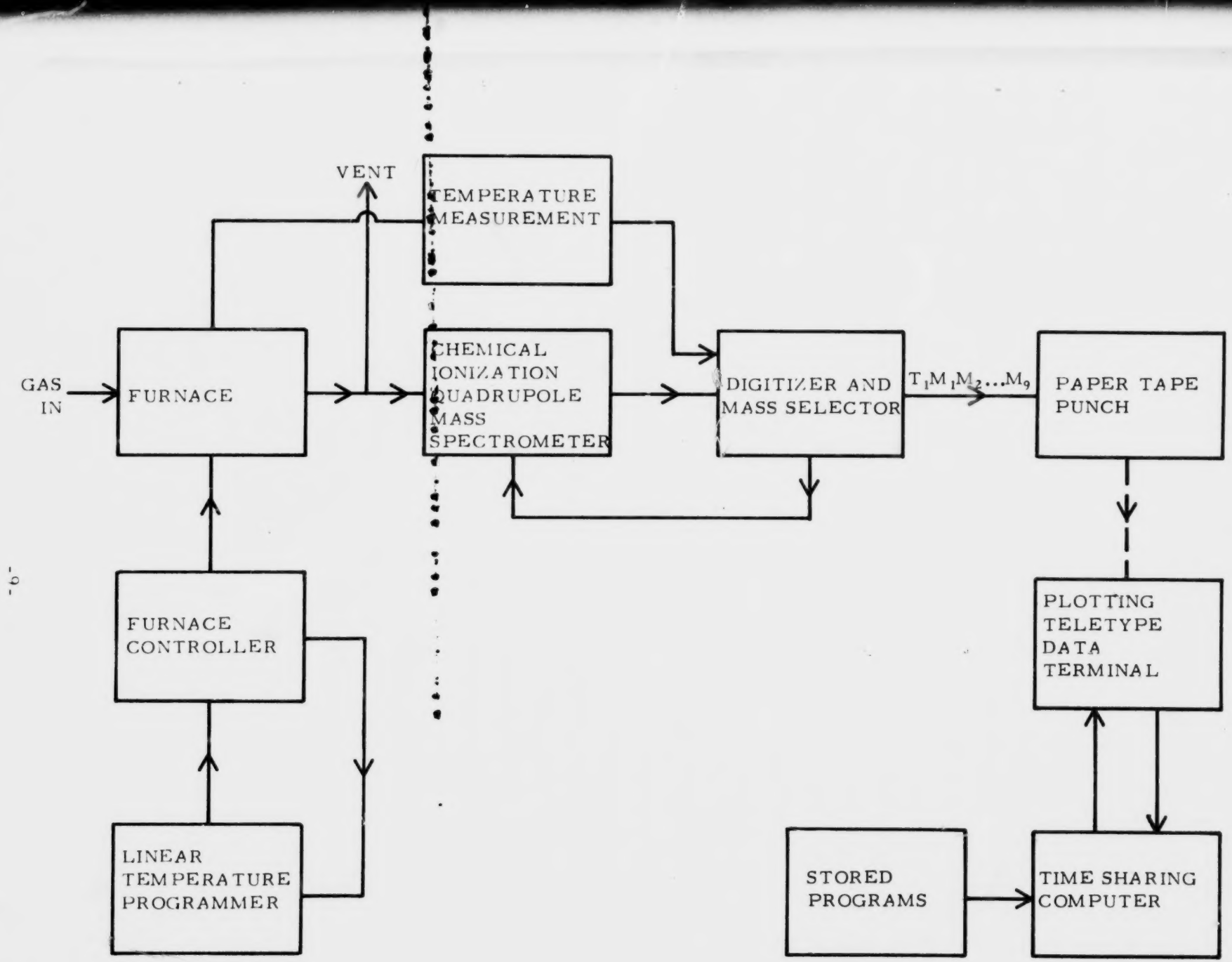

FIGURE 1. Block Diagram of the Non-Isothermal Kinetic Laboratory

The reactor is a stainless steel rod 3/4 inch diameter with a 1/4 inch hole bored through the center. The heating element is 22 gauge Chromel A resistance wire insulated with asbestos. The sample to be studied (coal, coke, pyrite, etc.) is placed in a quartz tube which, in turn, is placed in the 1/4 inch bore of the reactor. The reaction gas flows through the tube and is sampled by the chemical ionization quadrupole mass spectrometer immediately before it is vented through a hood to the atmosphere.

THE CHEMICAL IONIZATION QUADRUPOLE MASS SPECTROMETER

The chemical ionization quadrupole mass spectrometer monitors the gaseous reaction products evolved. This is accomplished by combining a quadrupole mass spectrometer with a chemical ionization source. The chemical ionization source, designed by Scientific Research Instruments Corporation is a practical application of the chemical ionization process discovered by Dr. F. Field[3]. This process differs from the normal electron-impact method of ionization. In electron-impact ionization the ions are formed by a beam of electrons striking gas molecules with sufficient energy to remove electrons from the neutral molecules thereby converting them to ions(See equation below). During the process of ion formation the pressure is low enough

$$H_2S + e^- \rightarrow H_2S^+ + 2e^-$$

(10^{-6} Torr) that the ions formed do not have time to react with other atoms or molecules before being analyzed in the mass spectrometer. Thus the intensity of the ions formed is dependent upon the number of collisions of the electrons with the neutral molcules. It, therefore, stand to reason that if there is a very low concentration of a particular neutral species present, its ionic concentration will be correspondingly low.

Chemical ionization, however, allows trace amounts of a substance to be observed with very high sensitivity. This is accomplished by using a high pressure ($\approx$ 1 Torr) source in which any ions formed will suffer numerous collisions with other gaseous species present in the source. Thus by using a reagent gas, a gas relatively high in concentration, the electrons will ionize a great number of these neutrals. These extremely abundant ions will then have opportunity to collide many times with other species (including like species) in the source before being drawn out and analyzed. By proper selection of the reagent gas these collisions, with the trace gases of interest, will result in charge exchange or proton transfer, producing new ions. These new ions being thermodynamically stable will not reverse react with reagent gas molecules but will be drawn out of the source and analyzed by the mass spectrometer. Thus it is seen that a very small concentration of neutrals can be made to produce a relatively large number of ions thereby enhancing the sensitivity of the instrument.

This process is illustrated for example in the equations below and is the method used in the analysis of the hydrodesulfurization of coal.

$$H_2 + e^- \rightarrow H_2 + 2e^-$$

$$H_2^+ + H_2 \rightarrow H_3^+ + H$$

$$H_3^+ + H_2S \rightarrow H_3S^+ + H_2$$

The reagent gas is hydrogen and the gas to be analyzed is H_2S. Note that the ion is one mass unit heavier then the parent neutral ($H_2S \rightarrow H_3S^+$).

Once the ions are formed in the chemical ionization source, they are drawn out and analyzed. The analyzer in this case is the quadrupole section of the mass spectrometer. The quadrupoles are four metal rods arranged parallel to each other on the four corners. of a square. The quadrupoles have an RF signal ($\sim$2MHz) and a D.C. potential applied to them. The RF is variable in amplitude and of fixed frequency. The D.C. applied to the quadrupoles is variable and so arranged that adjacent poles are of opposite polarity and equal amplitude.

When an ion of given mass to charge ratio enters the quardupole assembly, it will pass completely through and be counted by an electron multiplier if the RF amplitude and D.C. voltage are set correctly. If these parameters are not properly set, the ion will not pass through but will strike the quadrupole assembly. Thus ions of desired mass may be selected by properly setting the RF amplitude and D.C. voltage.

DIGITIZER AND MASS SELECTOR

The purpose of the digitizer and mass selector is to select the desired ion masses to be observed and to convert this analog voltage information of the mass spectrometer to digital information.

The mass selector sequentially selects the RF and D.C. voltages that determine a group of selected masses. In this system it is possible to observe as many as nine masses in sequence and relate their intensities to temperature. After the mass has been selected, the voltage information is converted to frequency and digitally counted. This count is stored and retrieved at a predetermined time to be fed into a paper tape punch.

The correlation of sequential voltages fed to the quadrupoles of the mass spectrometer and selection, storage and retrieval of information is achieved through a timing system within the digitizer and mass selector. This "clock" allows the storage of a temperature obtained from a thermocouple amplifier located in the temperature measurement block of Figure 1, delivery of the voltage to the quadrupole in the proper sequence, reading and storage of the mass intensity information and giving commands to the paper tape punch to record the information.

DATA STORAGE AND HANDLING

The paper tape punch is a Tally Model 420 and can punch up to 60 characters per second in the ASC 11 code. This is the code used by most time sharing computer systems. The paper tape when punched contains the following information: four digits temperature, 2 space, 4 digits M_1, 2 space, 4 digits M_2, 2 space. . . 4 digits M_9, carriage return, line feed, then repeats the sequence starting with temperature.

The finished tape is fed into the Telcomp PDP10D time sharing computer located in Cambridge, Massachusetts. The data are transmitted through the Typagraph plotting teletype terminal over telephone lines by means of an acoustic data coupler. The data are then named and graphed. They are then worked up using peak fitting rountines written especially for this project. The data work-up yields the kinetic data E, k_0, V_0 and a theoretically generated curve of gas evolution as a function of temperature which may then be plotted and visually compared with the empirical curve.

This automatic data acquisition and handling system has the advantage that it is a rapid and accurate system. It removes any error of measurement usually associated with experimental judgment and any error associated with hand transcription of data. The speed of the system may be seen if one considers that fact that it formerly took twelve hours to work up data and fit a curve for a single experiment when done by hand. At present, using a new automatic system, the same experimental work up requires one hour. In addition, the automatic system has 2-3 times the number of data points with which to work.

Finally the automatic data acquisition and handling system is very versatile, being adaptable to many gas-solid reaction systems. For instance, it is possible to adapt the system to any reaction in which the gas-solid interaction produces a new gaseous reaction product or series of gaseous reaction products. It is also possible to use the system to follow the source of a reaction in which gaseous reactant is absorbed or in which a thermal decomposition occurs, producing a product gas.

COMPUTER SYSTEM

The telcomp PDP10D time sharing computer system, employed in conjunction with the SRI non-isothermal laboratory, is shown in block diagram form in Figure 2. The purpose of the computer system is to take the experimental data, which is on punched tape, and perform the necessary calculations to extract from the raw data the desired kinetic data and graphic representations of the coal desulfurization process. The following is a description of the system with reference to Figure 2.

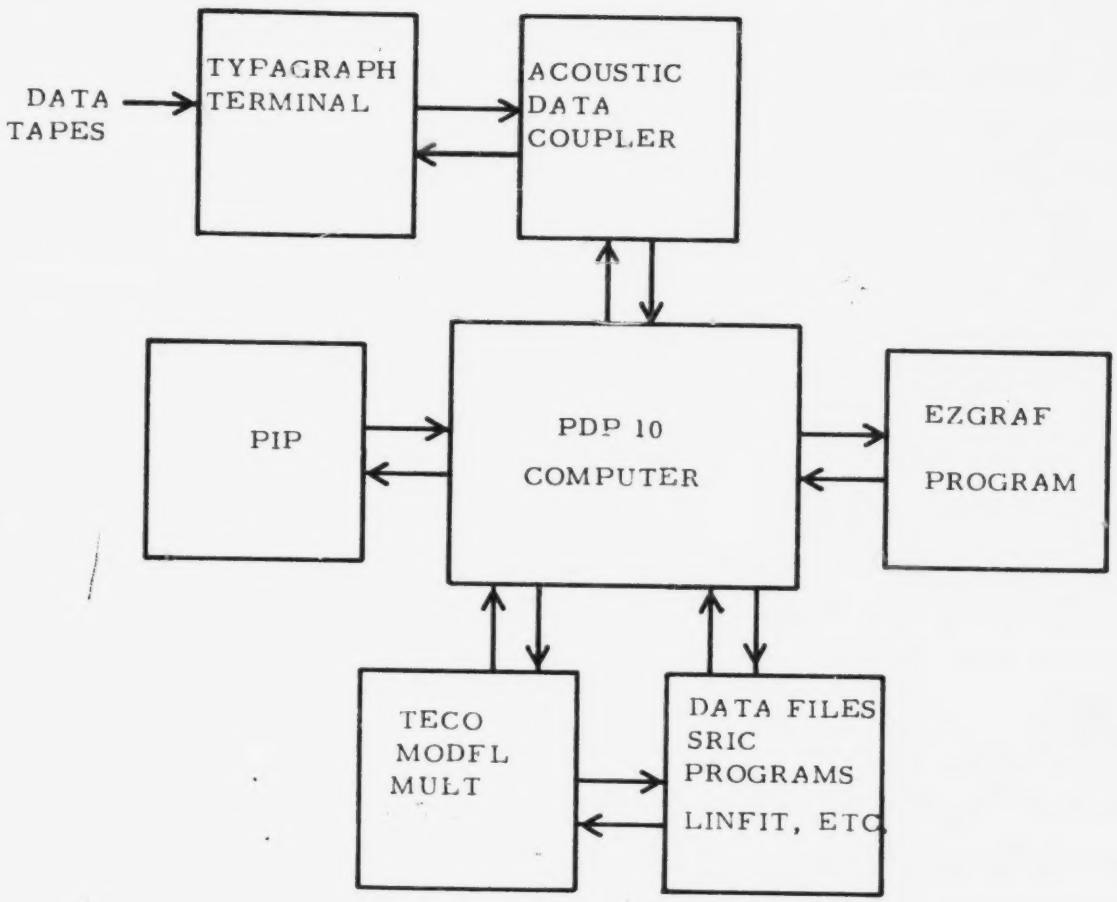

FIGURE 2. Block Diagram of the Computer System

There are two components of the system which are actually located on the premises of SRI Corporation. These are the TYPAGRAPH TERMINAL and the ACOUSTIC DATA COUPLER: the TYPAGRAPH TERMINAL is an advanced teletype apparatus which is able to draw high resolution graphs in addition to providing communication with the computer. Through this terminal, tapes may be introduced or typed commands may be made. The ACOUSTIC DATA COUPLER provides a link between the terminal and the PDP10D computer which is located in Cambridge, Massachusetts. This is accomplished by conversion of data into modulated audio signals which are transmitted over telephone lines to and from Cambridge, Massachusetts.

The data, usually consisting of temperature points with corresponding mass intensities, are fed from the terminal to the coupler and then into PIP (Peripheral Interchange Program) which is a program for naming and manipulating files. These data are then placed in storage data files. All data handling procedures operate with this area as reservoir of information. Once the data are stored they may be retrieved and manipulated by the existing computer programs.

The newly created data file is in the form of unscaled numbers which must be modified. For this purpose, MODFL has been written. MODFL converts the temperature from degrees Celsius to degrees Kelvin and adds any necessary correction factors to either the temperature or the intensity data. If the data have any irregular errors such as a gain change in mid run, the errors may be corrected after going through MODFL by using MULT. If the data file has any errors

due to transmission difficulties, such as line noise introducing nonsense symbols into the file, they may be removed by using TECO (Text editor and corrector). TECO allows data files or stored programs to be corrected by the operator.

Once the data file is named, corrected and stored, it may then be plotted. This is accomplished by using the EZGRAF program. This is a Typagraph supplied program which allows a graph to be drawn by the TYPAGRAPH TERMINAL. The subroutine permits the selection of vaious options, such as scales for the X and Y axes, length of the axes, and symbol with which the plot may be made. The graph, when finished, is complete with labels and titles and is suitable for publication. Examples of the EZGRAF output may be seen in Figures 7-10.

Once the data are stored they may be operated on by PEKFIT, which separates the various reactions occurring in the desulfurization process, determines the kinetic parameters E and k_0 and creates a data file which is a desulfurization curve calculated from the derived kinetic parameters. This "theory file" may then be plotted by the TYPAGRAPH TERMINAL and compared with the experimental curve. Successive repetitions of this curve fitting procedure by PEKFIT results in good fitting of the "theory file" with the experimental, hence best, values for E and k_0.

All the file manipulations, graph generations and curve fittings may be performed by a single person with a few hours training in the operation of the time sharing computer system.

KINETIC PROGRAMS

To better understand how some of the existing programs are used in computing the kinetic parameters, the following examples are presented. A summary of the kinetics programs currently used is given in Table II. The programs chosen for these examples are those which extend the utility of the non-isothermal kinetics treatment by mathematical modeling of the reaction systems. The evolution curves obtained from this best fit procedure may then be compared to the results obtained from analysis of the experimental data. In these examples, three H_2S evloution peaks corresponding to the pyrite reduction, the sulfide reduction, and the Organic III reaction are used. The kinetic parameters for these reactions, including reaction order, are chosen in advance to show that the fitting programs actually converge to the correct values. These parameters are shown in Table I.

TABLE I. KINETIC PARAMETERS CHOSEN FOR THE THREE H_2S EVOLUTION PEAKS USED IN THIS EXAMPLE

Peak	n	$\log_{10}(k_0)$	E	V_0
Pyrite	0.5	11.2	42.1	1
Sulfide	1	5.2	25.1	1
Organic III	2	7.4	38.1	0.5

The computer program LINFIT, used in combination with the sub-routines DVDTG, CAFILE, and certain library programs, LIB, available from the PDP-10 system is illustrated in Figure 3. This program uses as input variables the kinetic parameters E, k_0 and n as well as the experimental variable m, the heating rate,and

TABLE II. SUMMARY OF KINETICS PROGRAMS

Program Name	Purpose	External References
LINFIT	Calculation of best fit data from hypothetical kinetic parameters	DVDTG, CAFILE, Library
MDATA	Creation of theoretical non-isothermal evolution curves from best fit data of LINFIT. Temperature intervals are taken from an actual experimental run	DVDTG, CAFILE
MTM	Calculation of best fit kinetic parameters, E and k_0 for experimental data	CAFILE, LSTS
CURVE	Calculation of reaction order for experimental data using parameters determined in MTM	Library
E % GRAPH	Plotting program supplied in time-shared service software	Data File from experiments or theoretical calculations
MODFL	Creation of separate intensity/temperature data files from input raw data	CAFILE
CAFILE	File naming subroutine	
DVDTG	Differentiating subroutine $(\frac{dV}{dT})$	
LSTS	Least squares curve fitting subroutine	
Library	Various subroutines available as library functions in time-sharing service	

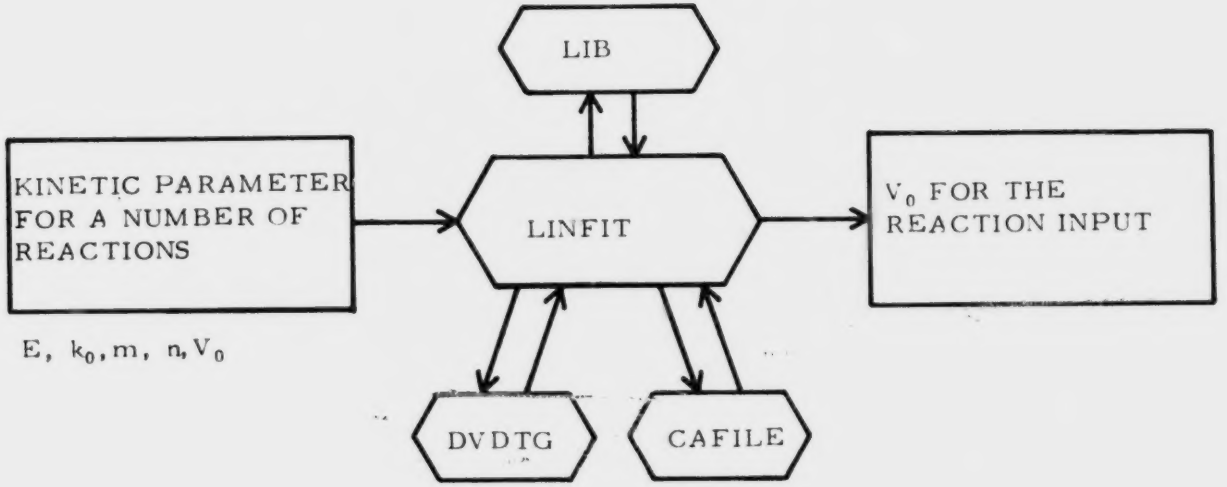

FIGURE 3. Block diagram of the program LINFIT

an initial guess for the variable V_0, the area under a particular curve. The purpose of the program is to produce a single parameter least squares fit for the variable V_0. The operation of this program is shown in Figure 4. For this example, the program was used to calculate V_0 for two values of m. With the best fit for V_0 in hand, the program MDATA, again in conjunction with CAFILE and DVDTG, is used to produce artificial data files from reaction parameters. This program is illustrated in Figure 5. The output is given in a form that may be plotted by using the EZGRAPH program, and has an option printing the curves in the form of a summation of the number of reaction being considered, or with the reactions resolved from each other. These options are illustrated in Figures 7-10 for the two different conditions of heating rate previously calculated by LINFIT. The operation of this program for one of the two heating rates is shown in Figure 6. The input of experimental data, SR XXX-DAT, shown in Figure 5, is seen from Figure 6 to be a means by which temperature intervals for the artificial data files are created. Temperature intervals unrelated to any experimental data could also have been used.

A second category of computer programs used in this work are those that are used primarily in analysis of real experimental data. The program MTM is based on Equation (1) which is derived from consideration of the non-isothermal kinetics treatment.

```
·LOAD LINFIT·F4,CAFILE·F4,DVDTG·F4,%LSSP△PSS△ SSP[LIBSSP]
FORTRAN:  LINFIT·F4
FORTRAN:  CAFILE·F4
FORTRAN:  DVDTG·F4
LOADING

LOADER 5K CORE

EXIT
'C

·START


ENTER MAX # OF FUNCTIONS, MAX # DATA POINTS
3,300

CORE SIZE IS NOW =  5

INPUT ANAME·EXT
SR224·DAT

INPUT TMIN,TMAX
550,1350

INPUT NUMBER OF REACTIONS, HEATING RATE
3,10

INPUT AN,LOG10(KO),E,VO FOR REACTION 1
·5,11·11,42100,1

 0·5000000     11·1100000      42100·0000000  1·0000000
INPUT AN,LOG10(KO),E,VO FOR REACTION 2
1,5·255,25100,1

 1·0000000      5·2550000      25100·0000000  1·0000000
INPUT AN,LOG10(KO),E,VO FOR REACTION 3
2,7·4,38100

 2·0000000      7·4000000      38100·0000000  0·0000000
FLOATING UNDERFLOW      PC=002433

FLOATING UNDERFLOW      PC=002433

IER= 1  IRES= 3

 0·0687638
 0·0089203      0·0382903
 77377·7100000 157922·1000000  46379·3200000
ERROR SQUARED=  0·6368313E+08
```

FIGURE 4. Computer Program LINFIT Calculating V_0 for m=10°C/min for Three Hypothetical Reactions.

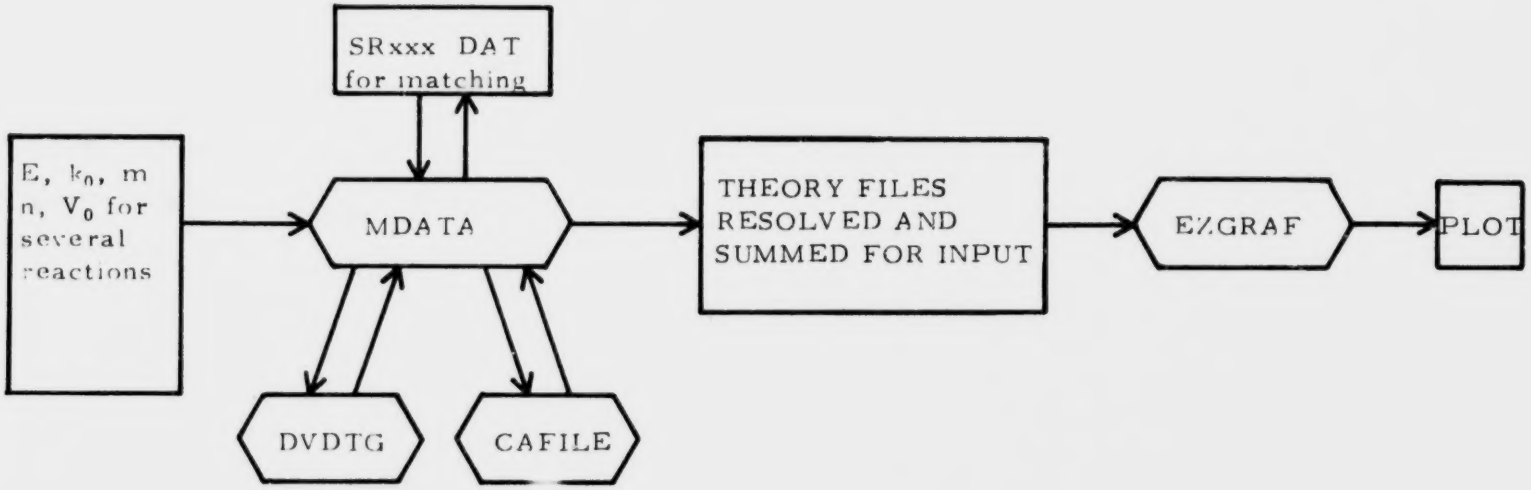

FIGURE 5. Block Diagram of the program MDATA

```
·EX MDATA·F4,CAFILE·REL,DVDTG·F4
FORTRAN:  MDATA·F4
LOADING

LOADER 4K CORE
EXECUTION

ENVELOPE

OUTPUT ANAME·EXT
SR224·ENV

INDIVIDUAL

OUTPUT ANAME·EXT
SR224·IND

TYPE 1 TO ENTER TEMPERATURES FROM FILE, 2 TO ENTER TZERO,DELT,AND NTEMPS
1

TEMPERATURE

INPUT ANAME·EXT
SR224·DAT

ENTER NUMBER OF REACTIONS, HEATING RATE
3,10

ENTER AN,LOG10(KO),E,VO
·5,11·11,42100,77378

ENTER AN,LOG10(KO),E,VO
1,5·255,25100,157922

FLOATING UNDERFLOW      PC=004175

FLOATING UNDERFLOW      PC=004175

ENTER AN,LOG10(KO),E,VO
2,7·4,38100,46379
```

FIGURE 6. Computer Program MDATA Creating Artifical Data Files SR224·ENV and SR224·IND, m=10°/min.

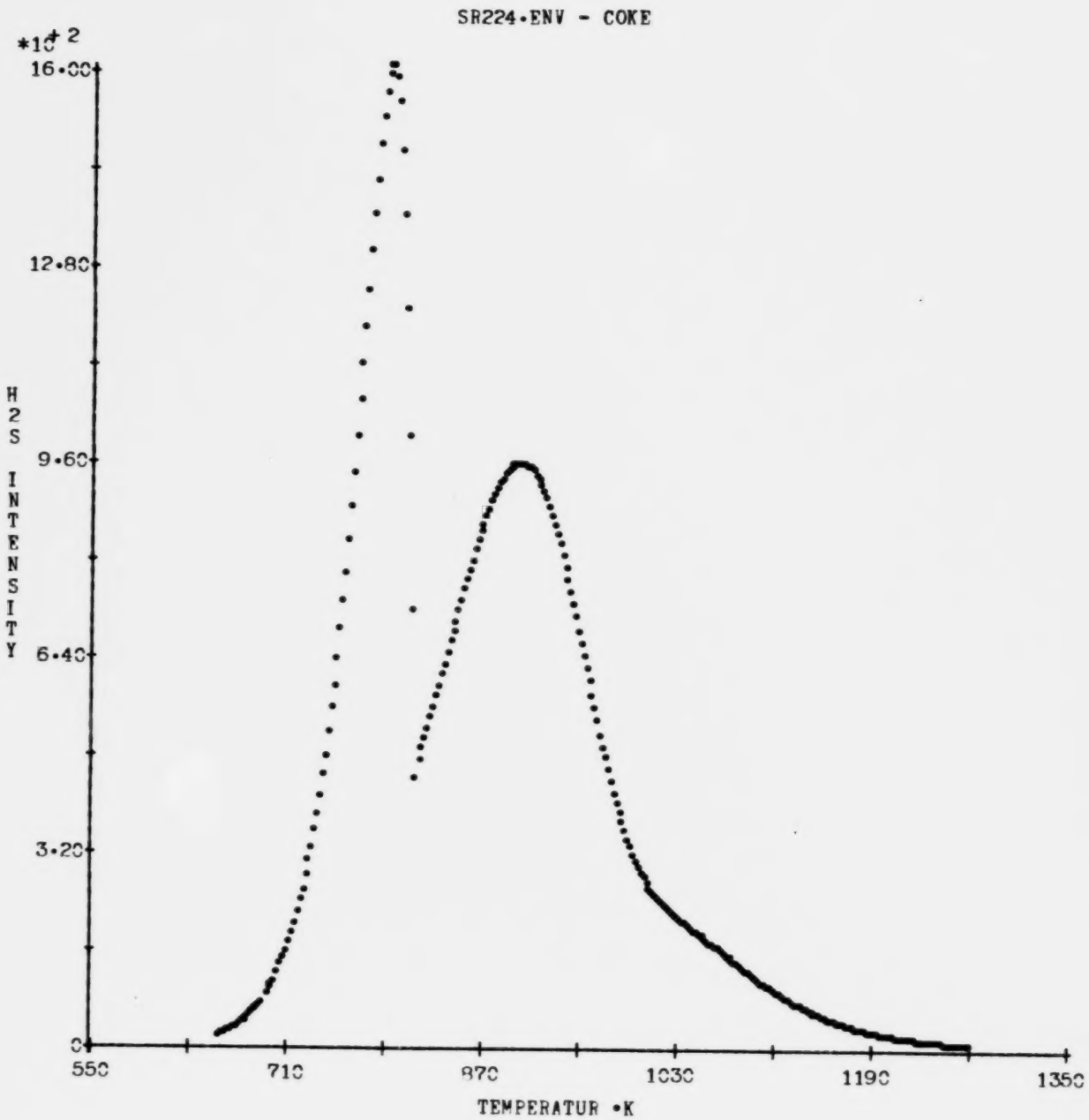

SYMBOL	NO.PTS.	LEGEND
•	278	

FIGURE 7. Output of LINFIT and MDATA for m=10°C/min. Overall Envelope.

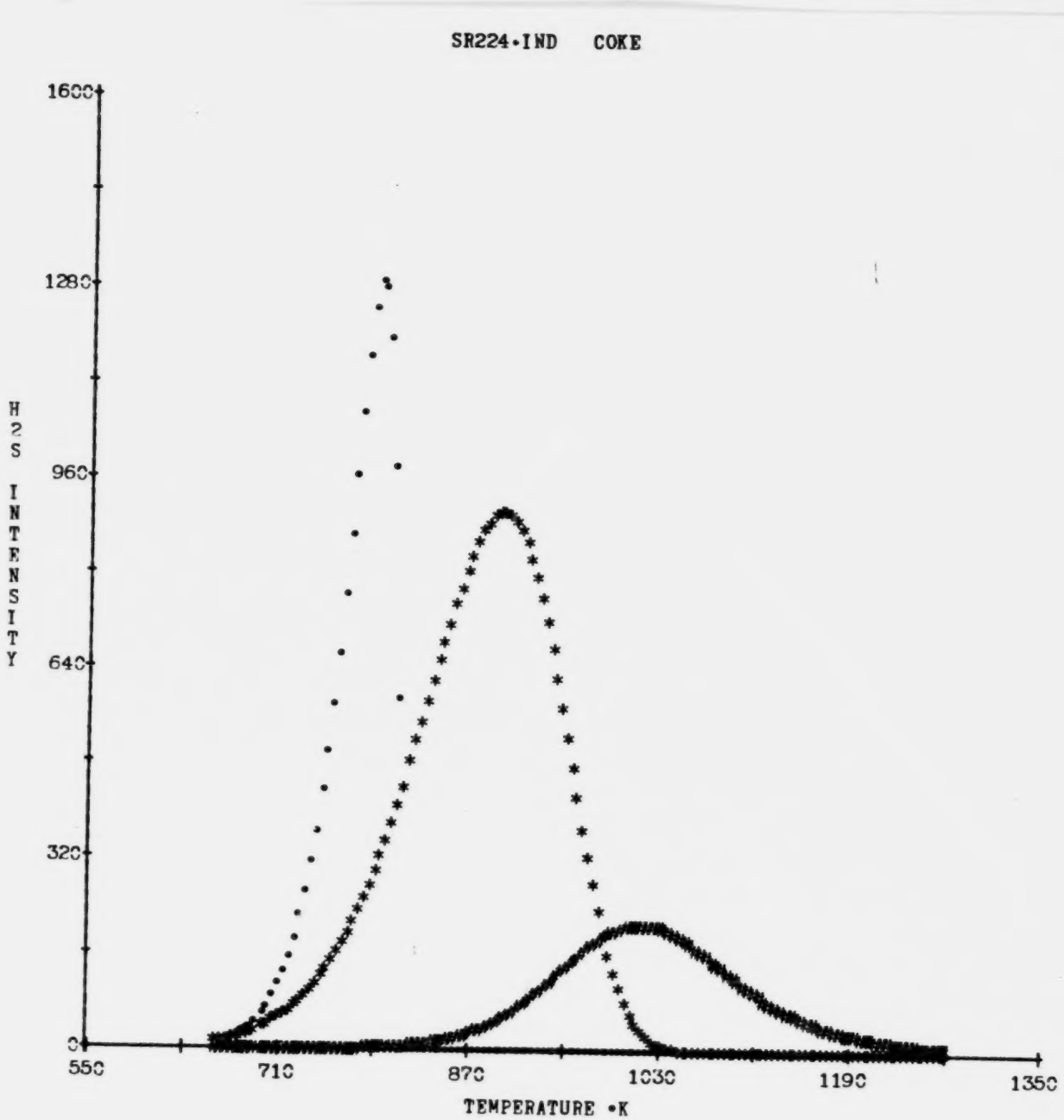

SYMBOL	NO.PTS.	LEGEND
•	139	PYRITE REACTION
*	139	SULFIDE REACTION
#	139	ORGANIC III REATION

FIGURE 8. Output of LINFIT and MDATA for m=10°C/min. Resolution of Three Reactions.

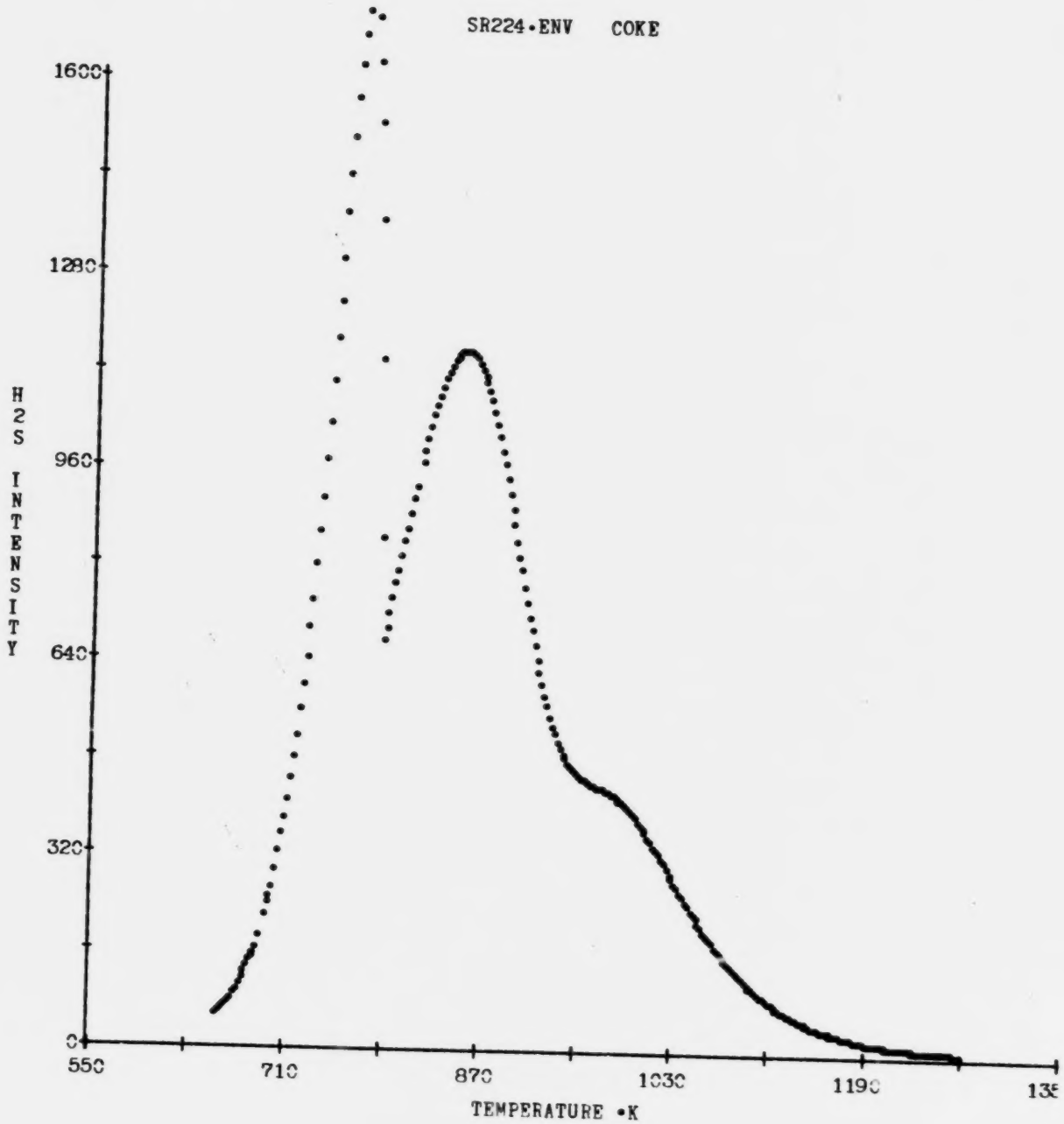

FIGURE 9. Output of LINFIT and MDATA for m=4°C/min. Overall Envelope.

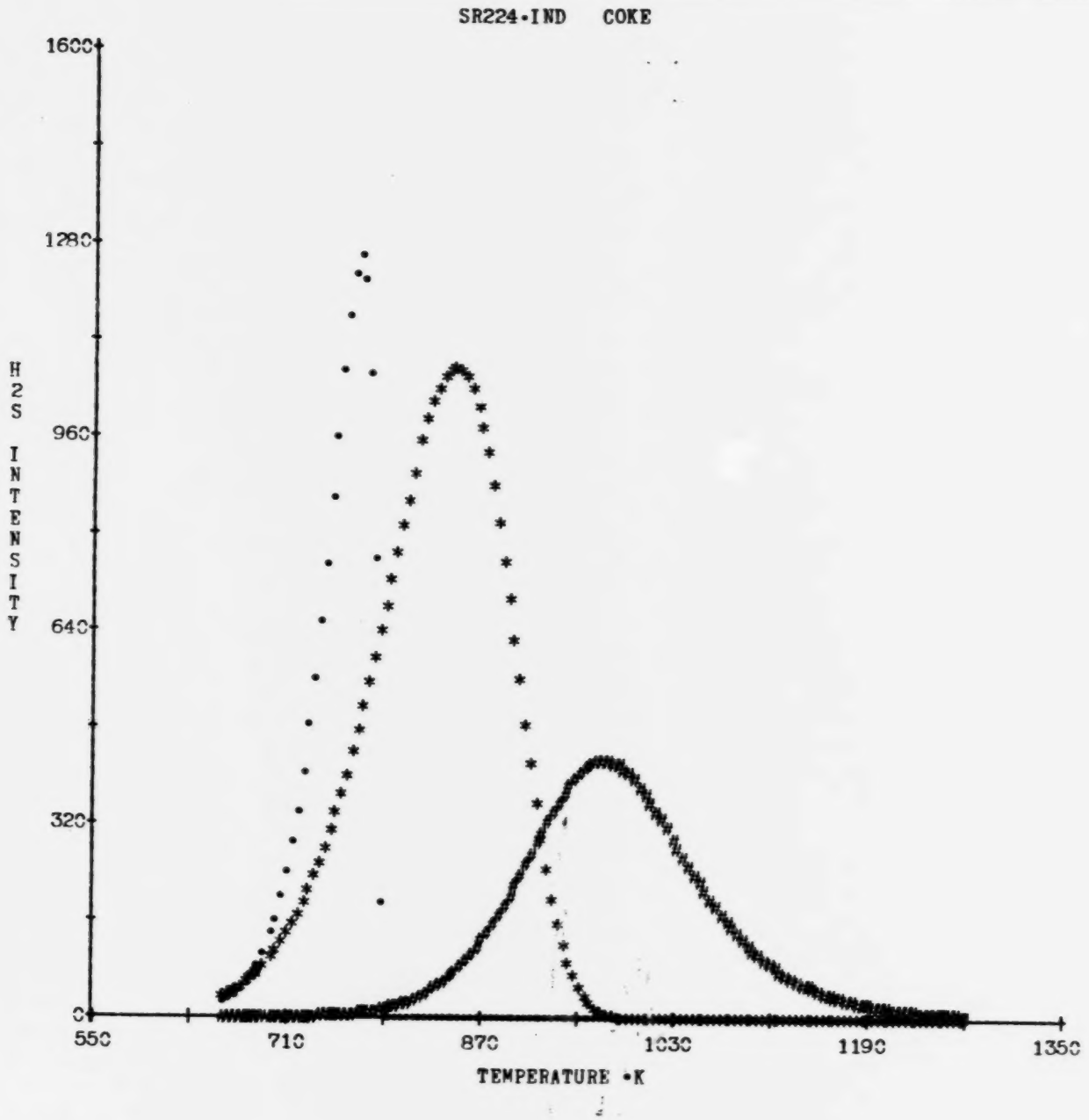

SYMBOL	NO.PTS.	LEGEND
•	139	PYRITE REACTION
*	139	SULFIDE REACYION
#	139	ORGANIC III REACTION

FIGURE 10. Output of LINFIT and MDATA for m=4 °C/min. Three Reactions Resolved.

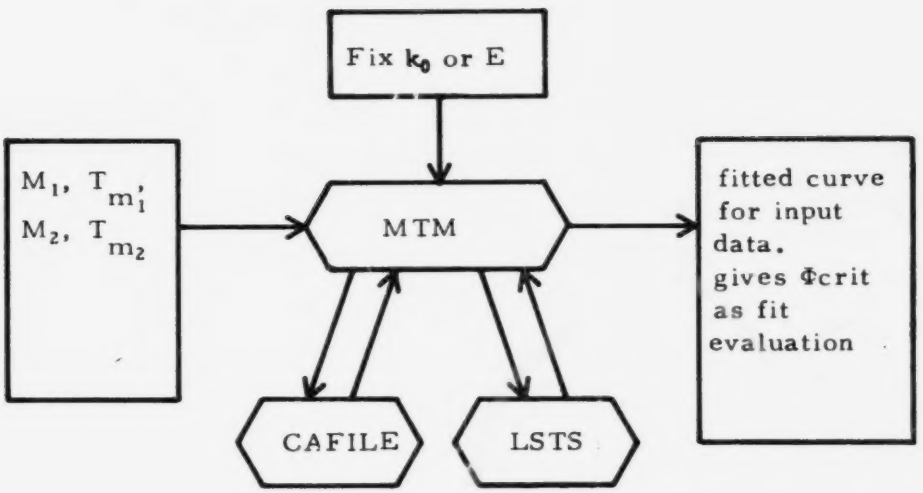

FIGURE 11. Block Diagram of the Program MTM

```
•START

INPUT AN,LOG10(KO),E,ISKIP
•5,10,42100,0

                                    Y=LOG(M/TM**2)        X=1/TM

INPUT M,TM, OR 0 TO TERMINATE
2,750

 2.0000000      750.0000000     -12.5470000       0.0013333
5,770

 5.0000000      770.0000000     -11.6833400       0.0012987
5,795

 5.0000000      795.0000000     -11.7219300       0.0012739
10,790

 10.0000000     790.0000000     -11.0414800       0.0012659
20.6,805

 20.6000000     805.0000000     -10.3563900       0.0012422
20,815

 20.0000000     815.0000000     -10.4106400       0.0012270
0

DO YOU WISH TO CREATE OUTPUT FILE?
YES

OUTPUT ANAME.EXT
PYRIT.DAT

DO YOU WANT A LEAST SQUARES FIT?
YES

NUMBER OF FIXED PARAMETERS?
1

FIXED PARAMETER INDEX?
2

EPSILON TEST

NONLINEAR CONFIDENCE LIMITS

PHI CRITICAL =  0.52475348E+00
CONVERGED TO THE FOLLOWING
LOG10(KO)= 11.1245200          E=  42100.0000000
```

Reproduced from best available copy.

FIGURE 12. Computer Program MTM Calculating E and k_0 for the Reaction of Iron Pyrite.

$$\frac{\ln m}{T_{max^2}} + \ln \frac{E}{Rk_0} = -\frac{E}{RT_{max}} \qquad (1)$$

Data for m, the heating rate, and T_{max}, the temperature in °K where the maximum of a particular envolution curve occurs, when used in Equation 1 yield a line having a slope of -E/R and an intercept of $-\ln E/Rk_0$. The MTM program illustrated in Figure 11, accepts m and T_{max} data from several non-isothermal runs, and in the normal case, keeping E fixed, yields a best fit straight line for the input data and an evaluation of the standard deviation of the points from that line. To determine the overall best fit value of E and k_0 to the experimental data, the values of the standard deviation quantity Φ critical, are plotted as a function of E, with the overall best fit being taken as the minimum of this curve. The operation of the MTM program is shown in Figure 12 for the case of actual data taken from reactions of pyritic sulfur. Figure 13 shows the use of the Φ critical plot for the same pyrite data to determine a value of E and thus a value of k_0, in an unambiguous manner. Figure 14 shows the MTM straight line for this same data in the case of the best fit for E and k_0. Figures 15-18 show critical curves and MTM straight lines for the best fits of experimental data from the reaction of sulfides and Organic III.

The computer program CURVE, illustrated in Figure 19 uses the kinetic parameters E and k_0 determined in the MTM procedure takes heating rate as fixed input and uses reaction order as a variable parameter to compute peak width at half maximum, FWHM, a shape factor of the experimental gas evolution curves. The plots resulting from this program are shown in Figures 20-22 for the cases of pyrite sulfide and Organic III respectively. A comparison of FWHM in °K from experimental evolution curves with these plots yields the reaction order for a particular process.

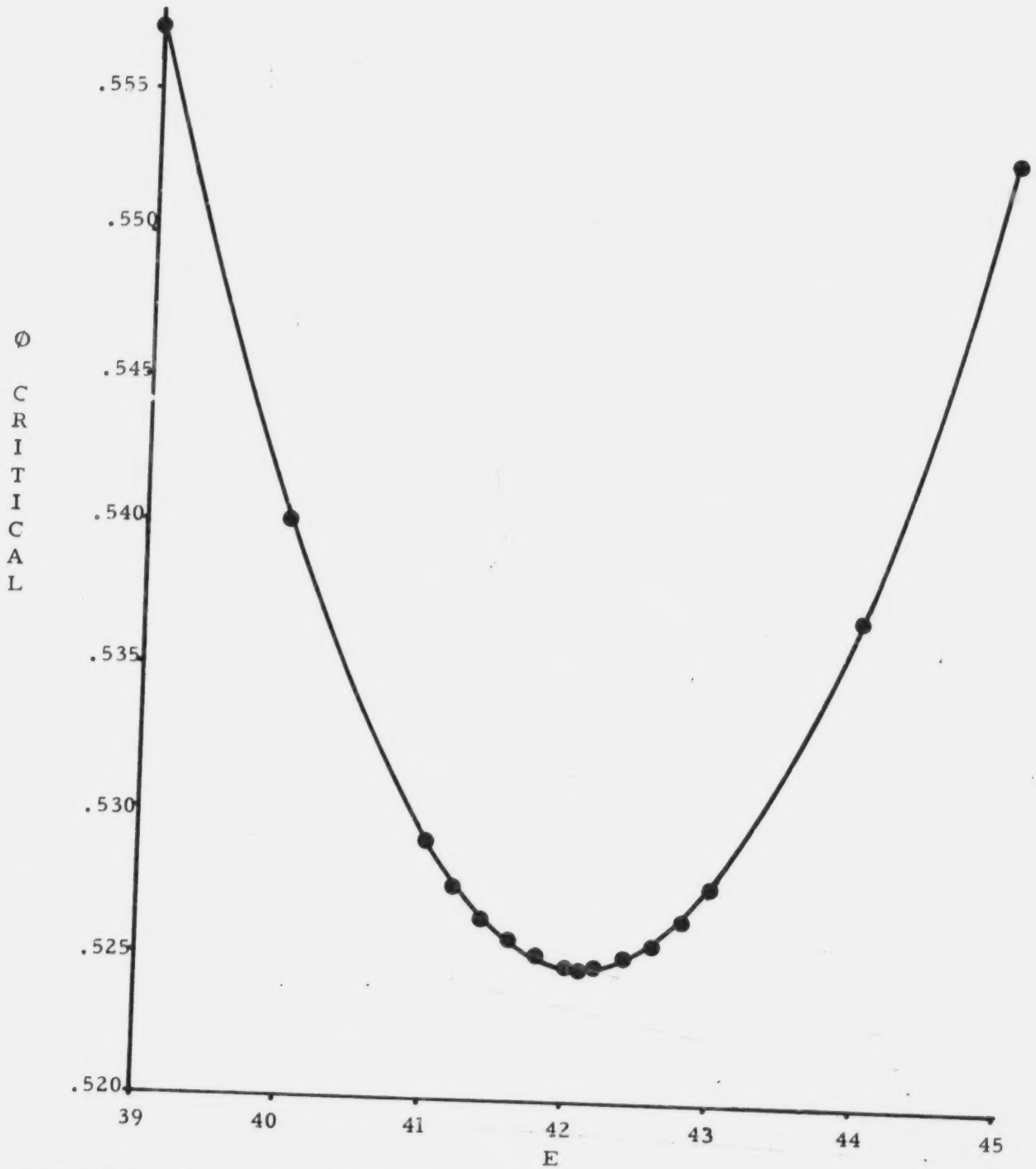

FIGURE 13. $\emptyset_{crit}$ vs E for Pyrite Reaction

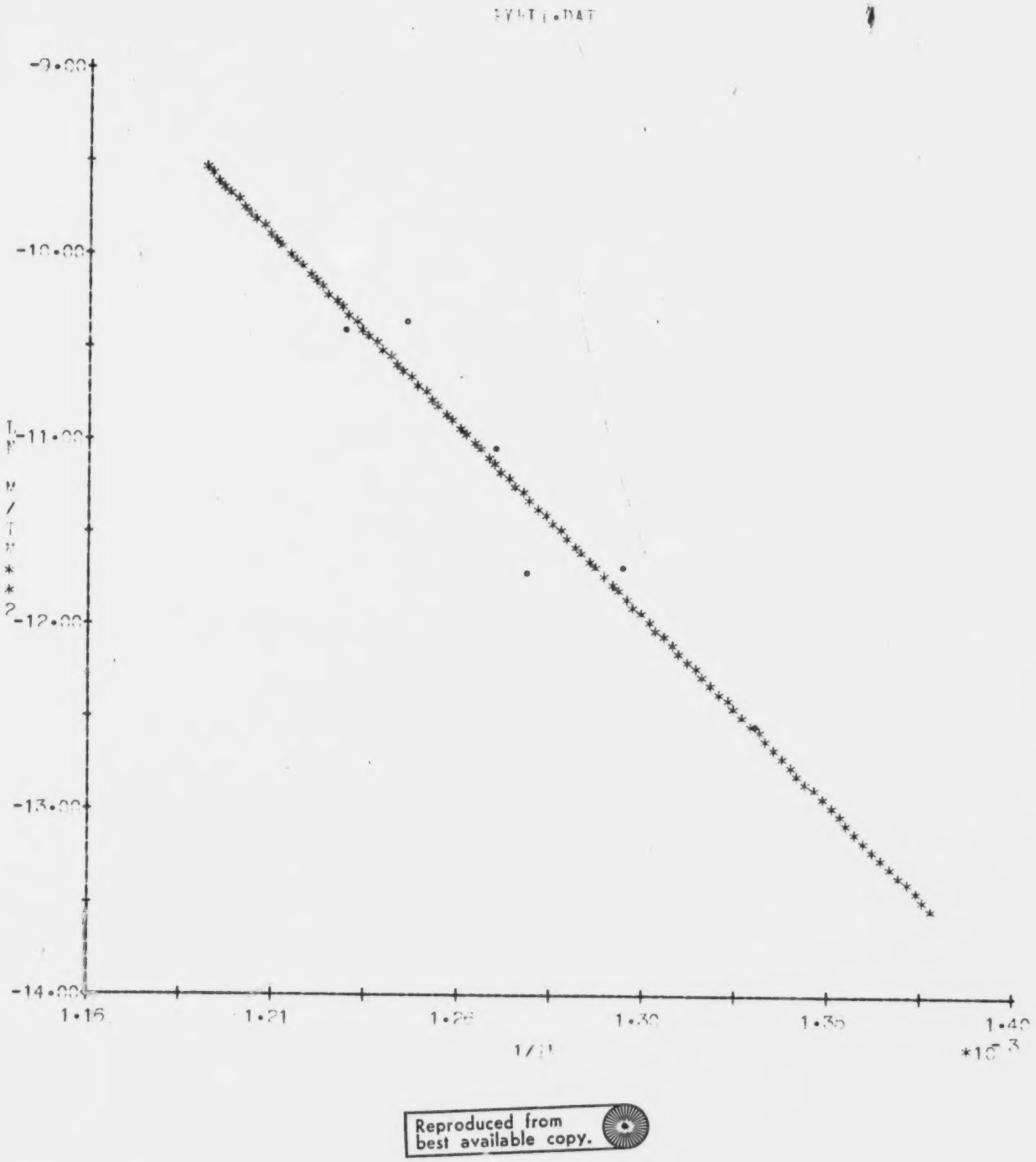

Reproduced from best available copy.

FIGURE 14. Best Fit for Tm Data from MTM Program and Φcrit Plot - Pyrite Reaction.

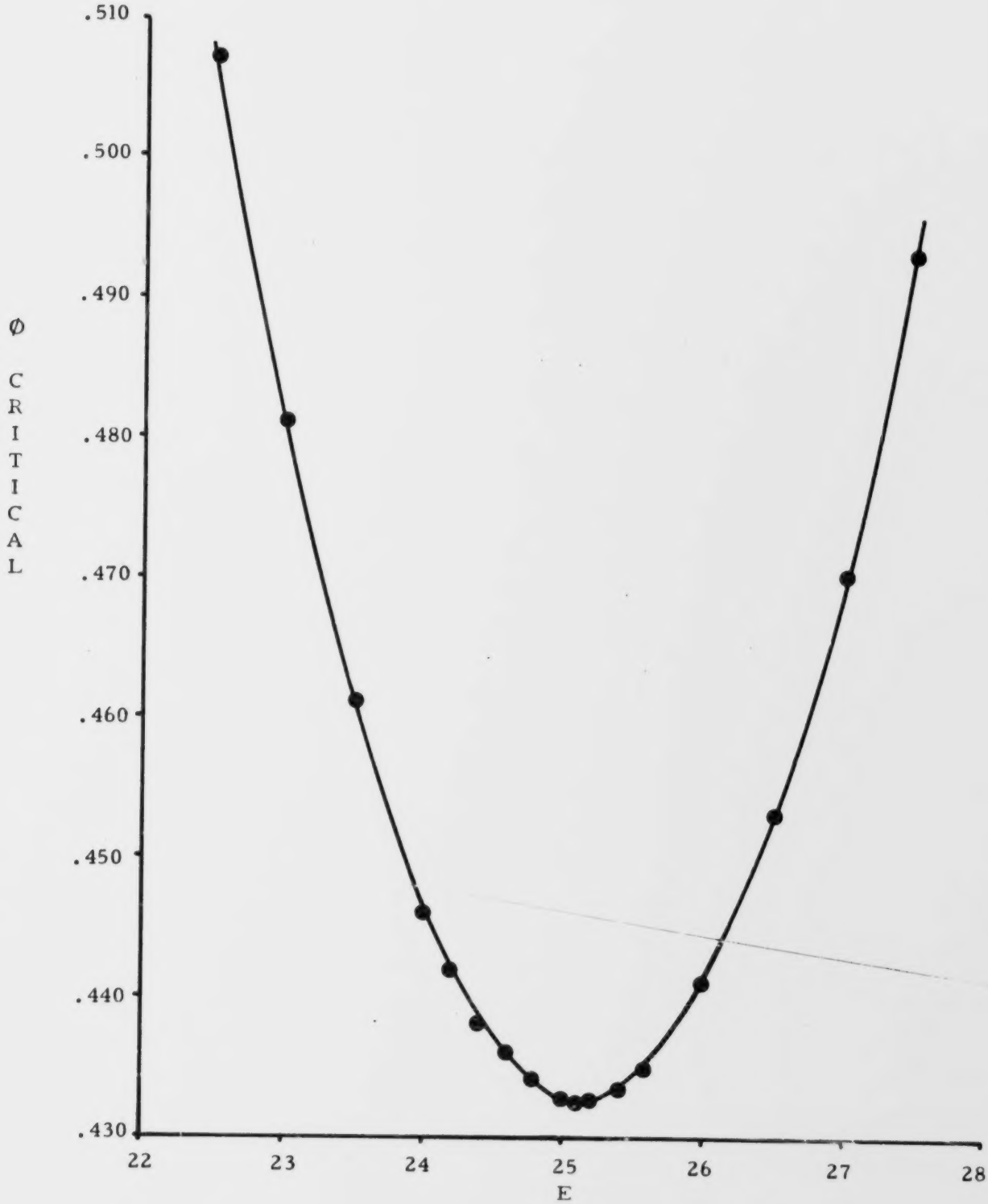

FIGURE 15. ϕ_{crit} vs E for Sulfide Reaction

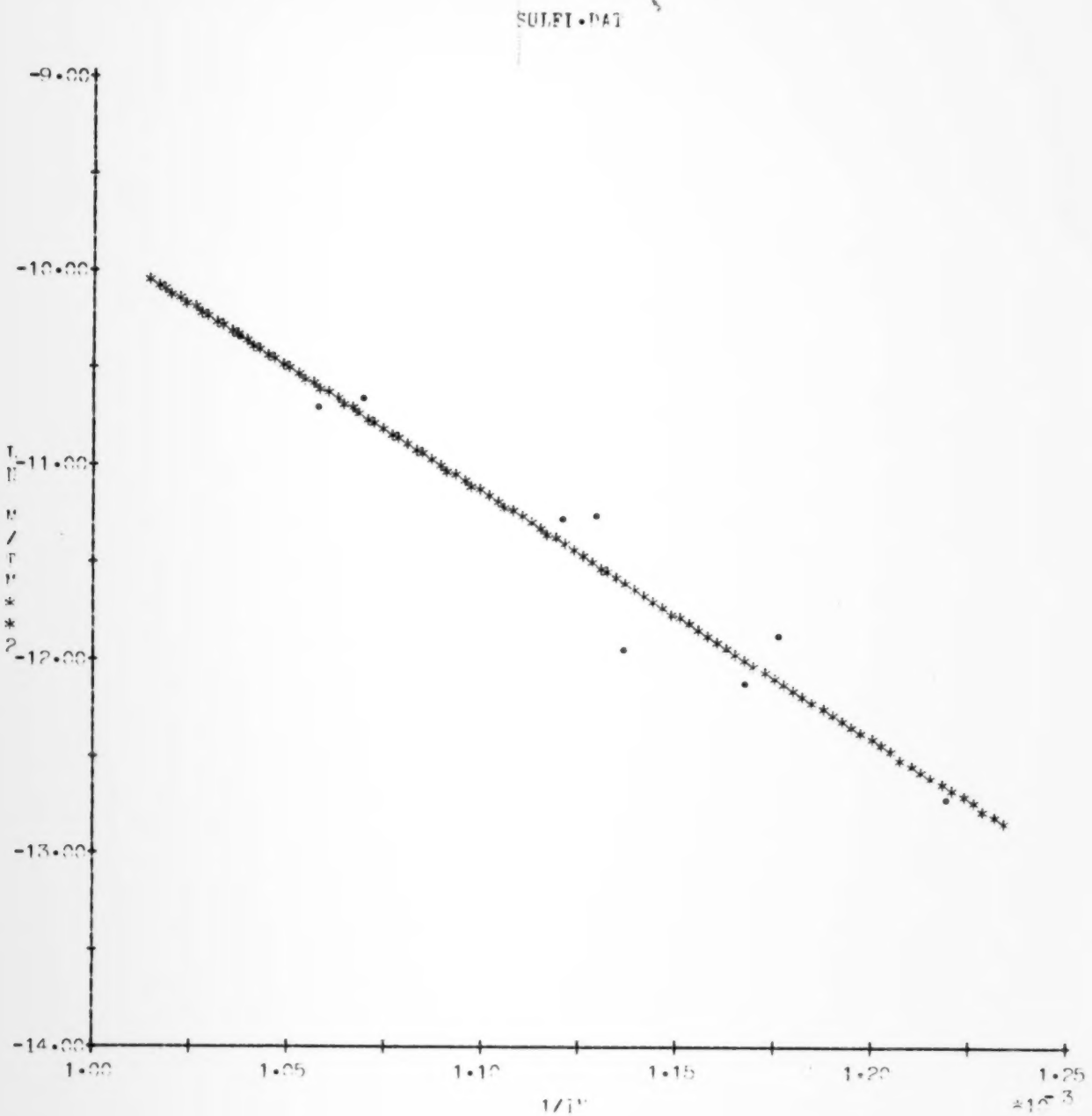

Reproduced from best available copy.

FIGURE 16. Best Fit for Tm Data from MTM Program and Φcrit Plot-Sulfide Reaction.

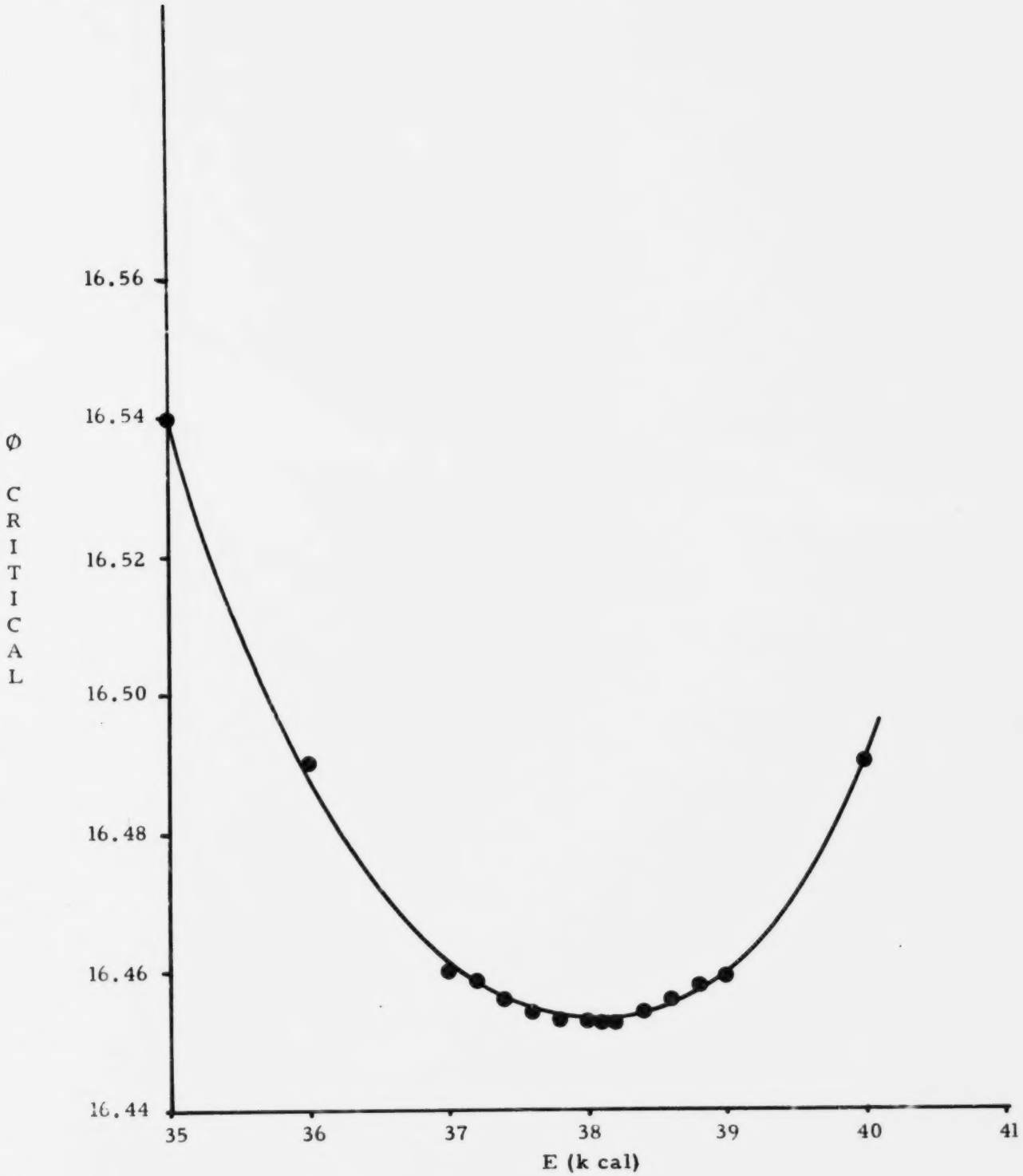

FIGURE 17. $\emptyset_{crit}$ vs E for Organic III Reaction

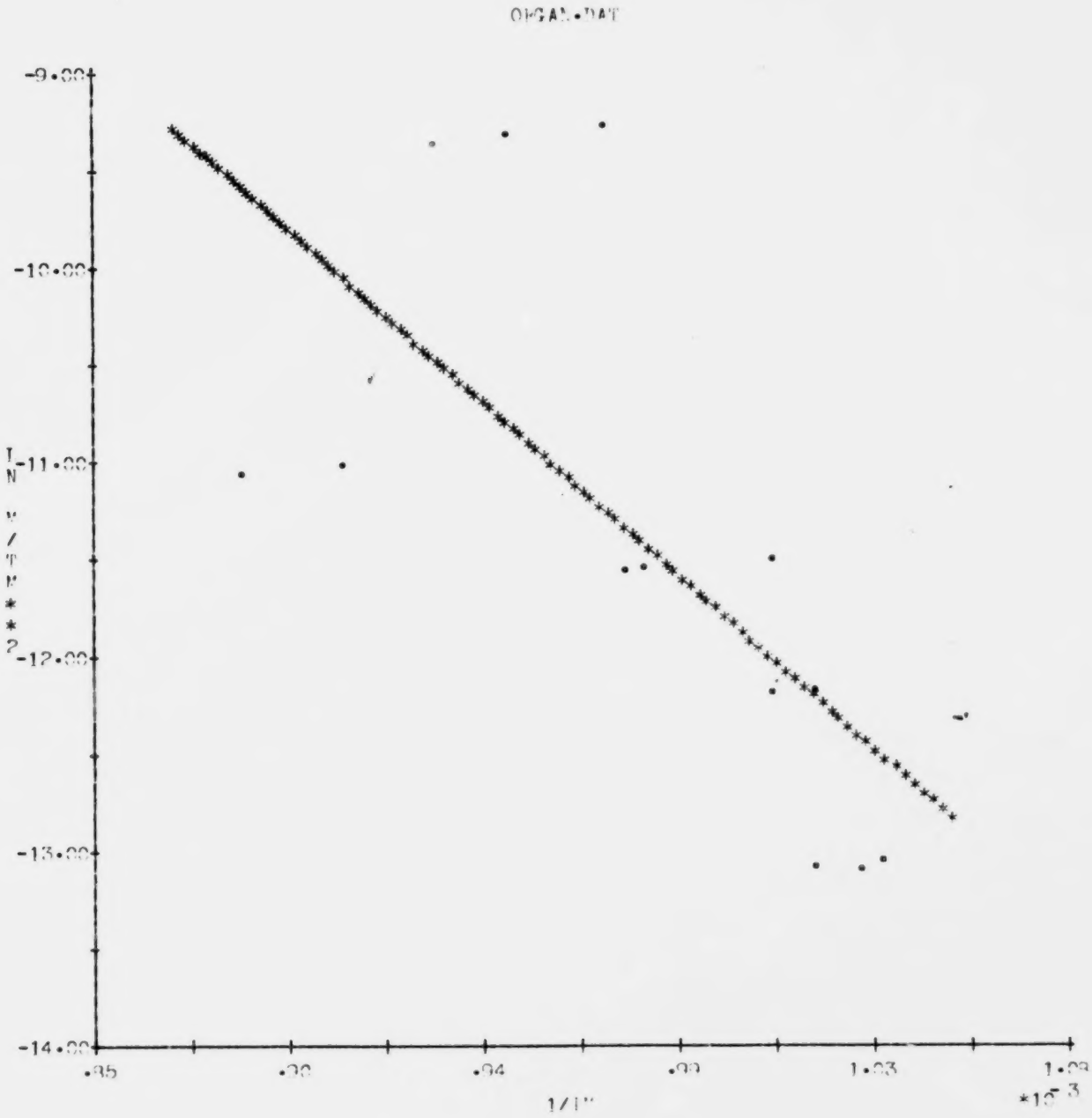

SYMBOL	NO.PTS.	LEGEND
•	13	CHARGES IL P-MAX AIR HEATING RATE FOR CORE IL 32

FIGURE 18. Best Fit for Tm Data from MTM Program and Φcrit Plot-Organic III Reaction.

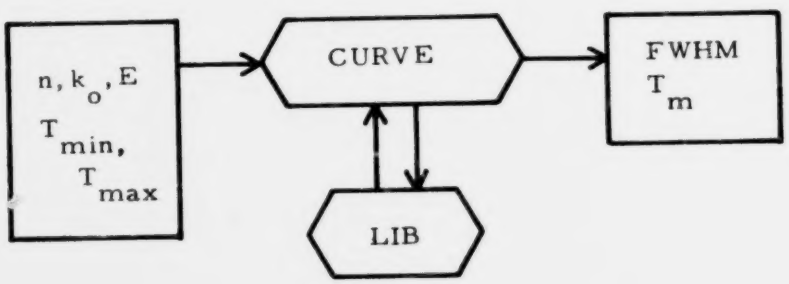

FIGURE 19. Block Diagram of the program CURVE

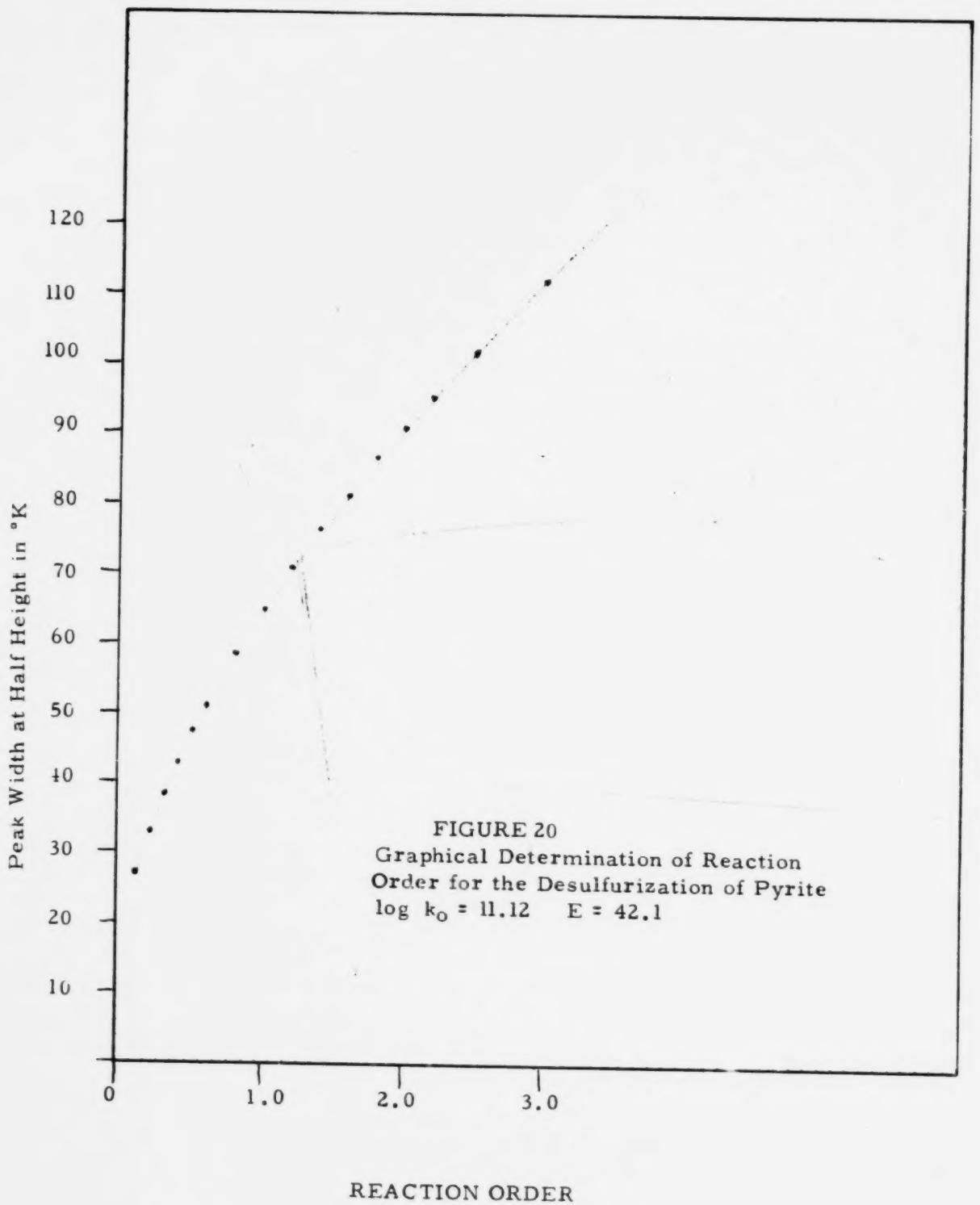

FIGURE 20
Graphical Determination of Reaction Order for the Desulfurization of Pyrite
log k_o = 11.12 E = 42.1

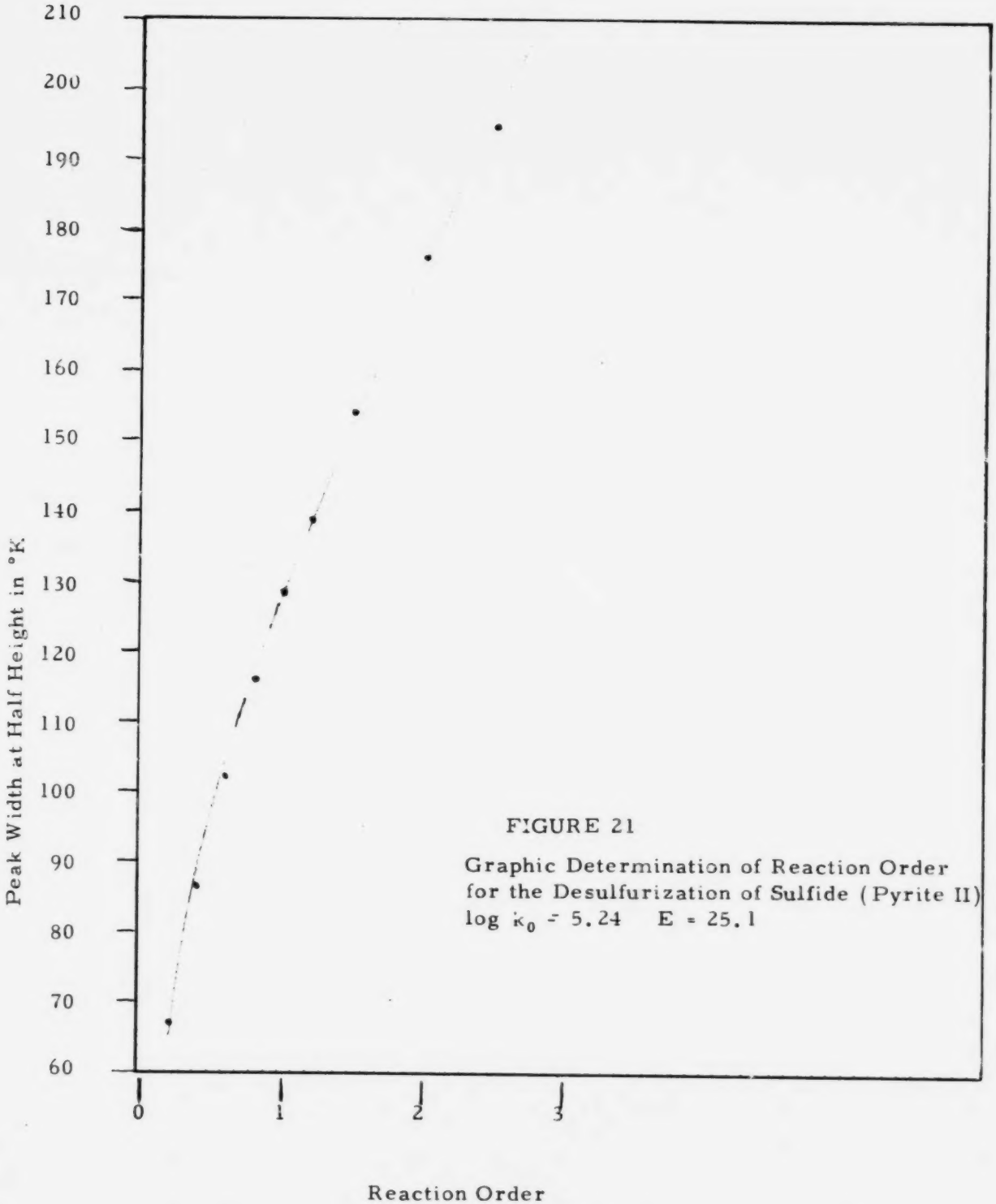

FIGURE 21

Graphic Determination of Reaction Order for the Desulfurization of Sulfide (Pyrite II)
$\log \kappa_0 = 5.24 \quad E = 25.1$

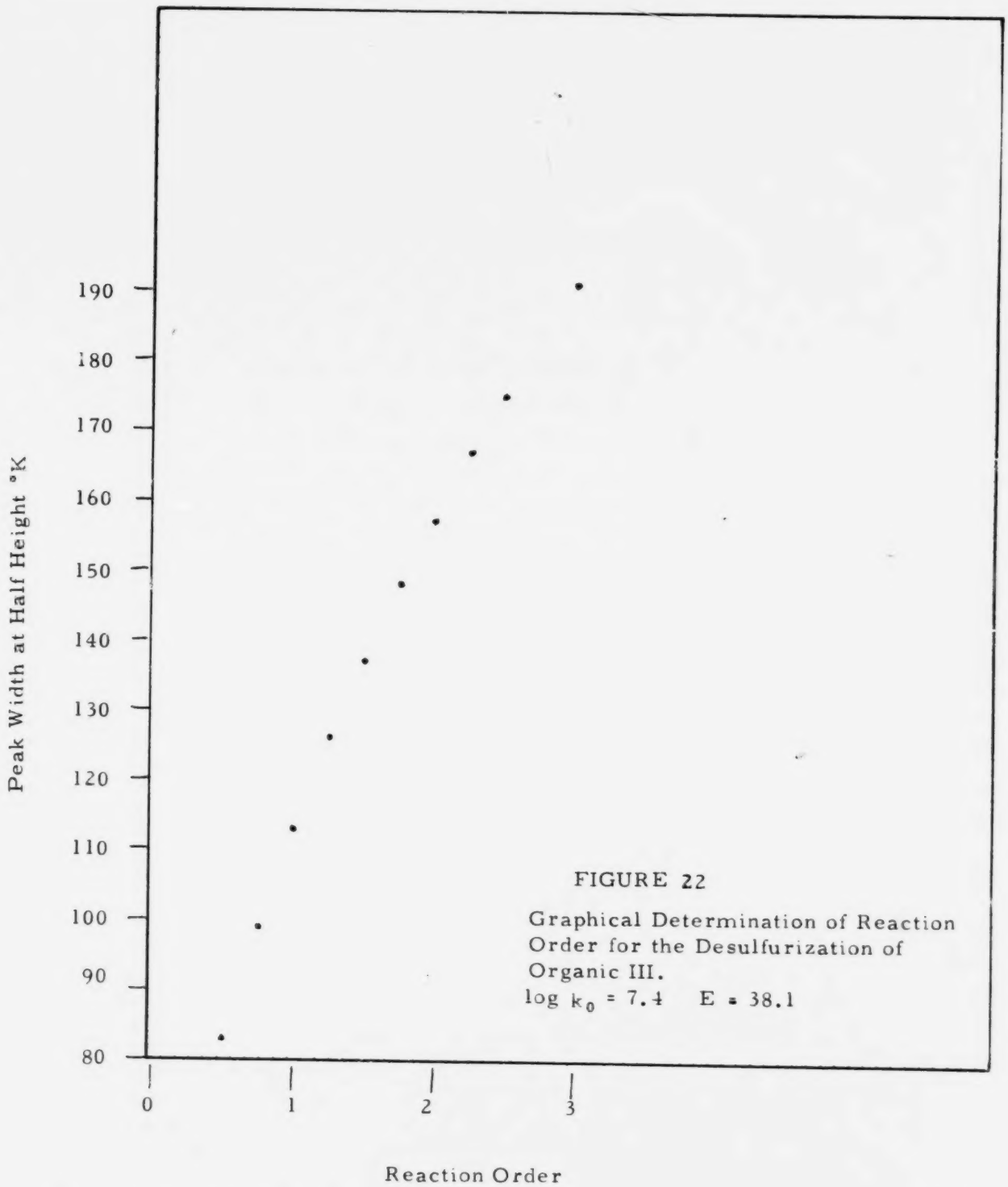

FIGURE 22

Graphical Determination of Reaction Order for the Desulfurization of Organic III.

$\log k_0 = 7.4 \quad E = 38.1$

THEORETICAL SUMMARY OF THE NON-ISOTHERMAL KINETIC METHOD

Sulfur is found in coal in a variety of different forms and we may depict the hydrodesulfurization of one of these typical forms by the chemical reaction (2), where A_j -S represents

$$(A_j\text{-}S)_{SOLID} + H_2 \rightarrow (A_j)_{SOLID} + H_2S \qquad (2)$$

one of the ways in which the sulfur is bound into the solid and A_j represents the pertinent site of this jth type of sulfur bonding after the sulfur has been removed. The rate of this reaction is given by the expression (3) where $[A_j\text{-}S]$ is the

$$-\frac{d[A_j\text{-}S]}{dt} = \left(\frac{d[H_2S]}{dt}\right)_j = k_j[H_2][A_j\text{-}S]^{n_j} \qquad (3)$$

concentration of solid reactant sites, $[H_2]$ is the molecular hydrogen concentration, n_j is the reaction order, t is the time, and k_j is the reaction rate constant. The reaction rate constant may be written in the usual Arrhenius form, viz:

$$k_j = k_{oj}\, e^{-E_j/RT} \qquad (4)$$

and there will be a rate equation such as (3) and a rate constant such as (4) for each type of hydrodesulfurization reaction.

As we have already discussed earlier, the shape of the H_2S evolution peak for a given process is also a function of E, k_0 and n. By combining our knowledge of k_0 and E for a given process with measurements of T_m for various heating rates, we may calculate the evolution curves for various assumed orders n, and thus construct a curve of the width of the H_2S evolution peak at half-height (the shape factor) as a function of order. Such plots are shown in Figures 20-22 for H_2S evolution from Pyrite, Sulfide, and Organic III. By comparing the experimental value of the peak width at half-height with these curves we may determine the order of the reaction that produces each peak.

RESULTS OF DESULFURIZATION STUDIES

REDUCING ATMOSPHERE

Hydrodesulfurization of sulfur bound as Organic I and Organic II appears to be described adequately by first-order irreversible reactions whose frequency factors and activation energies have been reported previously[2] but which for completeness are presented in Table III. There appears to be little difficulty in removing these forms of sulfur and we need not discuss them further.

The treatment described above, which, in principle, permits unambiguous determination of E, k_0, and n, assumes that the H_2S evolution curve for the process in question is resolved from those due to all other processes and also that the reaction is an irreversible one as given by (2). These assumptions appear to be valid for the H_2S evolution curve for pyrite sulfur, pointing to a desulfurization reaction that is one-half order in pyrite with an activation energy of 42.1 kcal/mole and a frequency factor of $10^{11.11}$. On the other hand, the assumptions mentioned above are only approximately valid for H_2S evolution from sulfide and Organic III; neither evolution peak is completely resolved and, moreover, there appears to be some evidence of complications due to the back reaction of (2) for these latter type hydrodesulfurization processes. None the less, applying the method described, as a means to obtain approximate values for the kinetic parameters, we find after consideration of many H_2S evolution curves that the Sulfide desulfurization is best represented by a first-order reaction having an activation energy of 25.1 kcal/mole and a frequency factor of $10^{5.24}$, while the Organic III desulfurization is best described by a second-order reaction having an activation energy of 38.1 kcal/mole and a frequency factor of $10^{7.4}$. The current best values for the kinetic parameters for all five processes are tabulated in Table III.

As shown in our previous reports[1,2], it is convenient to adopt the non-isothermal kinetic method of Jungten and follow these reactions by measurement of the H_2S evolved while hydrogen is flowing over a sample of coal that is being heated at a constant and known flow rate. Thus, after relating the concentration, $[A_j\text{-}S]$, to the amount of H_2S evolved, it has been shown that the following equation, (5), applies to each hydrodesulfurization reaction, in particular as shown in (5) to the $_j$th reaction:

$$\left(\frac{dV}{dT}\right)_j = \frac{k_{oj}}{m} e^{-\frac{E_j}{RT}} \left\{ V_{oj}^{-(n_j-1)} + (n_j-1)\frac{k_{oj}R}{mE_j} T^2 e^{-\frac{E_j}{RT}} \right\}^{-\binom{n_j}{n_j-1}}$$

(5)

In (5), V is the volume of H_2S evolved, at time t, V_0 is the volume evolved when reaction is complete, and m is the heating rate and the other symbols are as described previously. The H_2S concentration in the flowing gas is measured as a mass spectrometric peak intensity, i, that is related to dV/dT by the relationship (6),

$$\frac{dV}{dT} = \frac{Q}{mG}\beta i$$

(6)

where Q is the flow rate of gas, G is the weight of the coal sample, m is the heating rate, i is the intensity of the mass spectrometer peak and β is the proportionality factor relating the peak intensity to the fraction of the flowing gas that is H_2S. Thus if only the $_j$th process were operative the temperature dependence of i would be given by (5) and (6), which predict that i versus T should be a peak whose

shape and position depend upon k_0, E, n, and m. However, since a number of processes are superimposed which contribute to i, the actual temperature dependence of the observed mass spectral intensity is given by (7).

$$i = \frac{G}{Q\beta} \sum_j k_{oj} e^{-\frac{E_j}{RT}} \left\{ V_{oj}^{-(n_j-1)} + (n_j - 1) \frac{k_{oj} R}{m E_j} T^2 e^{-\frac{E_j}{RT}} \right\}^{-\binom{n_j}{n_j-1}} \tag{7}$$

Thus, as shown by (5) and (6), each hydrodesulfurization process yields a curve determined by the kinetic parameters k_0, E and n pertaining to that process and as shown by (7), the overall measurement of evolved H_2S is a superposition of those curves. A typical experimental curve is to be seen in Figure 23.

While it is undoubtedly true that the measurement of i versus T, such as shown in Figure 23 will not resolve a number of desulfurization processes, we have concluded, after numerous such measurements on a variety of coals, that we can consistently and at least partially resolve desulfurization curves due to forms of sulfur we have called Organic I, Organic II, Pyrite, Sulfide and Organic III. Further, by computer matching of the more-or-less resolved curves we can obtain the kinetic parameters E, k_0, and n. Thus for each of those five forms of sulfur in coal, whose H_2S evolution curves we can resolve, we may make an independent treatment according to (5) and (6).

As an example of the method of treatment consider (5) for the case of $n_j = n = 1$, that is, a first-order reaction. Utilization of (6) with (5) gives then (8) viz:

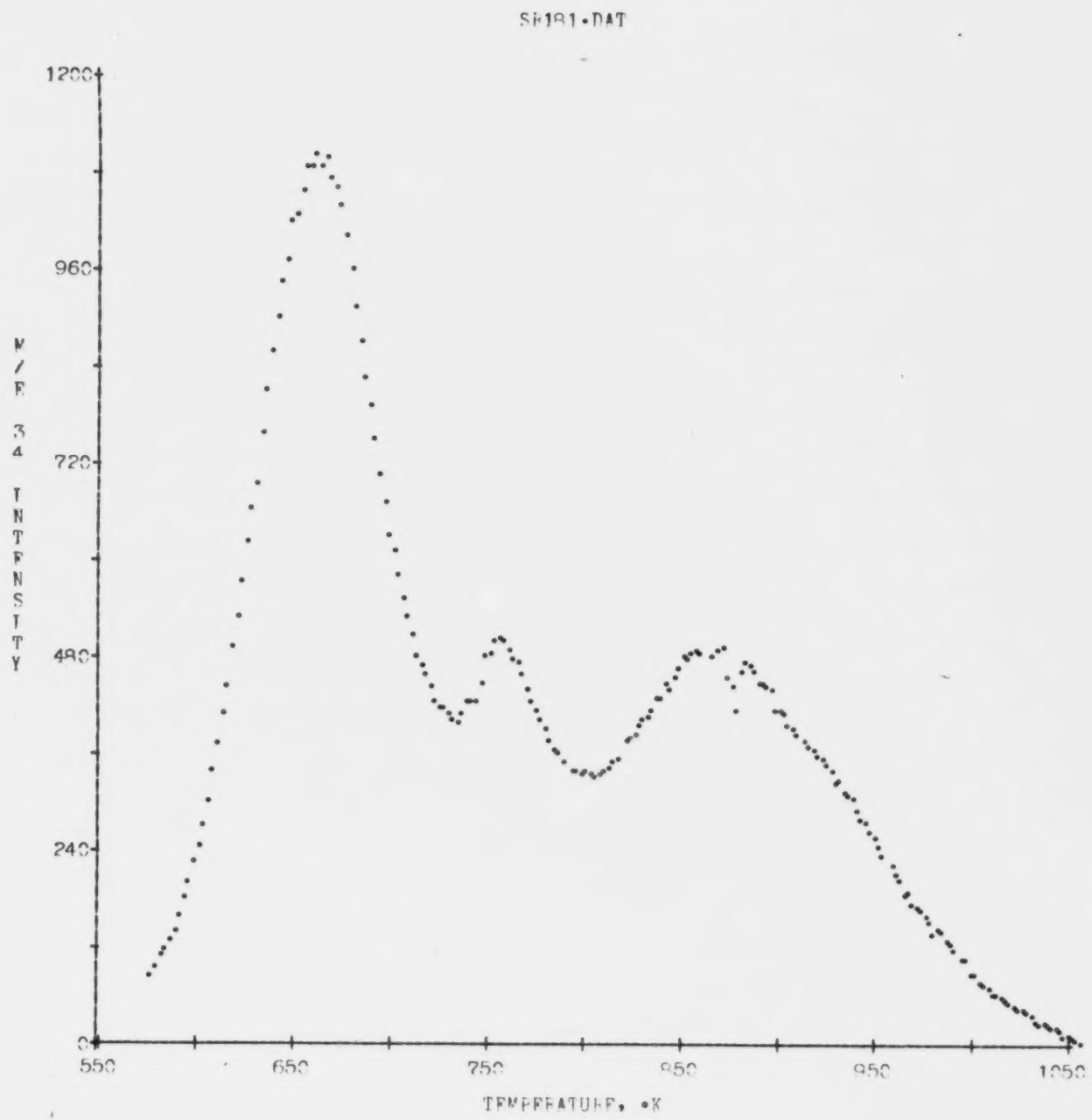

SYMBOL	NO. PTS.	LEGEND
•	207	

FIGURE 23. Typical Evolution Curve for H_2S in Treatment of Bituminous Coal with H_2.

$$i = \frac{GV_o k_o}{Q\beta} \exp\left[-\frac{E}{RT} - \frac{k_o RT^2}{mE} e^{-\frac{E}{RT}}\right]$$

(8)

and for a maximum in the i versus T curve, $(di/dT) = 0$, we have as long as $RT/E << 1$ the result, (9).

$$\frac{mE}{k_o RT^2_{MAX.}} = e^{-\frac{E}{RT_{MAX}}}$$

(9)

From (9) we have the useful result expressed by (10), namely

$$\ln\left(\frac{m}{T^2_{MAX}}\right) + \ln \frac{E}{k_o R} = -\frac{E}{R}\left(\frac{1}{T_{MAX}}\right)$$

(10)

Thus, if we measure the temperature of the maximum in i for a series of heating rates, l.e., and plot ln (l.c. and T_{m_2}) versus l and T_m a straight line is obtained whose slope yields E and whose slope and intercept give k_0. Most importantly, Equation (10) provides us with a most important tool, namely, independent of reaction order, we may determine E and k_0 from the measured positions of the peak intensity maxima as a function of heating rate. Typical plots of (10) for Pyrite, Sulfide, and Organic III are shown in Figures 14, 16, and 18 respectively.

TABLE III. KINETIC DATA FOR DESULFURIZATION OF COAL

Reaction	Order with respect to S-Containing Species	k_0	E kcal/mole.
$(Org\text{-}S)_I + H_2 \rightarrow H_2S$	1	3.1×10^{10}	34.5
$(Org\text{-}S)_{II} + H_2 \rightarrow H_2S$	1	2.8×10^{11}	41.5
$FeS_2 + H_2 \rightarrow FeS + H_2S$	1/2	1.3×10^{11}	42.1
$FeS + H_2 \rightarrow H_2S + Fe$	1	1.8×10^{5}	25.1
$(Org\text{-}S)_{III} + H_2 \rightarrow H_2S$	2	2.5×10^{7}	38.1

Pyrite Hydrodesulfurization ($FeS_2 + H_2 \rightarrow FeS + H_2S$)

This reaction appears to be one half order in FeS_2 with $k_0 = 10^{11.11}$ and E = 42.1 kcal/mole. Such a reaction order is easily rationalized by the following mechanism.

$$FeS_2 \rightleftarrows Fe + S_2\,(ads) \tag{11}$$

$$H_2 + S_2\,(ads) \rightarrow H_2S + S(ads) \tag{12}$$

$$Fe + S\,(ads) \rightarrow FeS \tag{13}$$

Assuming the first reaction is at equilibrium we have

$$K_1 = \frac{[Fe][S_2]_{ads}}{[FeS_2]} \tag{14}$$

and if (12) does not disturb the equilibrium significantly -that is, (12) is rate-determining we have

$$[Fe] \approx [S_2]_{ads} \tag{15}$$

and

$$\frac{d[H_2S]}{dt} = k_2 k_1^{1/2} [FeS_2]^{1/2} [H_2] \tag{16}$$

or

$$\frac{d[H_2S]}{dt} = k_2 k_1^{1/2} [FeS_2]^{1/2} [H_2] \tag{17}$$

Since (H_2) is maintained constant, we have finally

$$\frac{d[H_2S]}{dt} = k_2' k_1^{1/2} [FeS_2]^{1/2} \tag{18}$$

Hydrodesulfurization of Organic III

In this case the reaction appears to be second order in sulfur-containing species with E = 38.1 kcal/mole and $k_0 = k_0^1 [H_2] = 10^{7.4}$. Thus, for the rate equation we may write

$$\frac{d[H_2S]}{dt} = k'[H_2][A_J\text{-}S]^2 = k[A_J\text{-}S]^2 \tag{19}$$

Unfortunately, we do not know the nature of the bonding of sulfur in the solid but kinetics suggest the mechanism must be such that sulfur elimination between adjacent sites occurs. We may picture the Organic III removal, thus, as being of the form

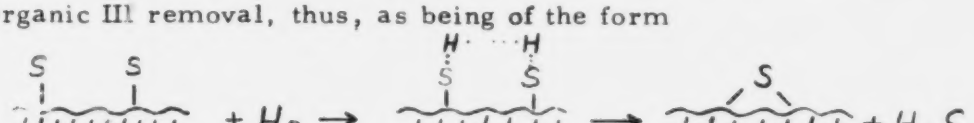

(20)

An example of such a reaction might be the hydrodesulfurization of thiophene to produce either a large cyclic thioether or a straight chain unsaturated thioether, or other isomer.

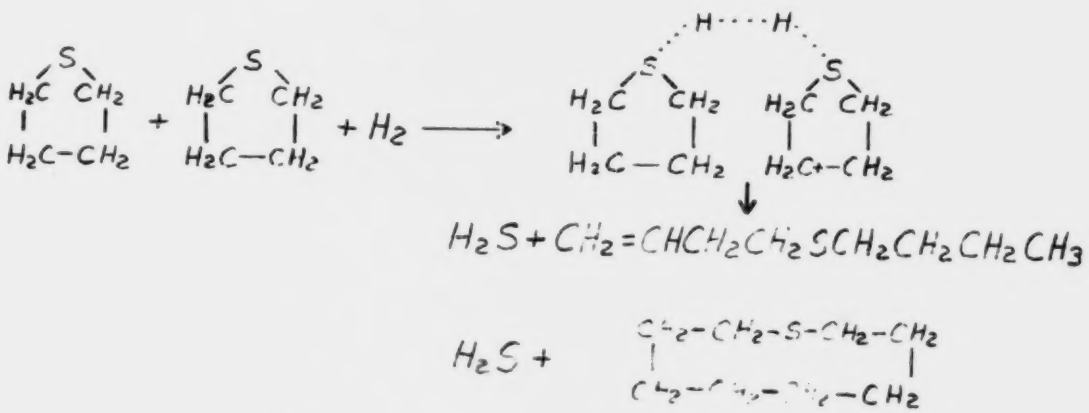

$$H_2S + CH_2{=}CHCH_2CH_2SCH_2CH_2CH_2CH_3$$

Reproduced from best available copy.

(21)

The kinetics tell us simply that two S-containing species must be involved in the rate-determining step.

OXIDIZING ATMOSPHERE

A total of 23 non-isothermal experiments (R 269-287, R 309-312) have been conducted in which a helium stream containing 1000 ppm of oxygen has been flowed over various solids. Samples so studied were pyrite, coals designated at SRI-Nos. 1-5, a coal char prepared from SRI No. 4, a sample of lignite and a sample of anthracite. An analysis summary of the coals used in this work is given in Appendix A. Most of the experiments were conducted at a heating rate of 20°C per minute although in two experiments (R 287 and R 310) a heating rate of 5°C per minute was used. All samples were of 100-200 mesh. The consumption of oxygen and the formation of SO_2, H_2S, H_2O, CH_4, CO, CO_2, and COS were measured in the computerized non-isothermal apparatus using chemical ionization mass spectrometry with He^+ as the reactant ion.

A summary of the experiments conducted in this oxidizing atmosphere is presented in Table IV.

Pyrite

Pyrite is a major source of sulfur in most coals and it is, therefore, of considerable value to examine the oxygen adsorption on this substance and the gas evolution subsequent to this adsorption as a function of temperature. In this way those processes occurring in actual coal samples which may be attributed to pyrite may be identified.

It is found that two specific oxygen adsorptions occur which exhibit peaks at 580° and 830°K, respectively, with a small possible adsorption occurring with a peak in the neighborhood of 720°K. A typical experimental curve showing these specific adsorptions as negative peaks may be seen in Figure 24. Sulfur dioxide evolution occurs by two processes, as may be seen in Figure 25 one exhibiting a peak at about 800°K and the second a peak at about 830°K. The first of these processes must occur specifically as a result of the first oxygen adsorption, namely, the adsorption peaking at 580°K, because, if only the first oxygen adsorption is permitted to occur (by removing the supply of oxygen at temperatures above 670°K) the second peak shown in Figure 25 is not observed. This may be appreciated by comparison of the O_2 adsorption curve in Figure 24 with SO_2 evolution curve in Figure 25, for which $He + O_2$ was supplied to the solid over the whole temperature range, and with the SO_2 evolution curve in Figure 26, for which O_2 was supplied only to 670°K. This appears to be an excellent example of a clear separation of two of the classical elementary steps of gas-solid reaction systems, namely, chemisorption and chemical reaction.

TABLE IV. OXIDIZING ATMOSPHERE EXPERIMENTS

Solid Reactant	Mesh	Heating Rate °C/Min.	Gases Studied m/e in ( )	Experiment Nos.	Remarks
Pyrite	200	20	O_2(32), SO_2(64), H_2S(34)	R282 A,B,D	
Pyrite	200	4.67	O_2(32), SO_2(64), H_2S(34)	R287 A,B,D	
Pyrite	200	20	O_2(32), SO_2(64), H_2S(34,35)	R309 A,B,C,D	He+O_2 to 677° He to 1200°
Pyrite	200	20	O_2(32), SO_2(64), H_2S(34)	R311, A,B,D	He+O_2 to 670° He to 1260°
Product of R311	-	20	O2(32), SO_2(64), H_2S(34)	R312 A,B,D	
Coal No. 1	100-200	20	H_2O(18,19), CH_4(16,17), CO(28,29) O_2(32), CO_2 (44,45)	R 278 A-I	
Coal No. 1	100-200	20	H_2(2), H_2S(34,35), COS(60), SO_2(64), O_2(32)	R279 A-F	
Coal No. 2	100-200	20	H_2(2), CO(29), H_2S(34,35), COS(60), SO_2(64)	R271 A-F	
Coal No. 2	100-200	20	CH_4(17), CO(28), O_2(32), CO_2(45)	R272 A-D	
Coal No. 2	100-200	5	O_2(32), H_2S(34), SO_2(60)	R310, A,C,D-COL	

OXIDATION EXPERIMENTS (Continued)

Solid Reactant	Mesh	Heating Rate °C/Min.	Gases Studied m/e in ( )	Experiment Nos.
Coal No. 3	100-200	20	H_2(2), O_2(32), H_2S(34,35), COS(60) SO_2(64)	R275 A-F
Coal No. 3	100-200	20	CH_4(16), H_2O(18), CO(28), O_2(32), CO_2(44)	R276 A-E
Coal No. 4	100-200	20	CH_4(17), H_2O(18,19), CO(29), O_2(32), CO_2(45)	R280 A-F
Coal No. 4	100-200	20	H_2(2,3), H_2S(34,35), COS(60,61), SO_2(64,65)	R281 A-H
Coal No. 5	100-200	20	CH_4(17), H_2O(19), CO(29), O_2(32), CO_2(45).	R269 A-E
Coal No. 5	100-200	20	H_2(2), CO(29), H_2S(34,35), COS(60), SO_2(64)	R270 A-F
Coal No. 5	100-200	20	CH_4(17), CO(29), O_2(32), CO_2(45)	R273 A-D
Coal No. 5	100-200	20	H_2(2), O_2(32), H_2S(34,35), COS(60) SO_2(64)	R274 A-F

OXIDATION EXPERIMENTS (Continued)

Solid Reactant	Mesh	Heating Rate °C/Min.	Gases Studied m/e in ( )	Experiment Nos.
Char No. 4	100-200	20	O_2(32), CH_4(17), H_2O(19), CO(29) CO_2(45)	R286 A-E
Lignite	100-200	20	O_2(32), H_2(2), H_2S(34), COS(60) SO_2(64)	R277 A,B,C, E,F
Lignite	100-200	20	O_2(32), CH_4(17), H_2O(19), CO(29) CO_2(45)	R285 A-E
Anthracite	100-200	20	O_2(32), CH_4(17), H_2O(19), CO(29) CO_2(45)	R283 A-E
Anthracite	100-200	20	O_2(32), H_2(3), H_2S(34, 35), SO_2(64)	R284 A,B, C,D,F

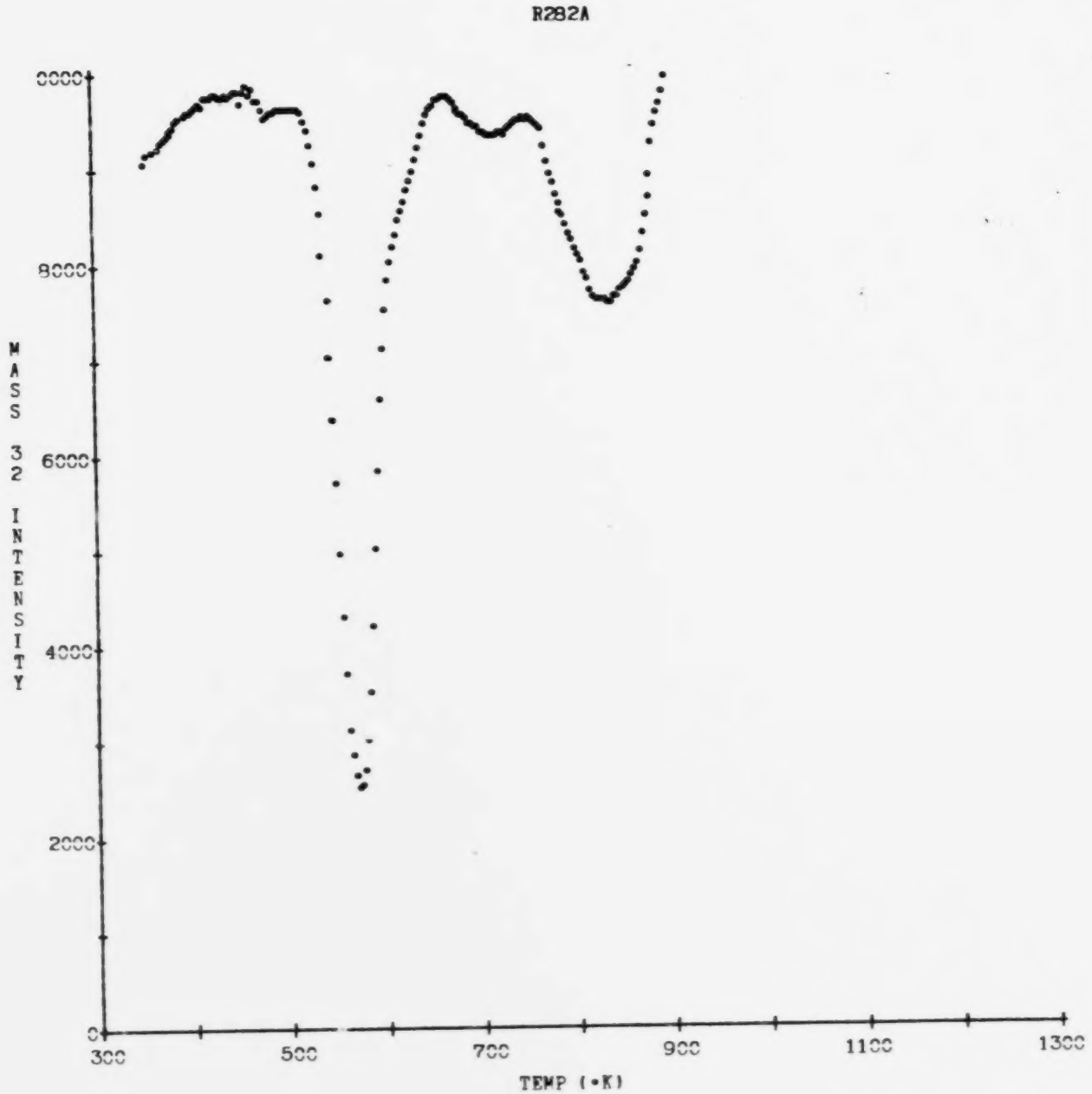

SYMBOL	NO.PTS.	LEGEND
•	178	02+ FROM PYRITE -200 MESH 20°/MIN

FIGURE 24. Non-isothermal Run of O_2 Adsorption on to Pyrite.

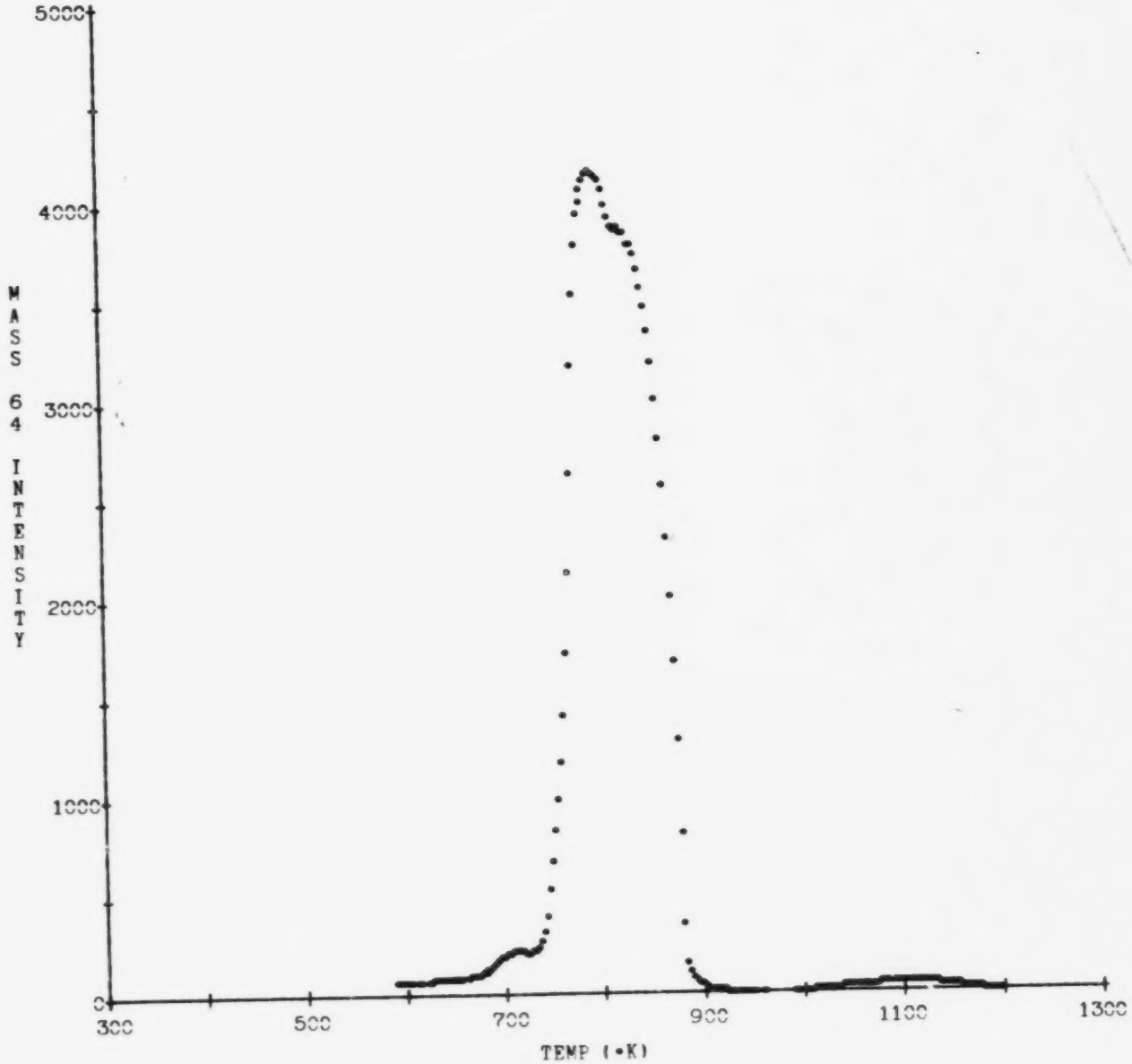

SYMBOL	NO.PTS.	LEGEND
•	191	SO2+ FROM PYRITE -200 MESH 20°/MIN

FIGURE 25. Non-isothermal Run of SO_2 Evolution from Pyrite.

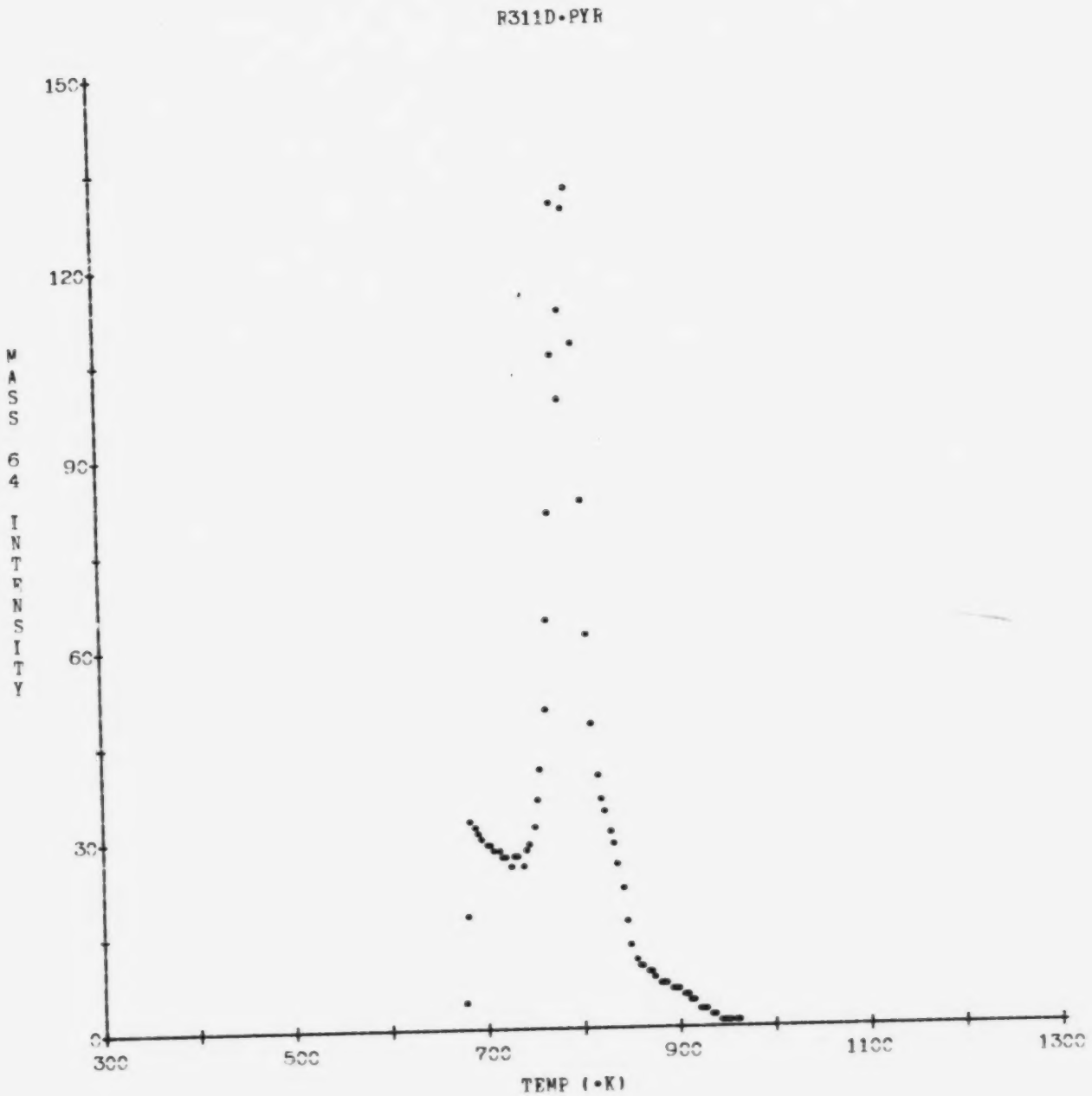

SYMBOL NO.PTS. LEGEND
• 70 SO2+ FROM PYRITE -200 MESH 20°/MIN HE + O2 TO 670°K, HE TO 1260°K

FIGURE 26. Non-isothermal Run of SO_2 Evolution from Pyrite, O_2 feed stopped at 670°K

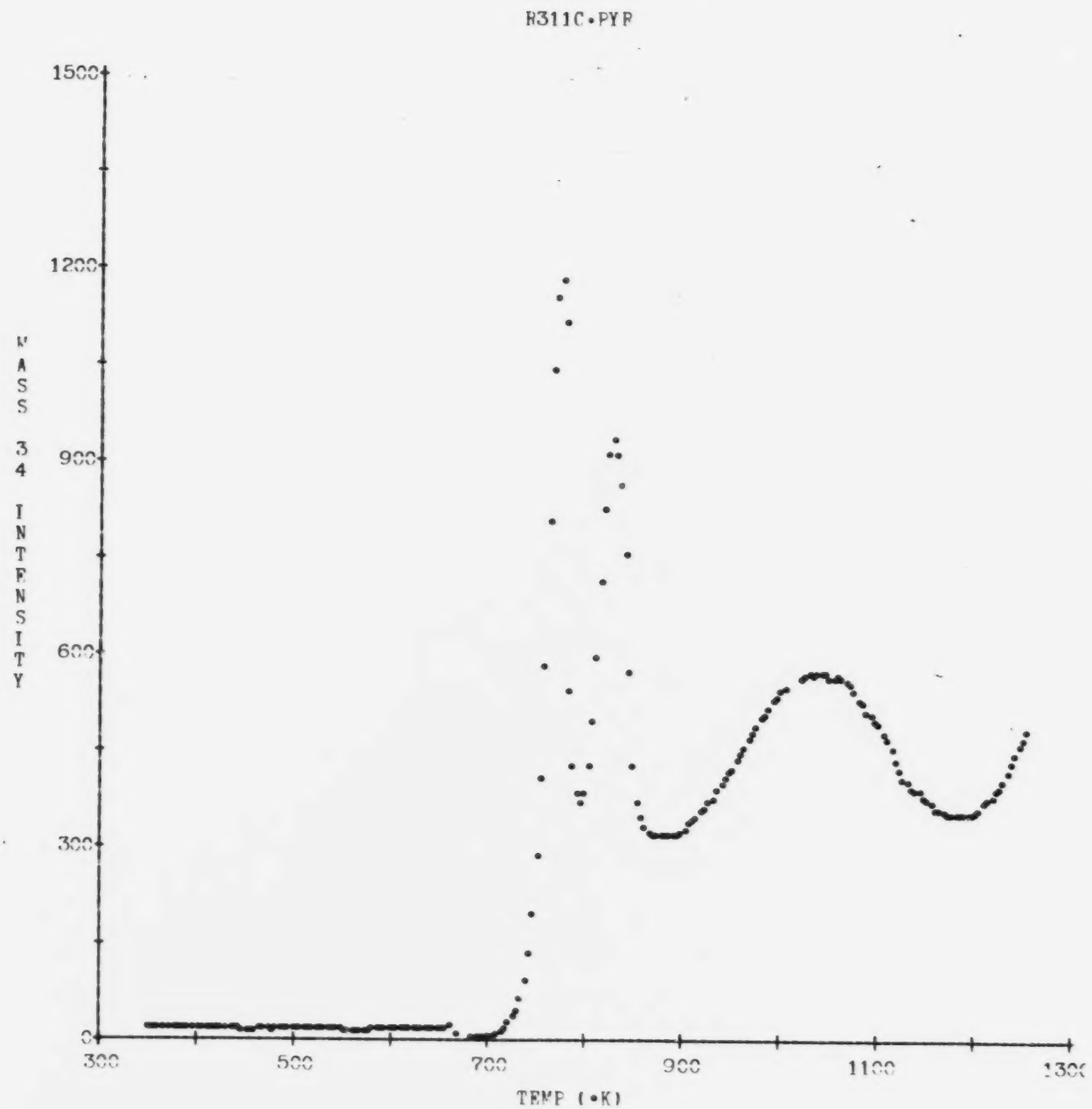

SYMBOL NO.PTS. LEGEND

• 212 H2S+ FROM PYRITE -200 MESH 20•/MIN HE + 02 TO 670•K, HE TO 1260•K

FIGURE 27. Non-isothermal Run of H_2S Evolution from Pyrite

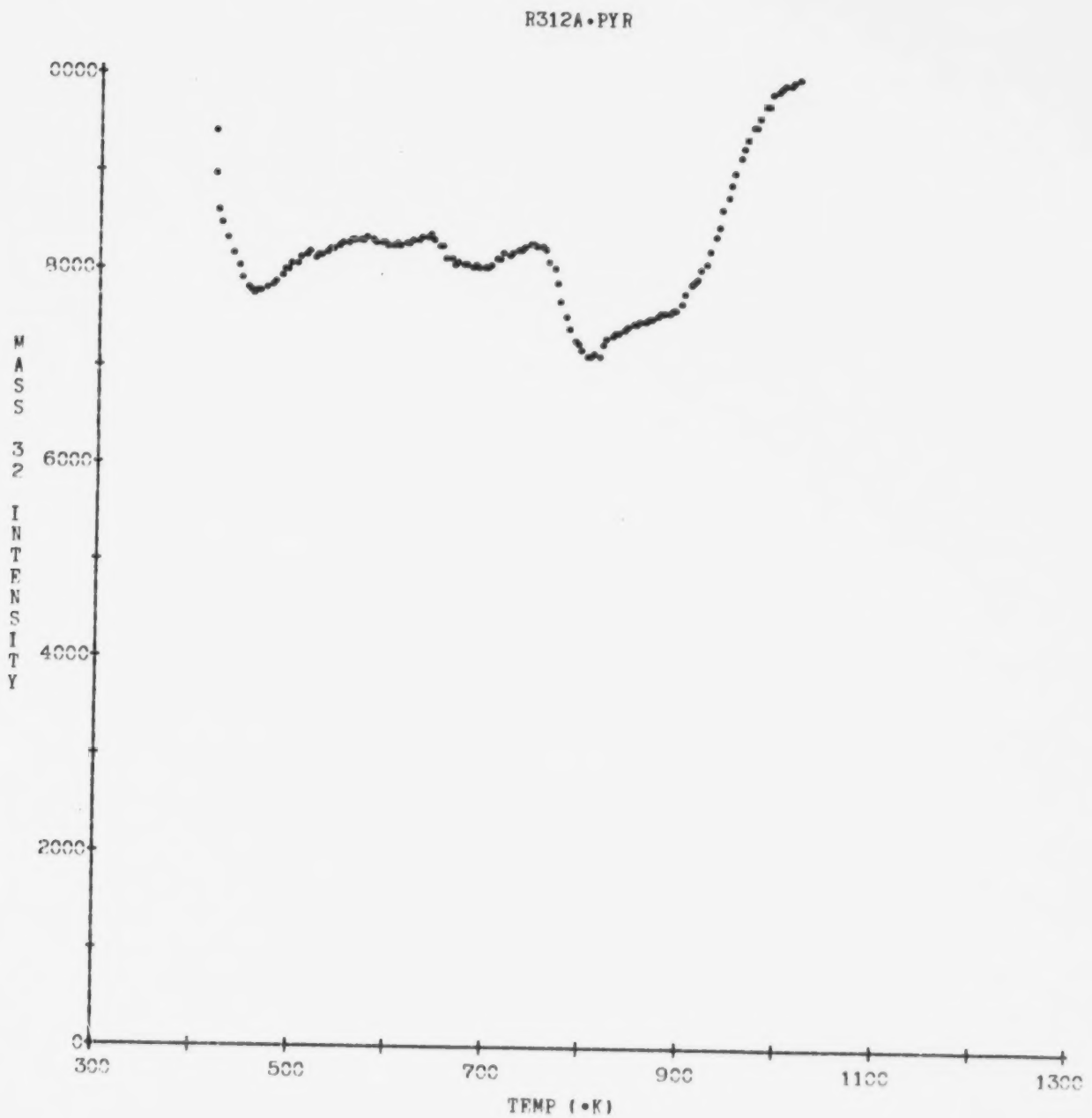

SYMBOL	NO.PTS.	LEGEND
•	142	O2+ FROM PYRITE(R311) 20•/MIN HE + O2 CARRIER GAS

FIGURE 28. Non-isothermal Run of O_2 Adsorption on to Pyrite - Rerun of Pyrite of FIGURE 26.

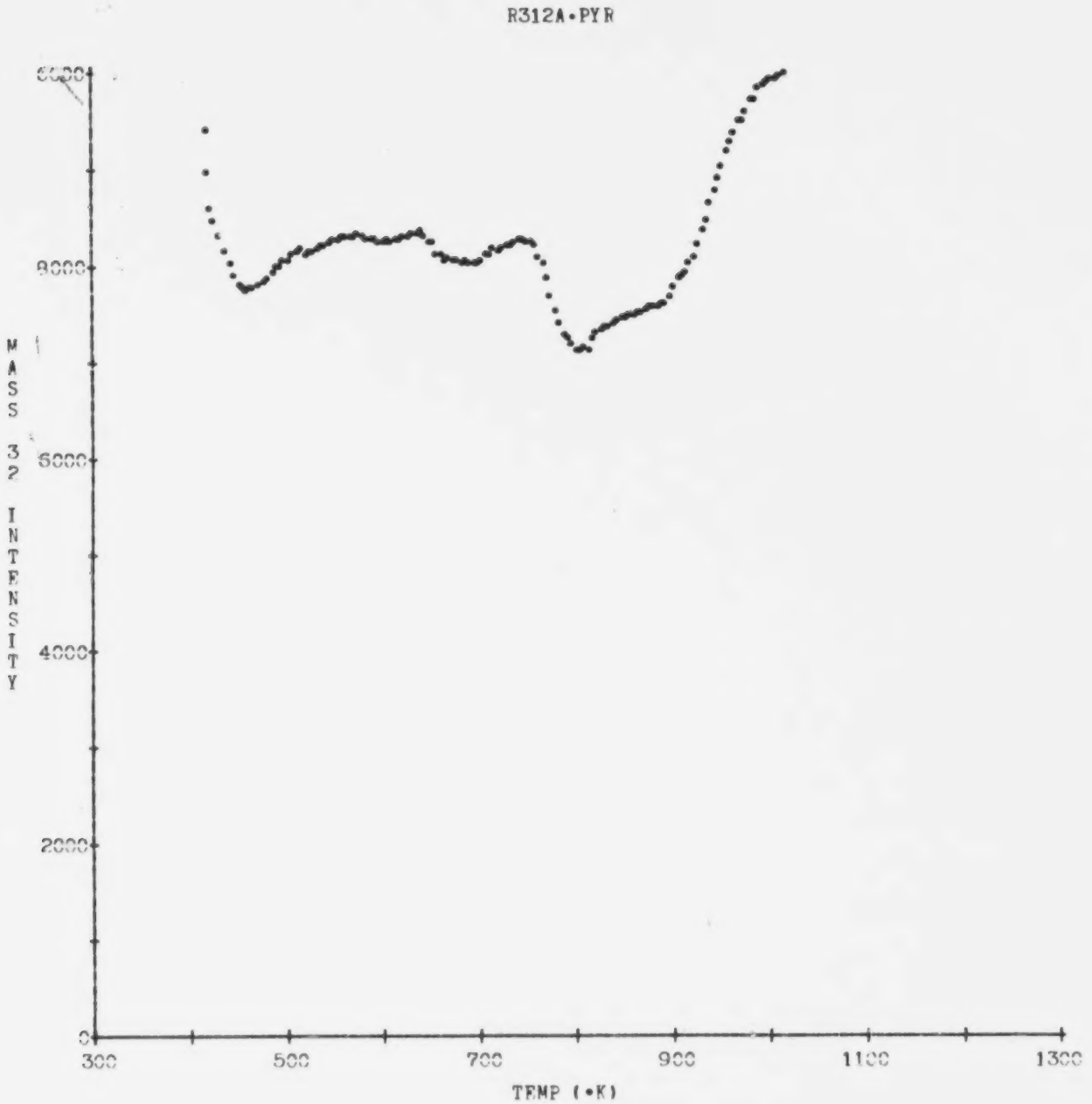

SYMBOL	NO.PTS.	LEGEND
•	142	O2+ FROM PYRITE(R311) 20•/MIN HE + O2 CARRIER GAS

FIGURE 28. Non-isothermal Run of O_2 Adsorption on to Pyrite - Rerun of Pyrite of FIGURE 26.

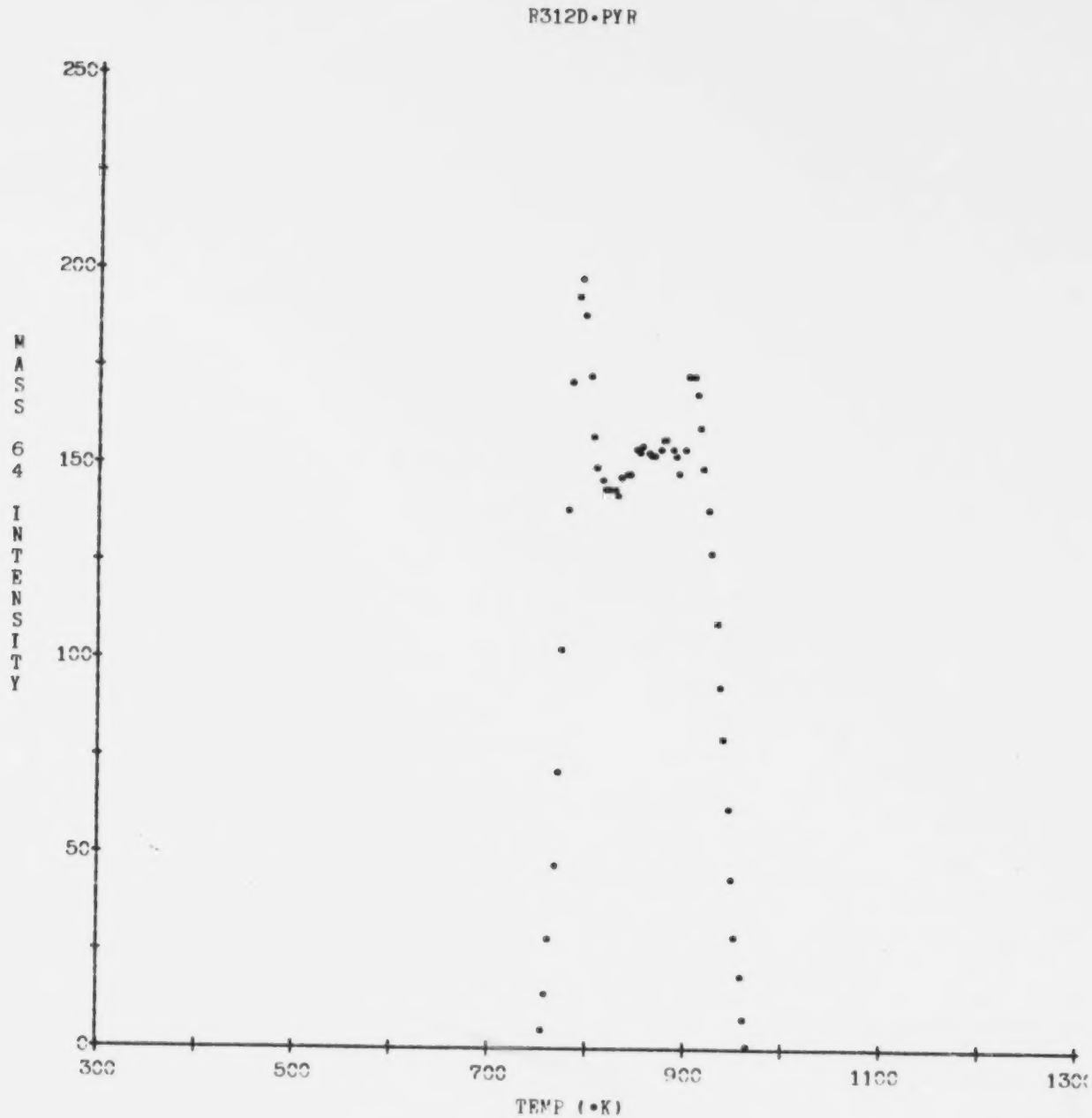

SYMBOL	NO•PTS•	LEGEND
•	51	SO2+ FROM PYRITE (R311) 20•/MIN HE + 02 CARRIER GAS

FIGURE 29. Non-isothermal Run of SO_2 Evolution from Pyrite- rerun of Pyrite of FIGURE 26

Hydrogen sulfide is also evolved in these non-isothermal experiments exhibiting two peaks at temperatures close to those of SO_2. These two peaks of H_2S behave similarly with heating rate to what is observed for SO_2 in these experiments and to what is observed for H_2S in a hydrogen atmosphere, the latter being shown in the preceding section to be due to a reaction of one-half order in pyrite. The source of the hydrogen to produce H_2S in these experiments is not completely clear. Removal of the O_2 supply above 670°K does not remove the second evolution peak of H_2S, as was the case for SO_2 and as may be seen from Figure 27. This suggests that the hydrogen impurity is present in the pyrite. Since examination of the evolution peak of H_2S in Figure 27 shows it to have very different kinetic parameters than the H_2S evolution in hydrogen atmospheres, it may be concluded in addition that the hydrogen impurity is not present as adsorbed hydrogen. Most probably, it is present as chemisorbed water.

As already mentioned, there is a 1:1 correspondence between the O_2 adsorption that occurs with a peak at 580°K and the SO_2 evolution process that exhibits a very narrow peak at about 800°K. Thus, if the O_2 is removed from the helium stream at temperatures above 670°K, thus permitting only the low temperature adsorption to occur, only this first narrow SO_2 evolution peak is observed (cf. Figures 24-26). If now the pyrite sample is cooled to room temperature and then treated with helium and oxygen as it is heated to about 1100°K, the low temperature oxygen adsorption peak is missing, as may be seen by inspection of Figure 28, but the high-temperature adsorption at ~800°K is still observed. In addition, as shown in Figure 29, the SO_2 evolution now exhibits the higher-temperature peak that was missing in the first treatment of this particular sample of pyrite (cf. Figure 26). It is thus concluded that the low-temperature oxygen adsorption and/or the subsequent reaction to yield the low-temperature SO_2 evolution peak saturates and destroys those sites in the solid responsible for the first oxygen adsorption. The

presence of the low-temperature SO_2 evolution peak in Figure 29 is most easily accounted for by assuming not all of the O_2 adsorbed originally (for temperatures up to 670) was reacted in the first run.

The similarity of the first SO_2 and H_2S evolution peaks, in these oxidizing atmosphere experiments, to the first H_2S evolution peak observed when iron pyrite is treated with hydrogen, leads us to the reasonable conclusion that the evolution of SO_2 and H_2S in the oxidizing experiments is also one half order in solid. As shown in the preceding section such a kinetic order is consistent with the following mechanism where $X_2 = H_2$, O_2, or H_2O:

$$FeS_2 \rightleftharpoons Fe + S_2\,(ads) \qquad (22)$$

$$X_2\,(g) \rightarrow X_2\,(ads) \qquad (23)$$

$$X_2\,(ads) + S_2\,(ads) \rightarrow X_2S + S(ads) \qquad (24)$$

$$Fe + S\,(ads) \rightleftharpoons FeS \qquad (25)$$

In this mechanism the rate-determining step of X_2S evolution is reaction (24) which, as shown in the preceding section, leads to one-half order kinetics for the X_2S evolution. Oxygen adsorption peaks correspond to reaction (23) which may or may not be reversible. Assuming that the oxygen adsorption is first-order in solid, treatment of the negative adsorption peaks as described in our previous work[1,2] lead to activation energies of 30 and 35 kcal/mole and frequency factors of 2×10^{11} and 6×10^{8} min^{-1}-$gram^{-1}$, for the low and high-temperature adsorptions, respectively. Assuming that the evolution of H_2S in the oxidizing experiments is due to adsorbed H_2O, treatment of the first evolution peaks of H_2S and SO_2 lead to the kinetic parameters for reaction (24) shown in Table V. Also shown in Table V for comparison are the kinetic parameters of (24) in the case of H_2.

TABLE V. KINETIC PARAMETERS FOR DESULFURIZATION

Reaction	E(kcal/mole)	k_0 (min^{-1}-$gram^{-1}$)
H_2 (ads) + S_2 (ads) $\rightarrow H_2S$ + S(ads)	42.1	1.3×10^{11}
O_2(ads) + S_2(ads) $\rightarrow SO_2$ + S(ads)	69	10^{18}
H_2O(ads) + S_2(ads) $\rightarrow H_2S$ + SO(ads)	85	10^{23}

In summary, we may say that specific oxygen adsorption processes that occur in coal samples as a result of the presence of pyrites may be recognized by the appearance of negative peaks of O_2 concentration in the neighborhood of 580°K and 830°K. In addition, SO_2 evolution peaks at ~800°K and 830°K may with some confidence be attributed to the iron pyrite present.

Bituminous Coal SRI Nos. 1-5

Adsorption of Oxygen: A typical non-isothermal oxygen consumption curve is shown in Figure 30 for the specific case of SRI-No. 3 coal. The behavior shown is, in general, reproduced for all five bituminous coals. As seen in Figure 30, the consumption of oxygen as a function of temperature consists of a number of specific narrow adsorption peaks superimposed on a continuous adsorption curve (which may be viewed as a very broad negative peak whose width extends over the entire temperature range.) The adsorption at 570°K is clearly due to the iron pyrite constituent of the coal, although the second adsorption found in pyrite at about 830°K is not observed because of the broad underlying continuous oxygen depletion. Note that the continuous oxygen adsorption curve is not observed when the solid reactant is iron pyrite (cf. Figures 24 and 28).

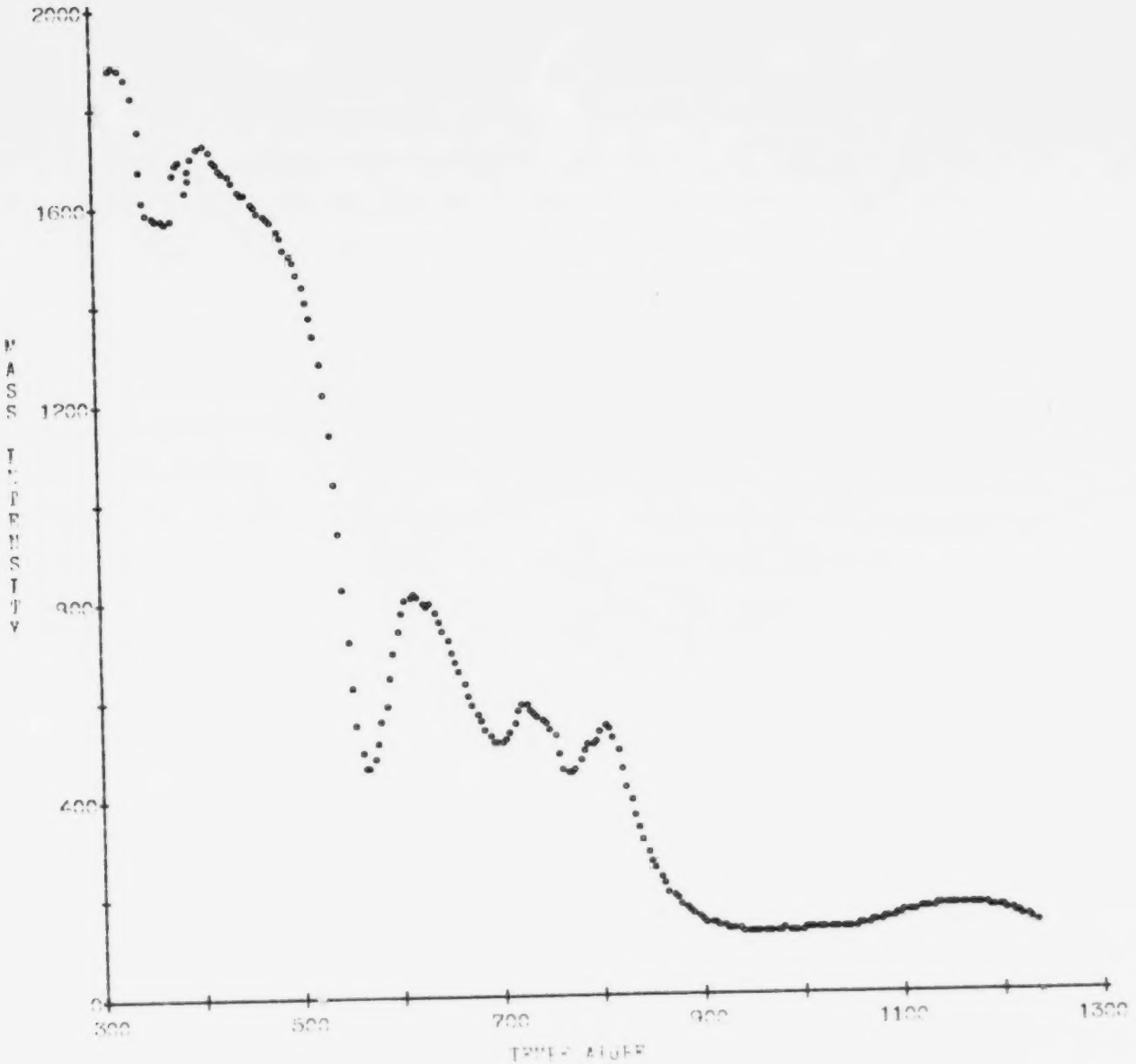

SYMBOL NO.-TS. [illegible]
• 222 [illegible]

Reproduced from best available copy.

FIGURE 30. Non-isothermal Run of Illinois 2.5% Coal.

In addition, to the pyrite adsorption, specific adsorption peaks of O_2 are observed at 370°, 700°, and 770°K. Similar specific adsorptions were found for all five coal samples. Assuming the adsorption process to be first-order in solid, the kinetic parameters derived from the peak locations and widths were estimated by methods described previously[1,2] and are shown in Table VI.

TABLE VI. SPECIFIC ACTIVATED ADSORPTION PROCESSES IN SRI NO. 3 COAL

Peak location (°K)	E(kcal/mole)	$k_0(min^{-1}gram^{-1})$
370	13	3×10^7
700	45	1×10^{14}
770	68	2×10^{19}

Previous workers[4] have accepted the view that chemisorption of oxygen is the first step in the oxidation of coal and that, moreover, this chemisorption process is continuous throughout the temperature range of 273-623°K with an activation energy of 3-4 kcal/mole. The overall activation energy for chemisorption of oxygen on coal is undoubtedly a suitably-weighted average of all actual processes involved, and is undoubtedly influenced overwhelmingly by the chemisorption one would observe on a fresh clean carbon surface. The methods employed to arrive at the low overall value of 3-4 kcal /mole[4] would not detect specific activation adsorption processes superimposed on this broad, continuous and low-activation energy process as are obvious in Figure 30, when the present technique is employed. Thus we attribute the broad underlying process in Figure 30 with an apparent minimum at around 900°K to the the low-energy (3-4 kcal) chemisorption of oxygen on carbon and we suggest that this predominant process weighs so heavily with respect to overall oxygen consumption that the methods used by previous workers[4] will reflect only this process.

However, our data show quite clearly as least four more specific activated chemisorption processes of considerably higher activation energies. We recognize one as being due to the pyrite component of coal and the other three must similarly represent chemisorption on surface sites containing specific coal constituents other than pure carbon. Further experimental work is necessary to attempt further identification of the nature of these sites, and this work is in progress. To our knowledge the data shown in Figure 30 is the first experimental demonstration of oxygen chemisorption processes on coal other than the low activation adsorption expected for pure carbon.

Evolution of SO_2: A typical curve obtained for the evolution of SO_2 from coal in an oxidizing atmosphere is shown in Figure 31 for the particular case of SRI Coal No. 2. The general features of these curves are similar to those obtained for H_2S evolution from coals in a reducing atmosphere[2] with the exception that there is a peak common to all of SO_2 curves at about 540°K for which there has been no corresponding evolution of H_2S observed. Earlier data obtained on coal reactions in a hydrogen stream[1] show the evolution of small amounts of SO_2 at 540°K, and studies of sulfate decompositions[2] show a similar peak from the pyrolysis of $FeSO_4$ in a reducing atmosphere. These data all seem to indicate that the coal sulfur which is in the form of sulfates is liberated as SO_2 at temperatures of about 540°K.

The five remaining peaks in Figure 31, including the shoulder at 750°K, appear to correspond to reactions of Organic I, Organic II Pyrite, Sulfide and Organic III having T_m values of 620, 750, 800, 920, and 1050°K respectively. The production of SO_2 from the reaction

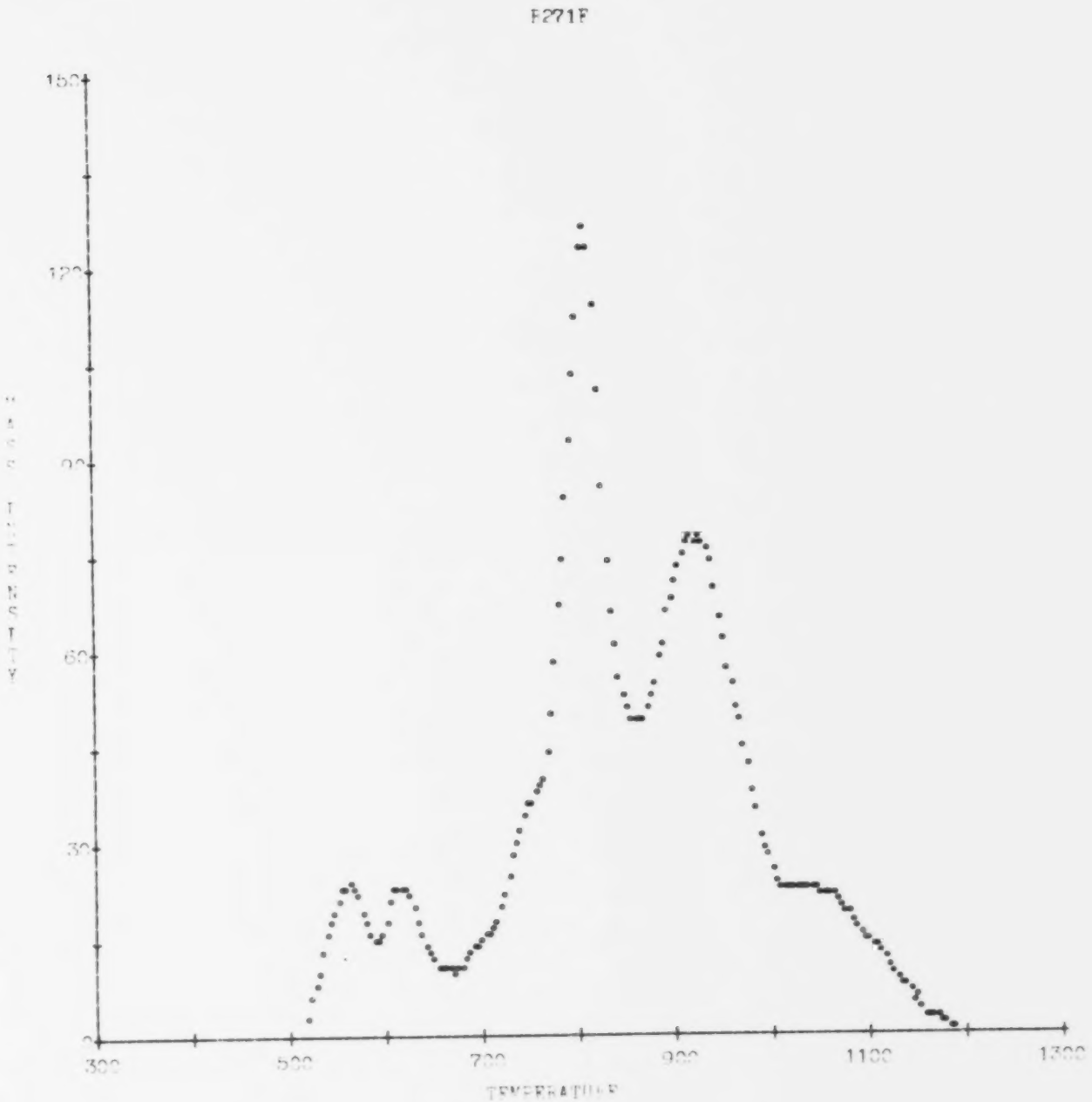

Reproduced from best available copy.

FIGURE 31. Non-isothermal Run of Illinois 1% Coal - SO_2 Evolution.

of Organic III sulfur results in small evolutions possibly because of competition with carbon combustion to produce CO_2. Kinetic parameters can be estimated for all of the reactions seen in Figure 31, except for the combustion of Organic III, using a previously discussed procedure[2]. First order kinetics for sulfur containing species are taken for Organic I, Organic II, and Sulfide[2], half - order kinetics have been demonstrated for the Pyrite sulfur reaction, and a first order decomposition of sulfates will be assumed. The estimates are shown in Table VI. Kinetic parameters for the Organic III reaction are not estimated here because of the difficulty in resolving this process from the pyrite and sulfide reactions.

TABLE VII. ESTIMATED KINETIC PARAMETERS FOR SO_2 EVOLUTION FROM COALS IN AN OXIDIZING ATMOSPHERE

Sulfur Species	E(kcal/mole)	log k_0
Sulfate	25	12.9
Organic I	34	11.4
Organic II	40	12.0
Pyrite	40	10.0
Sulfide	40	9.0

Comparison of the data in Table VII with those in Table III shows very good agreement between activation energies and frequency factors for the reactions of Organic I, Organic II, and Pyrite, and poor agreement for the reaction of Sulfide. The reason for the differences in the sulfide reaction parameters is not known at this time. On the other hand, the agreement in the values for kinetic parameters for Organic I and Organic II reactions in both oxidizing and reducing atmospheres

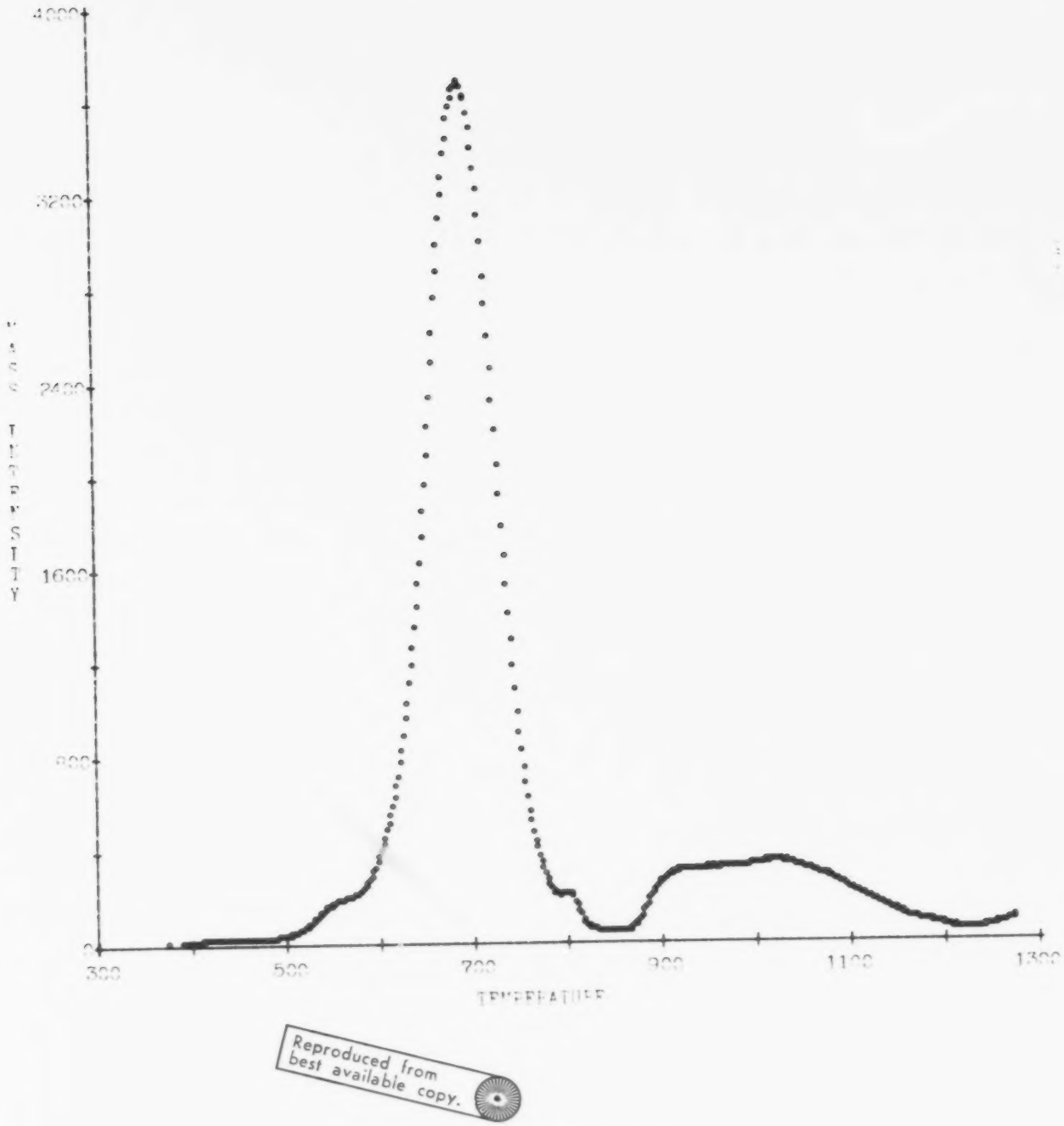

Reproduced from best available copy.

FIGURE 32. Non-isothermal Run of Illinois 4.5% Coal - H_2S Evolution.

appears to indicate that these reactions are independent of the adsorbed gas and that the kinetics are limited by the rupturing of the carbon-sulfur bonds in the coal. The difference between the values for the pyrite reaction reported in Tables III and VII are, however, not resolved at this time.

Evolution of H_2S: A curve typical of the evolution of H_2S from coal in an oxidizing atmosphere is shown in Figure 32 for the specific case of SRI Coal No. 5. The prominent feature of this curve, common to all H_2S evolutions in this series of experiments, is a peak with a T_m corresponding to the reaction of Organic II in a reducing atmosphere. The other peak that is present appears to correspond to a reaction of the Organic III sulfur compounds. Absence of peaks for the reactions of Pyrite, Sulfide and Organic I, compared to the presence of these peaks in the SO_2 evolution curve of Figure 32 seems to indicate that oxygen competes more effectively for the adsorption sites of these sulfur species that does the internal hydrogen source. A further comparison of Figures 31 and 32 indicates, however, that the source of Organic II sulfur may be rich in internal hydrogen since the reaction of this sulfur species in an oxidizing atmosphere favors the production of H_2S over the production of SO_2.

Evolution of CO and CO_2: Examples of curves obtained for the evolution of CO and CO_2 from coals in an oxidizing atmosphere are presented in Figures 33 and 34. The general features seen in both of these and in the other curves for CO and CO_2 evolution are the low level processes for gas production in the region of 600-700°K, the increase of intensity above 800°K and reaching a maximum between 1100 and 1200°K. All of the CO_2 evolution curves have a plateau in the general upward trend occurring between 950 and 1050°K. In addition to showing the anticipated

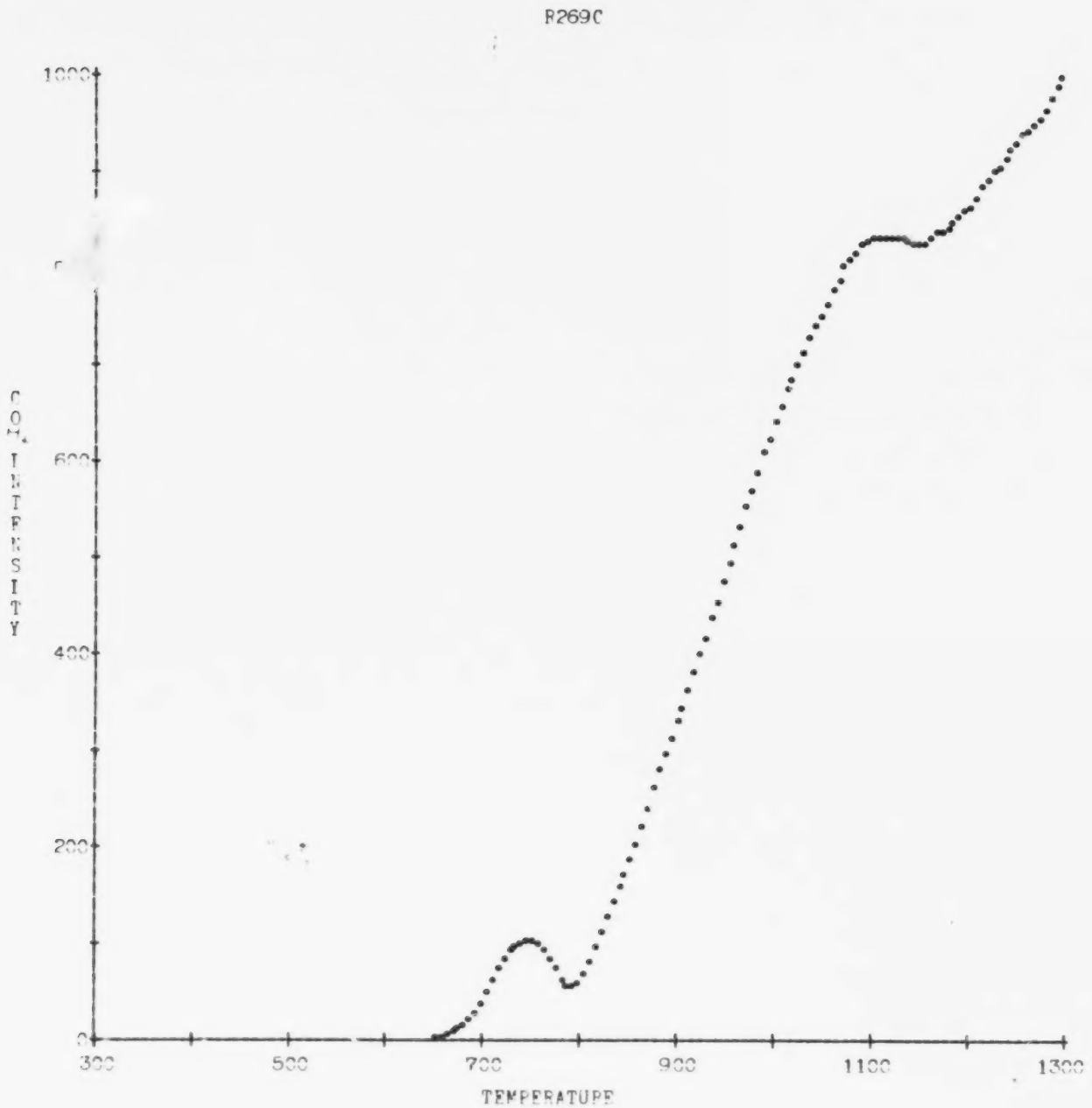

Reproduced from best available copy.

FIGURE 33. Non-isothermal Run of Illinois 4.5% Coal - CO Evolution.

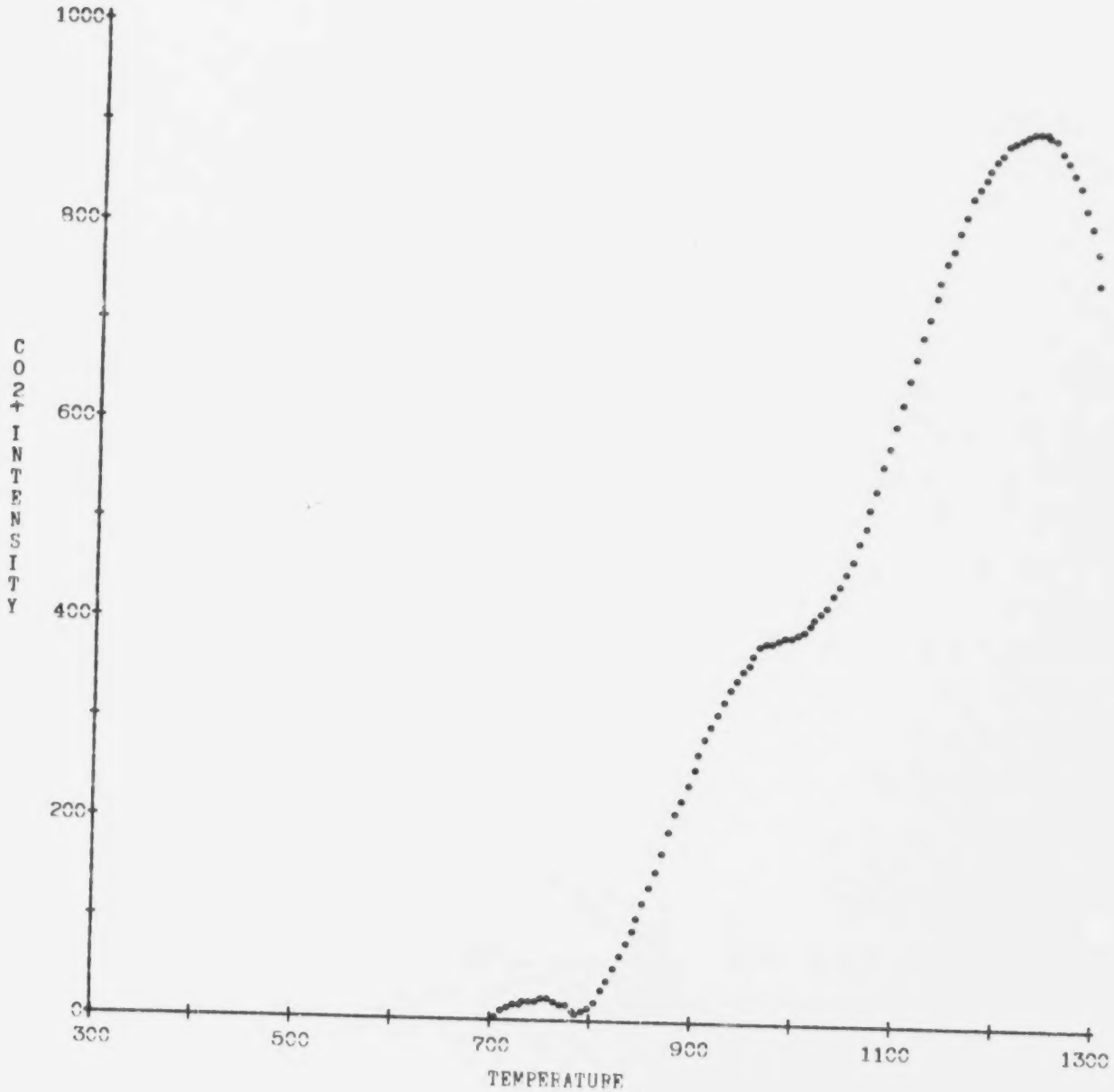

FIGURE 34. Non-isothermal Run of Illinois 4.5% Coal - CO_2 Evolution.

combustion process for carbon in oxygen, these curves illustrate the reason for the lowered intensity of SO_2 in the reaction of Organic III. A comparison of Figures 31 and 34 in the region of 900 to 1000°K shows that the low SO_2 evolution is accounted for by an increasingly large production of CO_2.

Anthracite and Lignite

Adsorption of oxygen and evolution of SO_2 are shown in the curves of Figures 35 and 36 for the reaction of anthracite. The maxima of the SO_2 evolutions in Figure 35 occur at temperatures corresponding to the reactions of Organic II, Pyrite and Sulfide, the latter two peaks being poorly resolved. The oxygen adsorption of Figure 36 shows the characteristic minimum at 560°K corresponding to adsorption on to a pyritic sulfur site. The H_2S evolution from anthracite, is of very low intensity indicating that, in this low sulfur material, the oxygen reactions with sulfur almost exclude the production of H_2S. Carbon dioxide evolves in a fashion quite like those processes yielding CO_2 from the bituminous coals.

The curves for SO_2 and O_2 for the reaction of lignite are shown in Figures 37 and 38 respectively. Notably absent from the SO_2 curve is any peak corresponding to the reaction of pyritic sulfur. The peak at about 750°K probably corresponds to the reaction of Organic II while the one at 920°K must result from a form of sulfur which is present only in lignite, since it has no precedent in our studies. The oxygen adsorption curve of Figure 38 shows three adsorptions, the ones at 390 and 720°K having been observed for bituminous coals and reported in Table V. The adsorption at 540°K is in the region where the adsorptions for pyritic sulfur are found, but the lack of any SO_2 from pyrites seems to indicate that this large specific

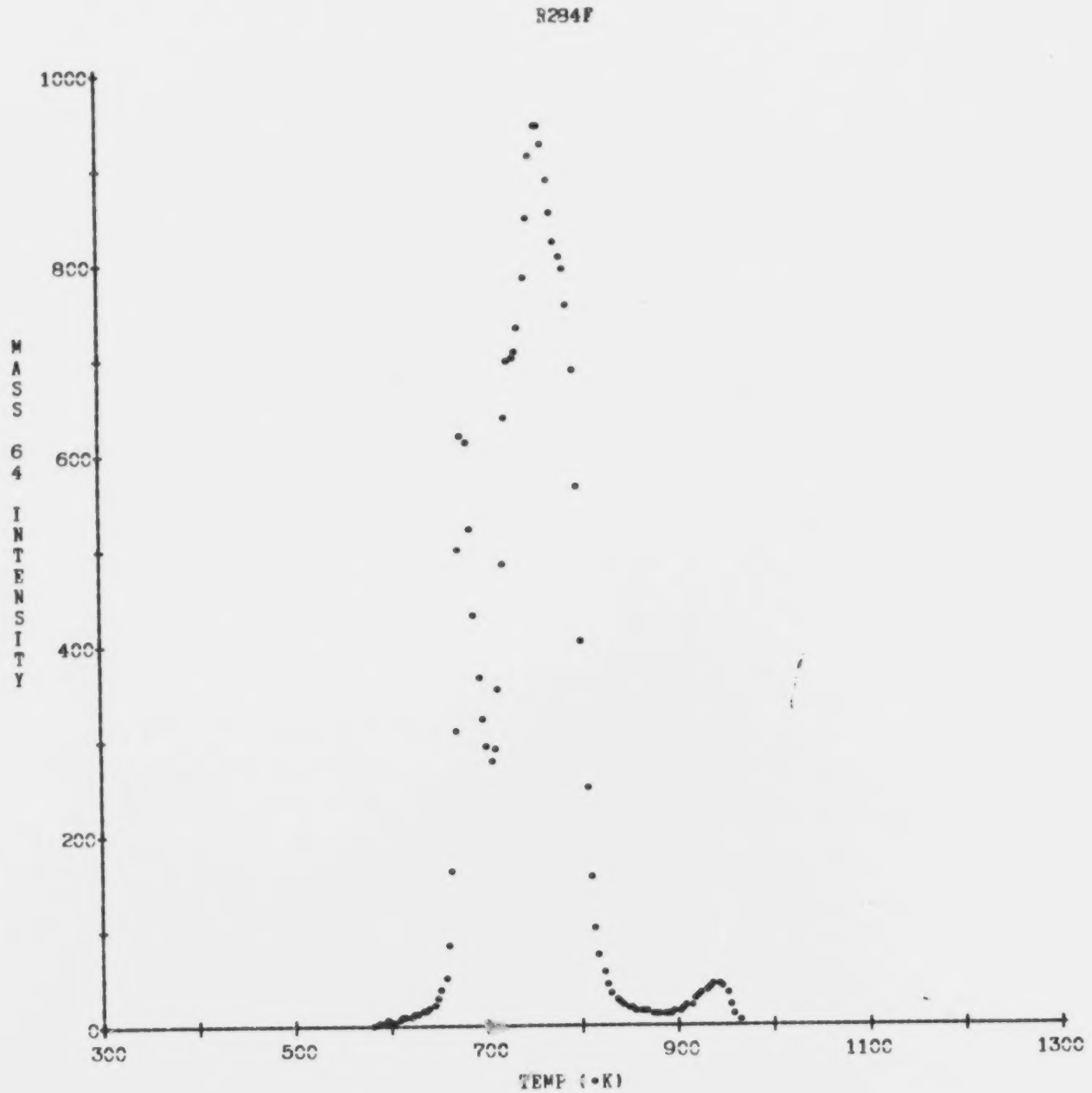

SYMBOL NO.PTS. LEGEND
• 93 SO2+ FROM ANTHRACITE 100-200 MESH 20°/MIN

FIGURE 35. Non-isothermal Run of Anthracite - SO_2 Evolution.

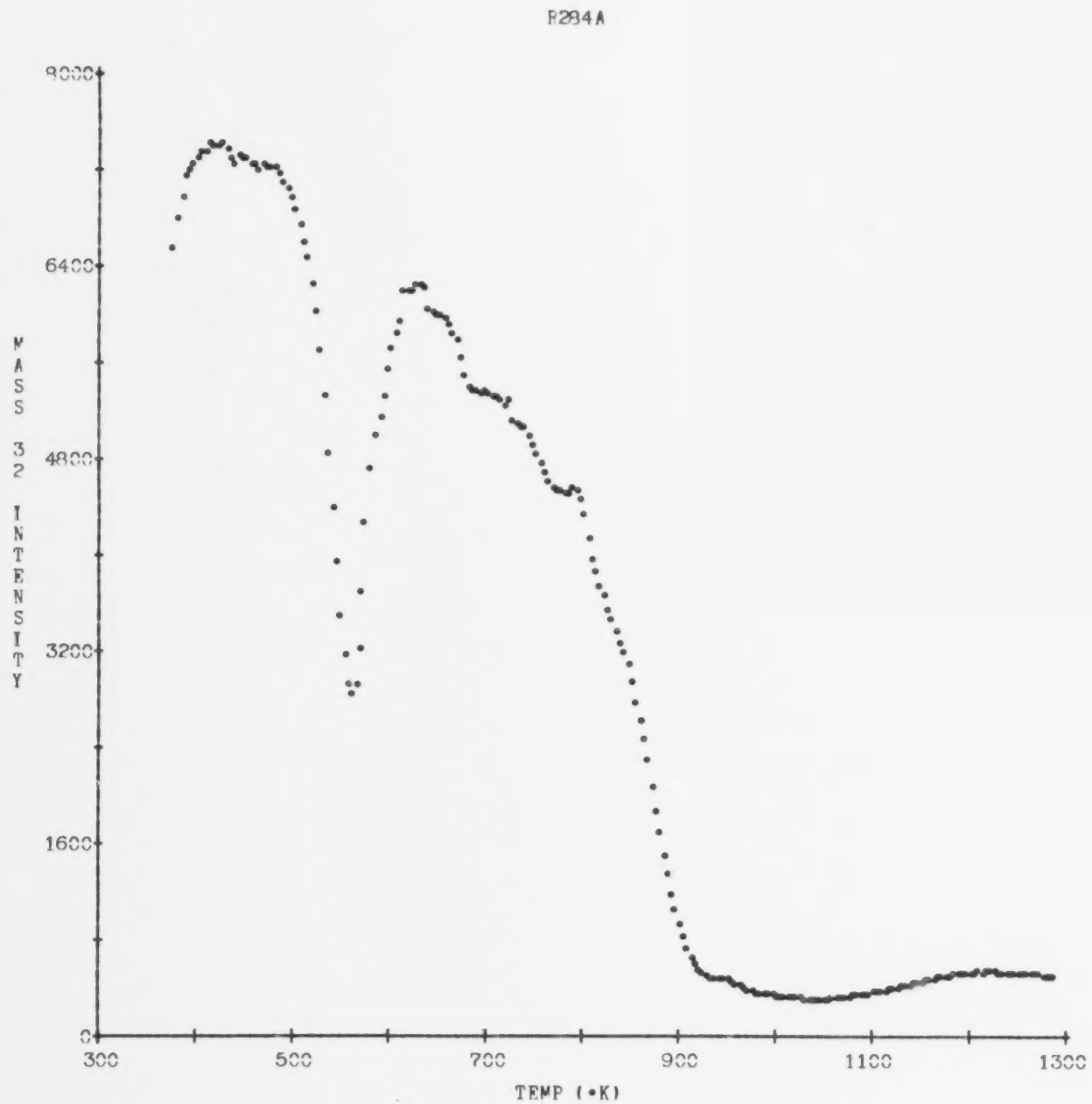

FIGURE 36. Non-isothermal Run of Anthracite - O_2 Adsorption

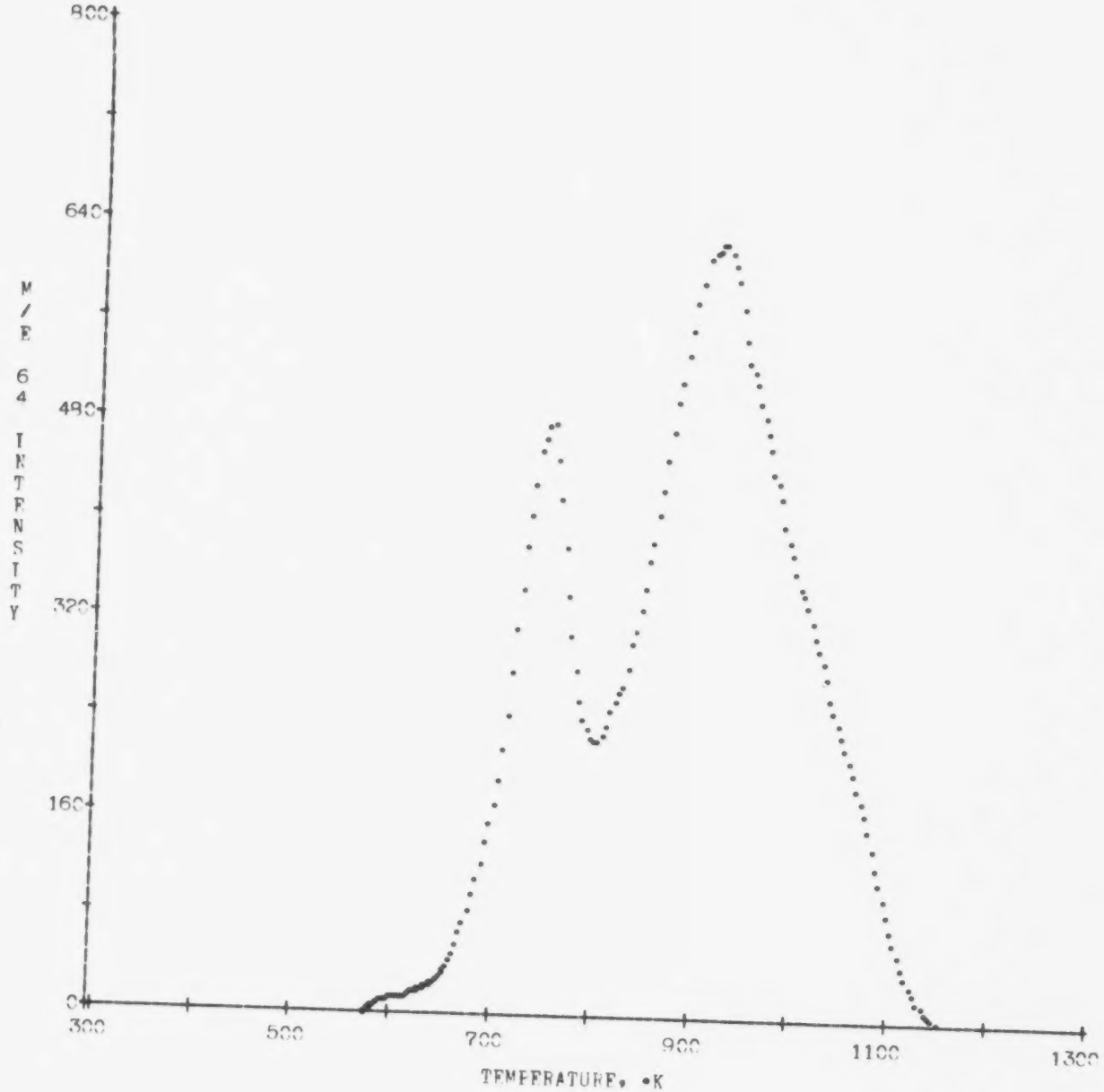

SYMBOL NO.PTS. LEGEND

• 163 SO2+ FROM LIGNITE 100-200 MESH 20°/MIN

Figure 37. Non-isothermal Run of Lignite - SO_2 Evolution

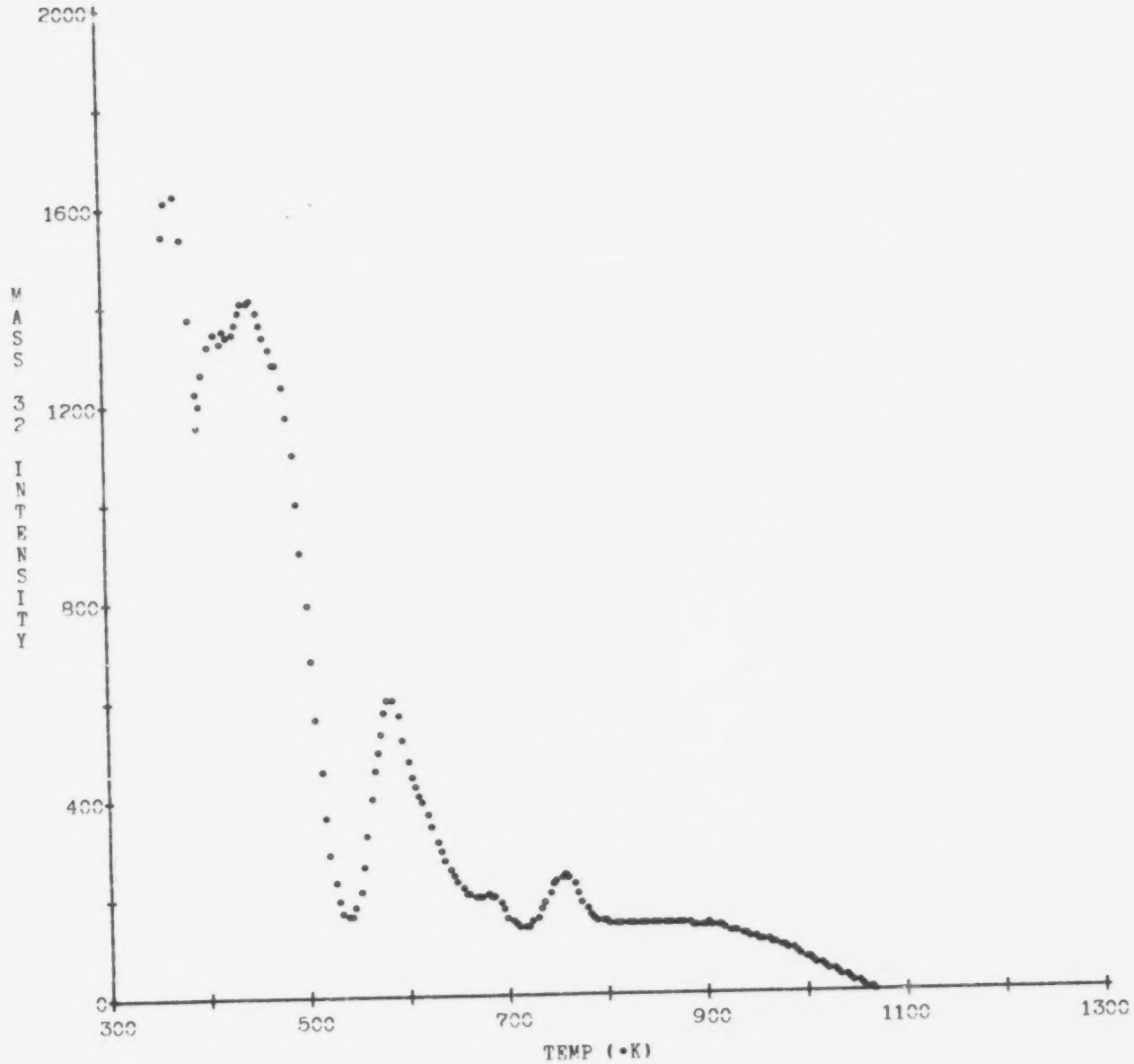

SYMBOL	NO.PTS.	LEGEND
•	169	02+ FROM LIGNITE 100-200 MESH 20°/MIN

FIGURE 38. Non-isothermal Run of Lignite - O_2 Adsorption

oxygen adsorption may be connected to the SO_2 evolution at 920°K. H_2S production is a low intensity process as in the case of anthracite, while the evolution of carbon dioxide is similar to the behavior observed for other coals.

Table VIII presents results of ASTM sulfur analysis on both the anthracite and lignite used in these experiments. The data in the table are presented as the forms of sulfur as percent of dried coal, mineral analysis as percent of ashed coal, and percent sulfur in fixed carbon.

TABLE VIII. SULFUR ANALYSIS OF ANTHRACITE AND LIGNITE

Forms of Sulfur (Dry Basis)

	Anthracite	Lignite
Sulfate Sulfur, as S	0.03	0.07
Pyrite, as S	0.14	0.06
Organic Sulfur (by diff.), as S	0.51	0.65
Total Sulfur, as S	0.68	0.78

Mineral Analysis (% of Ash)

Total Iron, as Fe	3.77	7.82
Pyritic Iron, as Fe	0.91	0.43
Calcium, as Ca	1.35	17.17
Magnesium, as Mg	0.38	4.62
Sulfur, as S	0.56	3.87
Sulfur, as S, in Fixed Carbon	0.80%	1.08%

MODEL COMPOUNDS

A series of experiments designed to determine specifically the kinds of carbon-bound sulfur present in coal as Organic I, II, III were performed by using several different simple organic sulfur compounds as models.

In each of the experiments a compound was adsorbed on to activated carbon, swept with either helium or hydrogen and heated as in the normal non-isothermal kinetic study. Thianthrene was the adsorbate in five experiments (R-288-292), dibenzothiophene in two (R-293 and 294) and methylmercaptan in two (R-295 and 296).

Sweeping the adsorbates with helium yielded H_2S^+ peaks that did not correspond to any evolutions observed from similar experiments with coal. The results of sweeping with hydrogen show one H_2S^+ peak in every compound having a T_m at 1040°K. This temperature corresponds to the peak observed for the Organic III from bituminous coal in a reducing atmosphere. A possible second correlation between the model compounds swept with hydrogen and the coals in a reducing atmosphere is the peak in the model compounds having a T_m between 810° and 860°K. This may correspond to the peak observed for sulfides in coal at 870°K. If during the pyrite reduction, the unreacted sulfur atom is transferred from the iron atom to elsewhere in the coal matrix, the peak from the model and sulfide could possibly have the same origin. There are no low temperature H_2S^+ peaks observed from the model compound studies which correspond to the T_m of either the Organic I or II reactions observed in the coals.

The three compounds chosen as models appear to be adequate for only one, perhaps two, of the forms of sulfur present in coal. It appears that small molecules adsorbed on to carbon, even when these molecules are

heterocyclic aromatic ring compounds, cannot represent Organic I and Organic II. Furture experiments directed toward obtaining an adequate representation of Organic I and II will include the use of sulfur cross-linked rubbers as model compounds.

REMOVAL OF H_2S FROM PRODUCT GASES

Calcination of Dolomite

Kinetic experiments have been conducted on the calcination of dolomite, $CaMg(CO_3)_2$. Three samples (R-265, 266, 267) of 200 mesh dolomite No 1930 were heated at 20°/min. in helium flowing at 50 cc/min. CO_2 was the species monitored in all of these experiments[2].

A typical CO_2 evolution curve is shown in Figure 39. In addition to the small low temperature peak at a T_m of 580°K, a large evolution composed of two incompletely resolved peaks is centered at about 860°K. In earlier studies of dolomite calcination performed at a heating rate of 4°/min.[2] only one large broad peak having a T_m of about 950°K was observed. Because of the large difference in T_m between the present and past experiments as well as the insufficient resolution of the high temperature peaks and the intensity of the low temperature peak, kinetic data for dolomite calcination cannot be presented at this time. Future experiments will be directed toward obtaining these data.

Other studies of calcination have concentrated on single carbonates. Juntgen observed two processes for CO_2 production in $MgCO_3$[5] while our earlier work on precipitated $CaCO_3$[2] revealed one process producing CO_2. The T_m values of the present experiments on dolomites differ from the temperature maxima of both Jungten's $MgCO_3$ and our $CaCO_3$. Comparison of the present studies with the work on $MgCO_3$ and $CaCO_3$ indicates that the multiple processes producing CO_2 from dolomite probably are different than the processes which yield CO_2 in the heating of the simple carbonates.

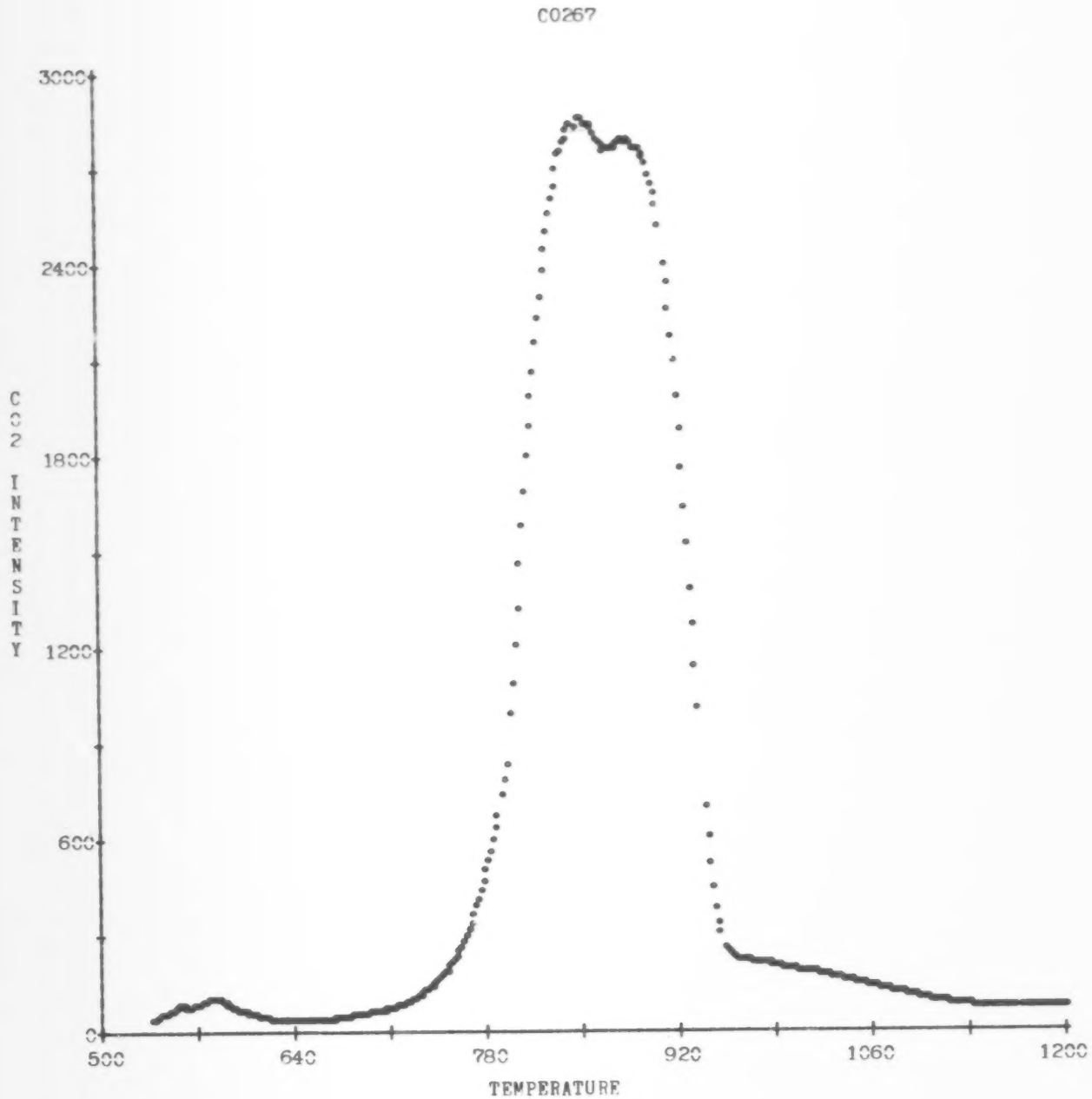

FIGURE 39. Non-isothermal Run of CO_2 Evolution from Dolomite.

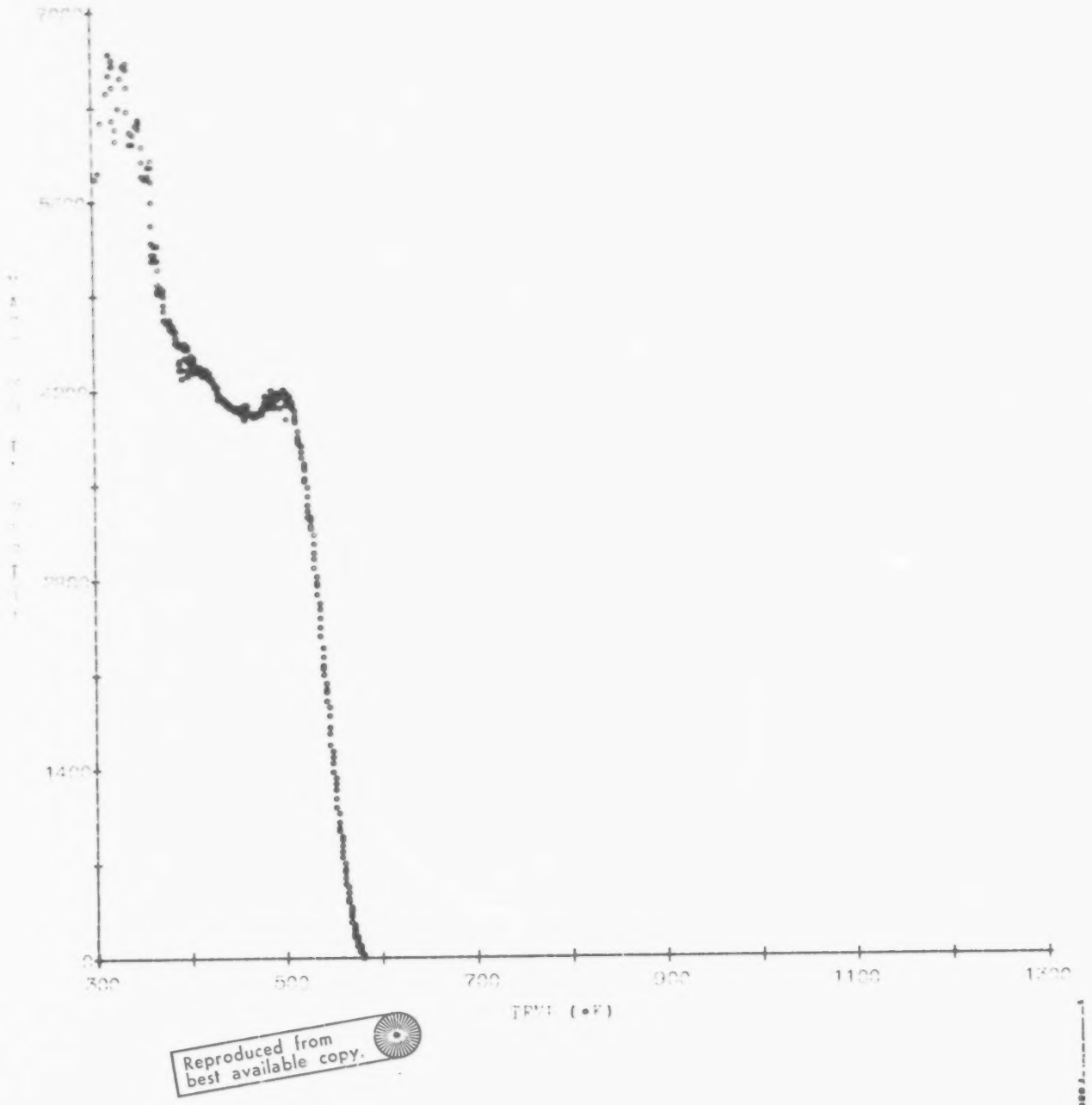

FIGURE 40. Non-isothermal Run of H_2O Evolution from Calcined Dolomite

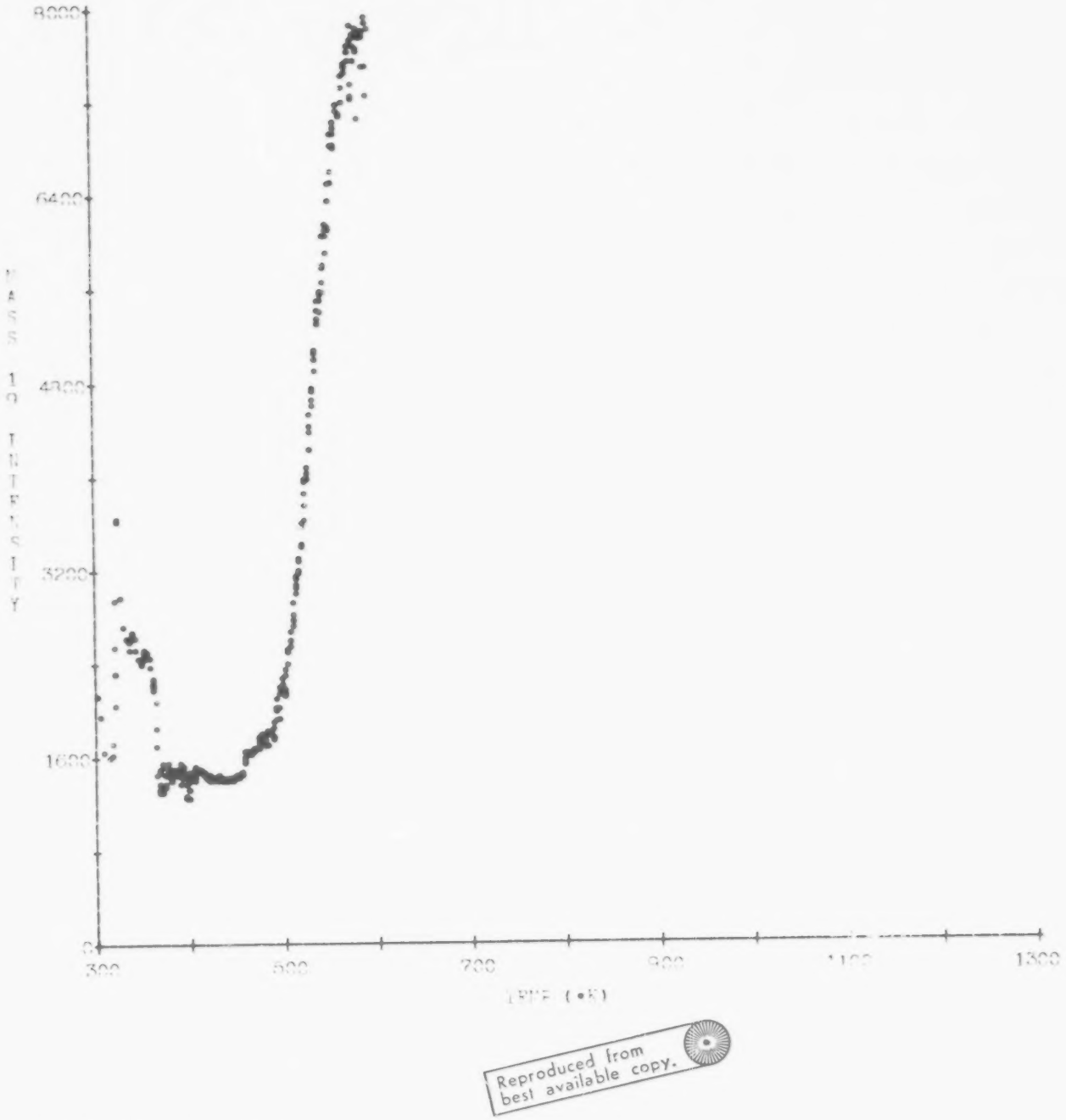

Reproduced from best available copy.

SYMBOL POINTS. LEGEND

° 373 H2O+ FROM CALCINED CAO(1930 DOLOMITE) 5°/MIN N2 + H2S CARRIER GAS

FIGURE 41. Non-isothermal Run of H_2S Adsorption on to Calcined Dolomite

Adsorption of H_2S

Three experiments were conducted on the adsorption of H_2S by calcined specimens of dolomite No. 1930. In each experiment 200 mesh calcined dolomite was treated by blowing 50 cc/min N_2 containing 1000 ppm H_2S over it. H_3S^+ and H_3O^+ ions were monitored at heating rates of 5°/min and 20°/min, and in addition, at 10°/min the ions H_2S^+ and H_2O^+ were monitored. Although, in general only the unprotonated species are seen in nitrogen chemical ionization, in this experiment some of the protonated species were observed.

The H_3S^+ curve from the experiment at 5°/min is shown in Figure 40. The intensity is seen to diminish from its initial high value to a small minimum at 475°K, and then, above 525°K, to fall precipitously reaching zero intensity at 575°K. Figure 41 shows the water levels off by 475°K, and then above 500°K the loss increases very rapidly reaching a maximum at 575°K. Behavior similar to that seen for H_2S adsorption and H_2O evolution at 5°/min is seen in the experiments conducted at higher heating rates. There is good agreement between the temperatures obtained for the first minimum in the H_2S adsorption, the complete adsorption of H_2S, and the maximum evolution of H_2O in the experiments performed at 5°/min and 20°/min. Higher temperatures for the two adsorptions of H_2S and the evolution of H_2O result from the experiment conducted at 10°/min. The small H_2O minimum occurs at 525°K and the H_2S intensity reaches zero at 725°K. The H_2O maximum is seen at 725°K, but there is an additional peak in the water curve at 575°K.

It appears to be clear from these experiments that we have observed the adsorption of H_2S by CaO according to the reaction:

$$CaO + H_2S \rightarrow CaS + H_2O$$

The temperature at which the adsorption reaches a maximum has not yet been well defined, but on the basis of these experiments, it is between 575° and 725°K. The processes occurring during adsorption appear to be an initial take up of H_2S^+ curves. Figure 41 shows that the initial adsorption of H_2S may possibly be accompanied by a corresponding evolution of water. At higher temperatures, water begins to evolve vigorously, and simultaneously H_2S is rapidly adsorbed.

The principal experiments to be performed in the future on this system will be directed towards obtaining a well defined temperature for the adsorption maximum of H_2S.

EXPERIMENTAL DESULFURIZATION REACTORS

CONFORMANCE STUDIES ON EXPERIMENTAL REACTORS

The kinetic parameters obtained from experiments with the computerized non-isothermal kinetic laboratory are used for the derivation of generalized equations for predicting the sulfur which remains in a char after processing. This experiment is intended to demonstrate that there may exist an upper limit to the amount of sulfur which can be removed from a given coal because of the mineral content of that coal. The equations derived for this experiment have been tested experimentally.

Consider the experiment shown in Figure 42. The tube containing alternate layers of coal and CaO, Figure 42a, is heated at some heating rate, m, to a final temperature, T, and then held at this final temperature for a time, t. The temperature history of the experiment is shown in Figure 42b. After the experiment the coal (coke) is analyzed for sulfur containment. During passage through the coal, the various hydrodesulfurization reactions occur to produce H_2S which is then removed from the gas by reaction with CaO. This CaO is shown in Figure 42a as separate layers, but additionally, the calcium content of coals is taken to be in the form of CaO.

As a first approximation we shall assume that we have a sufficiently large number of sufficiently thin layers of coal such that immediate take-up of H_2S by CaO in layers prevents any reverse reactions such as Organic III formation, from occurring. Under these conditions, we may write for the hydrodesulfurization reactions

$$V_j\text{-}S + H_2 \rightarrow H_2S + N_j \qquad (26)$$

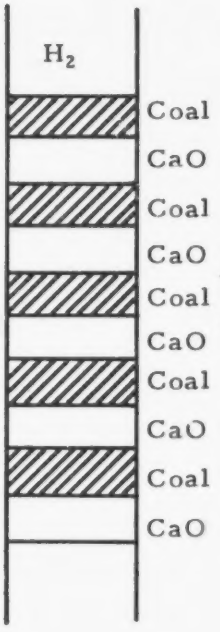

FIGURE 42a. Schematic of the reactor used in equation derivation and experimental measurement

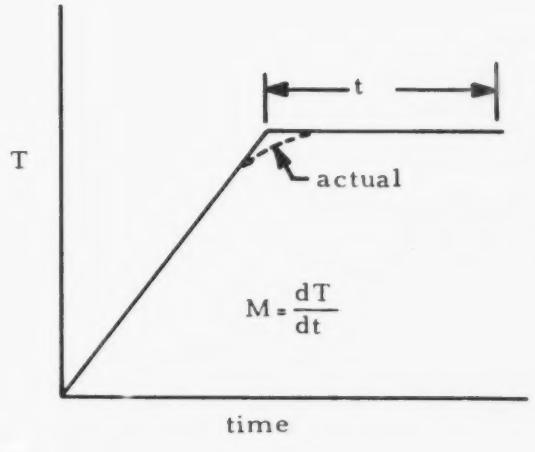

FIGURE 42b. Schematic diagram of experiment showing heating curve.

followed immediately by

$$H_2S + CaO \rightarrow CaS + H_2O \qquad (27)$$

so that H_2S produced in Equation 26 reacts always with layered CaO. Then for the desulfurization process we have

$$-\frac{d[N_j - S]}{dt} = k'[H_2][N_j - S]^n = k[N_j - S]^n \qquad (28)$$

Reproduced from best available copy.

where n is the order of the reaction.

For $n \neq 1$ we have

$$-[N_j - S]^{-n} \, d[N_j - S] = k\,dt \qquad (29)$$

$$[N_j - S]^{n-1} - [N_j - S]_0^{n-1} = (n-1)\int k\,dt \qquad (30)$$

During the heating region in Figure 42b where the temperature is changing with time, and which we shall call region I,

$$\int k\,dt = k_o \int e^{-E/RT}\,\frac{1}{m}\,dT = \frac{k_o}{m}\,\frac{RT^2}{E}\,e^{-E/RT}$$

SEE REFERENCE 1

(31)

while on the other hand, during the isothermal region (region II)

$$\int k\,dt = kt = k_o e^{-E/RT} t$$

(32)

Substituting these values for the integrals into the two regions we have:

$$\frac{[N_j - S]_I^{n-1}}{[N_j - S]_o^{n-1}} = \frac{1}{1 + \frac{(n-1)[N_j - S]_o^{n-1} k_o}{m}\,\frac{RT^2}{E}\,e^{-E/RT}}$$

(33)

and

$$\frac{[N_j - S]_{II}^{n-1}}{[N_j - S]_I^{n-1}} = \frac{1}{1 + (n-1)[N_j - S]_I^{n-1} k_o e^{-E/RT} t}$$

(34)

Multiplying Equations 33 and 34 together and substituting for $[N_j\text{-}S]_I^{n-1}$ in Equation 34, we get for the fraction of sulfur sites of the j^{th} type remaining after time t, the equation

$$\left(\frac{[N_j\text{-}S]}{[N_j\text{-}S]_o}\right)^{n-1} = \frac{1}{1+\frac{(n-1)[N_j\text{-}S]_o^{n-1}k_o}{m}\frac{RT^2}{E}e^{-E/RT}+(n-1)[N_j\text{-}S]^{n-1}k_o e^{-E/RT}t} \quad (35)$$

$$\left(\frac{[N_j\text{-}S]}{[N_j\text{-}S]_o}\right) = \left(\frac{1}{1+(n-1)[N_j\text{-}S]_o^{n-1}k_o e^{-E/RT}\left(\frac{RT^2}{mE}+t\right)}\right)^{1/n-1} \quad (36)$$

Reproduced from best available copy.

For the case of n = 1 we obtain the result

$$\frac{[N_j\text{-}S]}{[N_j\text{-}S]_o} = exp\left[-k_o e^{-E/RT}\left(\frac{RT^2}{mE}+t\right)\right] \quad (37)$$

Intra Layer Trapping of H_2S by CaO

The above derivation, predicts that desulfurization of all types of sulfur containing sites should be essentially complete, thus leaving no sulfur in the coal. Empirically however, it has been found for SRI. No. 4 (5%S) and SRI No. 5 (4.5%S) coals that the percent sulfur remaining in the char was 0.96% and 0.61% respectively. This suggests that reverse reactions or competing reactions within the coal are important. One component of the coal which could pose a problem is the calcium contained in the coal.

Assuming that this calcium is in the form of CaO and acts as sulfur acceptor, the following treatment is presented.

We are interested in knowing whether a molecule of H_2S, produced in a thin layer of coal by hydrodesulfurization, will leave the coal layer by being swept out by the flowing hydrogen, then being trapped in a CaO layer as a mineral component in coal and thus be trapped in the coal layer as CaS. In the latter case the trapped sulfur will be found by analysis in the layer of coke. We assume in the remainder of this treatment that trapping refers to H_2S being trapped by residual CaO in the coal, and any H_2S escaping the coal layer is trapped by the adjacent CaO layer.

Thus we are dealing with the competing reactions, viz:

$$H_2S + CaO \longrightarrow CaS + H_2O \qquad (38)$$

$$H_2S \rightarrow \text{Escapes the layer of coal} \qquad (39)$$

and the probability <u>for any rate of production of H_2S</u> that the H_2S will be trapped as CaS will be given by

Probability of Trapping in Coal Layer $= P_T = \frac{R_1}{R_1 + R_2}$

(40)

where R_1 and R_2 are the rates of Equations 38 and 39, respectively. Defining an effective H_2S concentration within the layer by (H_2S), these rates are:

$$R_1 = k_1 [H_2S][CaO]$$

(41)

$$R_2 = \frac{[H_2S]}{\tau}$$

Reproduced from best available copy.

(42)

Thus

$$P_T = \frac{R_1}{R_1 + R_2} = \frac{k_1 [H_2S][CaO]}{\frac{[H_2S]}{\tau} + k_1 [H_2S][CaO]}$$

(43)

or

$$P_T = \frac{k_1 \tau [CaO]}{1 + k_1 \tau [CaO]}$$

(44)

Where τ = residence time of flowing gas within the layer, viz:

$$\tau = \frac{Ad}{Q} \qquad (45)$$

where A is cross-sectional area of layer of coal, d is the thickness of the layer and Q is the flow rate of gas in volume per unit time.

From our measurements on CaO,

$$k_1 = 4.7 \times 10^{13} e^{-\frac{38000}{RT}} \quad min^{-1} gram^{-1}$$

In the experiments with the alternate trays (0.3g layers of coal)

$$\tau = 9.4 \times 10^{-4} \; min$$

Then knowing the Ca content we may calculate the probability of trapping of H_2S on this residual Ca for various coals as a function of T. That is

$$P_T = \frac{4.4 \times 10^{10} e^{-\frac{38000}{RT}} [CaO]}{1 + 4.4 \times 10^{10} e^{-\frac{38000}{RT}} [CaO]} \qquad (46)$$

This function is shown in Figure 43 for two coals SRI-4 and SRI-5. (CaO) is the number of grams of Ca in the layer of coal. In the case of SRI-4 and SRI-5 coals, with 0.3g layers, (CaO) is 0.0042g and .0003g respectively.

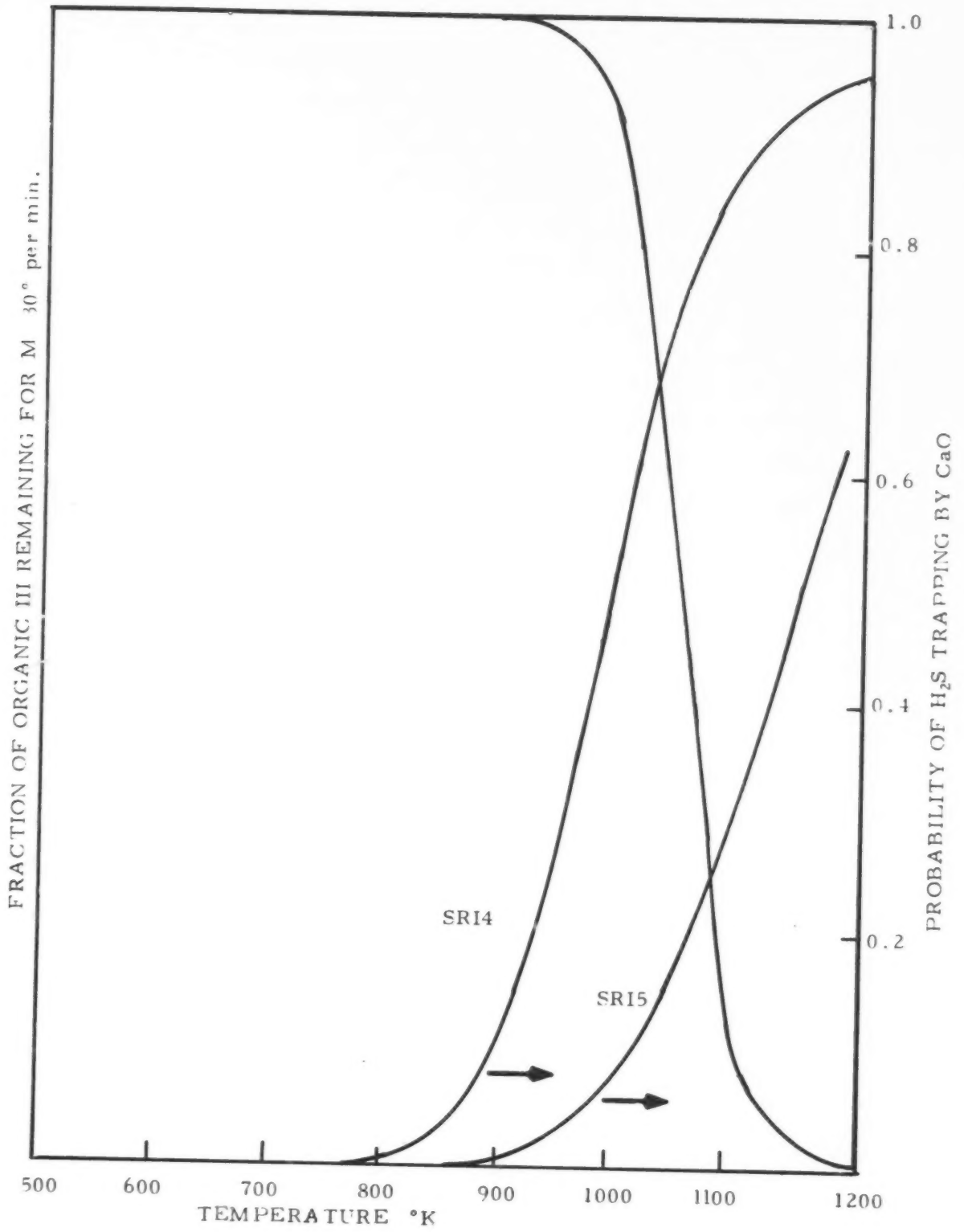

Figure 43. Plot of fraction of Organic III remaining for M= 30°/min and the probability of H_2S trapping by CaO for SRI #4 and SRI #5 coals.

Kinetic consideration of the rates of S-removal from the various forms of coal, namely, from Organic I, Organic II, Pyrite, Sulfide, and Organic III indicate that during the heating-up period, even at 30° per minute, essentially all the forms of sulfur except Organic III are removed at temperatures below those for which the probability of trapping by CaO is significant. That is to say, with the small amounts of CaO present in coals, the trapping of H_2S is unimportant below the temperatures at which Organic III decomposes. Thus we may consider here that only sulfur from Organic III can be trapped within a layer by CaO.

For an experiment with alternate trays in which M=30°/min and in which the coal is heated to 1000°C and held at that temperature for 20 minutes, the fraction of any form remaining at temperature T is expressed in Equation 36.

For the removal of S from Organic III, n=2. Equation 36 for n=2 is plotted in Figure 43 in general form. Inspection of Figure 43 shows that a very significant part of Organic III sulfur is removed during the heating up period in temperature ranges at which the probability of trapping is significant.

Let us now use Figure 43 to calculate the amount of Organic III retained in the char as a result of Ca trapping as CaS.

TABLE IX. DATA FROM FIGURE 38 FOR SRI COAL NO. 4

Temperature Range °K	Fraction of Organic III-S Removed	Average P_T in Range	$\langle P_T \rangle$ (Fraction Removed)
900- 950	0.010	0.183	0.002
950-1000	0.084	0.389	0.033
1000-1050	0.356	0.609	0.216
1050-1100	0.436	0.782	0.341
1100-1150	0.080	0.886	0.071
1150-1200	0.036	0.906	0.033
	1.002		

The fraction of Organic III sulfur trapped by CaO is thus the sum of the fourth column or

Fraction Organic III Trapped = 0.696

This number represents the entire amount of Organic III sulfur which is trapped, both in the coal CaO and in the layer of CaO. According to earlier work, the weight per cent of S in SRI-4 is 5.0%, and of this total S, 16% is in the form of Organic III. Thus, we predict that the %S to be found in the char for SRI-4 is:

$$\%S \text{ in char} = 5.0 \times 0.16 \times 0.696 \times \frac{\text{wt. coal}}{\text{wt. char}}$$

$$\%S \text{ in char} = 0.56 \times \frac{\text{wt. coal}}{\text{wt. char}}$$

As the ratio of weight of coal to weight of char is about 2, we get

%S in char (SRI-4) = 1.1%

Similarly for SRI Coal No. 5, the calculation is repeated.

Organic III comprises 24% of a total S content of 4.2% according to the table in a previous report[2].

TABLE X. DATA FROM FIGURE 38 FOR SRI COAL NO. 5

Temperature Range in °K	Fraction of Organic III Removed	Average P_T in Range	$\langle P_T \rangle$ (Fraction Removed)
900- 950	0.010	0.017	0.0002
950-1000	0.084	0.046	0.0039
1000-1050	0.356	0.109	0.0388
1050-1100	0.436	0.222	0.0969
1100-1150	0.080	0.372	0.0298
1150-1200	0.036	0.541	0.0195

From summing last column.

Fraction Organic III Trapped = 0.189

$$\%S \text{ in char (SRI-5)} = 0.24 \times 0.189 \times 4.2 \times \frac{\text{wt. coal}}{\text{wt. char}} = 0.191 \times \frac{\text{wt. coal}}{\text{wt. char}}$$

$$\approx 0.38\%$$

For SRI-4 coal the percent sulfur remaining in the char after the experiment is predicted to be 1.1% and is empirically determined to be 0.96%. Similarly SRI-5 coal is predicted to have 0.38% sulfur in the char whereas it is empirically determined to be 0.61%. The agreement between prediction and experiment is quite good considering the simplicity of the treatment of the problem.

EVALUATION OF THE DUAL CHANNEL CASCADE REACTOR FOR THE HYDRODESULFURIZATION OF COAL

INTRODUCTION

Based upon our kinetic measurements on coal desulfurization, we have proposed a method for the efficient desulfurization of high sulfur coal in the dual channel cascade heat exchange reactor. The design is such that coal and calcined dolomite can be introduced into the top in parallel flows each separately mixed intimately with an upflowing gas so that there is a rapid and complete evolution of sulfur in a gaseous state from the coal and an efficient absorption on to the calcined dolomite without physical mixing of the two parallel particle streams. Our schematic design of such a reactor together with the conceptual system for desulfurization are shown in Figures 44 and 45. We have analyzed the energy flow system of this chemistry and find this to be favorable as shown in the heat flow diagram, Plate I.

In order that the overall rate process be commercial, the residence times of the coal and calcium oxide particles must be long enough to complete the desulfurization reactions and the consequent absorption of H_2S by the CaO. Also the oscillations of gas flow between the coal channel and the channel of calcined dolomite must have appropriate gas residence times to capture the H_2S by the calcium oxide without the recapture in the reverse reaction of Organic III by the char. Our kinetic measurements have shown that the following requirements should be met: (a) One second

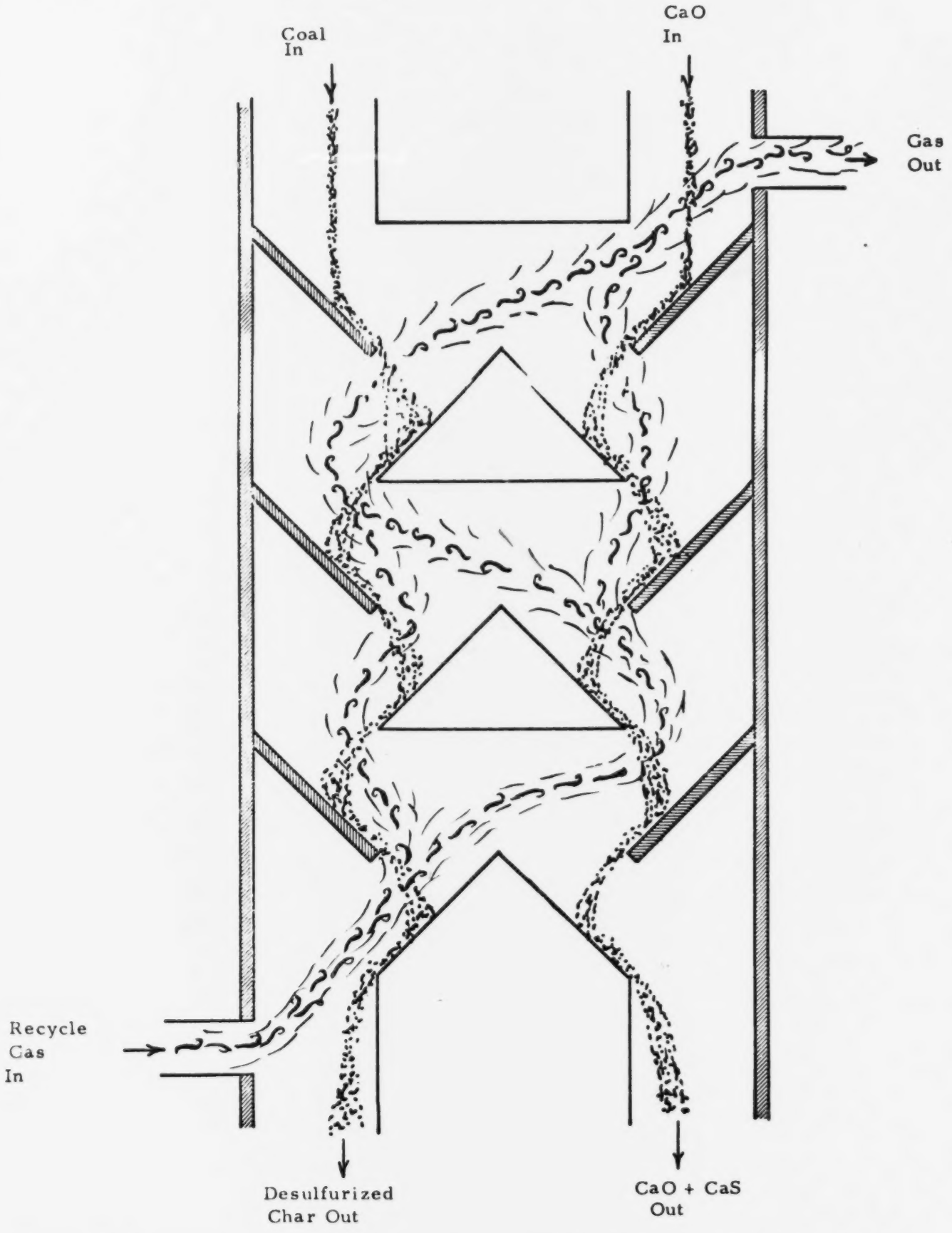

Figure 44. Schematic Diagram Of A Short Section Of The Proposed Dual Channel Baffled Cascade Desulfurization Reactor.

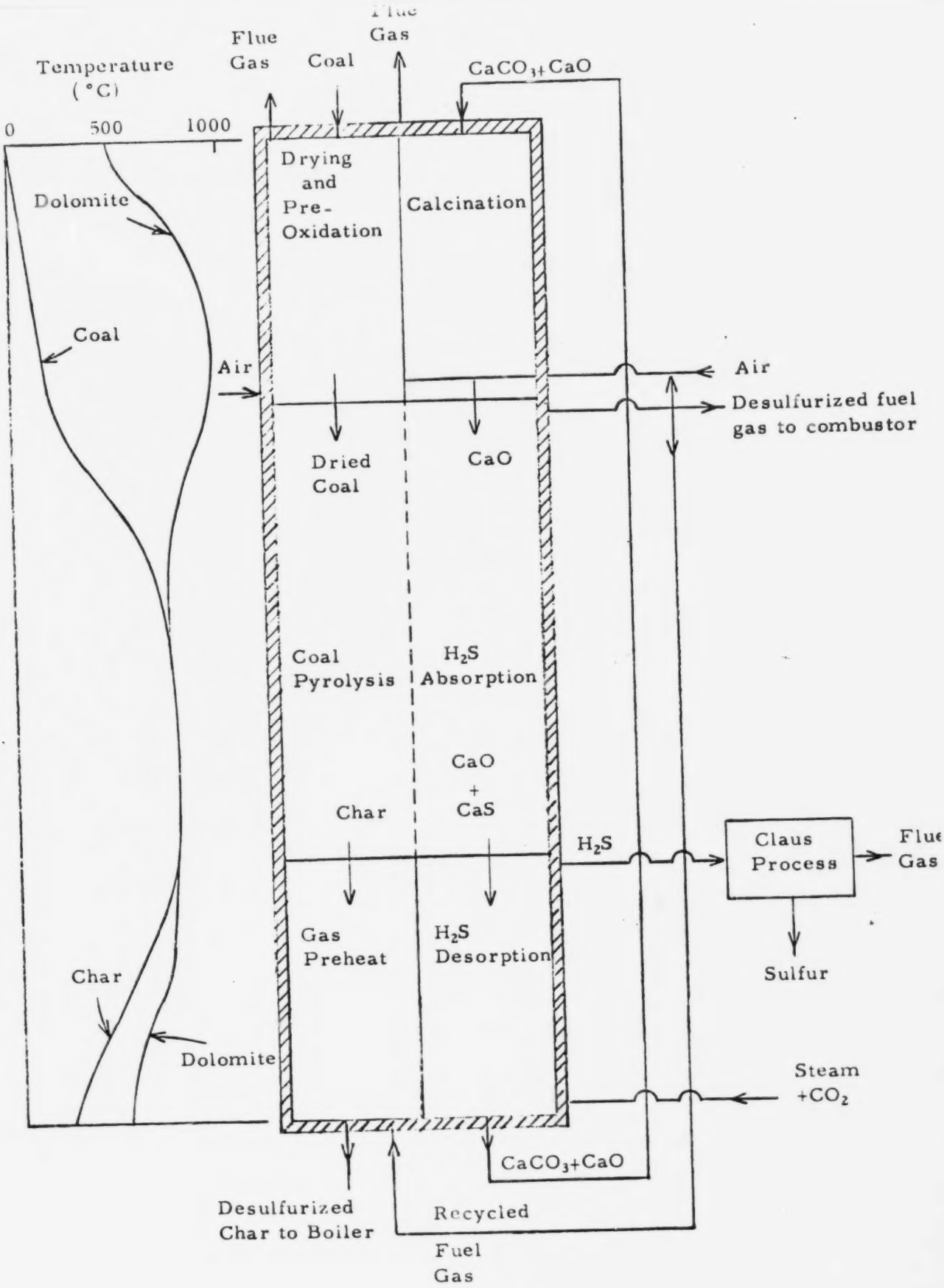

Figure 45 Simplified Block Diagram of Complete Conceptual Desulfurization System

per vertical foot residence time for the solid particles and (b) 90% gas transfer from one channel of the reactor to the other within one second.

A laboratory scale-model of the proposed dual channel reactor was constructed and measurements of the residence times of the solid streams and of the gaseous transfer times were made. Mass spectrometric sampling of a carbon dioxide tracer gas at the various stages was employed to determine gas flow patterns.

Results indicated that the above requirements will be satisfied by this design. Literature studies suggest that this reactor is patentable. These model data together with the engineering calculations based upon the kinetic measurements recommend this reactor as an attractive candidate for production of a low sulfur content char from a high sulfur content coals.

DESCRIPTION OF THE DESULFURIZATION PROCESS

In the simplified block diagram of Figure 45, the coal entering the top of the reactor is first dried and lightly preoxidized to reduce agglomerization tendencies. The coal then enters the pyrolyzer stage where it is treated by convection of the recycled pyrolysis gas between the hot (1000°C) calcined dolomite and the coal. The heat required in this reactor is provided by preheating the incoming recycled gas against the exiting char and by the hot incoming CaO. The heat required for calcination of the dolomite may be provided by combustion of char fines carried over with the dolomite and by combustion of a fraction of the fuel gas produced from the pyrolzer. An approximate temperature profile for the reactors is shown in this figure.

While many detailed features of such a reactor system must be developed, this proposed system satisfies, in principle, many of the requirements indicated by our kinetic studies for an efficient desulfurization system. Some of these requirements are the following:

1. The easily removable forms of sulfur are eliminated during heating of the coal without significant transfer of sulfur into the more difficult to remove forms.

2. The counterflow of gas and solid with the gas oscillating between the coal and the calcined dolomite maintains the average H_2S concentration in contact with the coal at a very low level, thus inhibiting the back reactions allowing effective desulfurization with short treatment times.

3. The H_2S can be efficiently desorbed from the absorbent at sufficiently high concentrations for effective use of the commerical Claus process for converting recovered H_2S into elemental sulfur as a marketable by-product.

The feasible energetics of this concept are confirmed by the energy flow analysis which we have previously published in the Proceedings of the Symposium on Hydrogen Process of Solid and Liquid Fuels, American Chemical Society, September, 1970. The heat flow diagram is shown in Plate I.

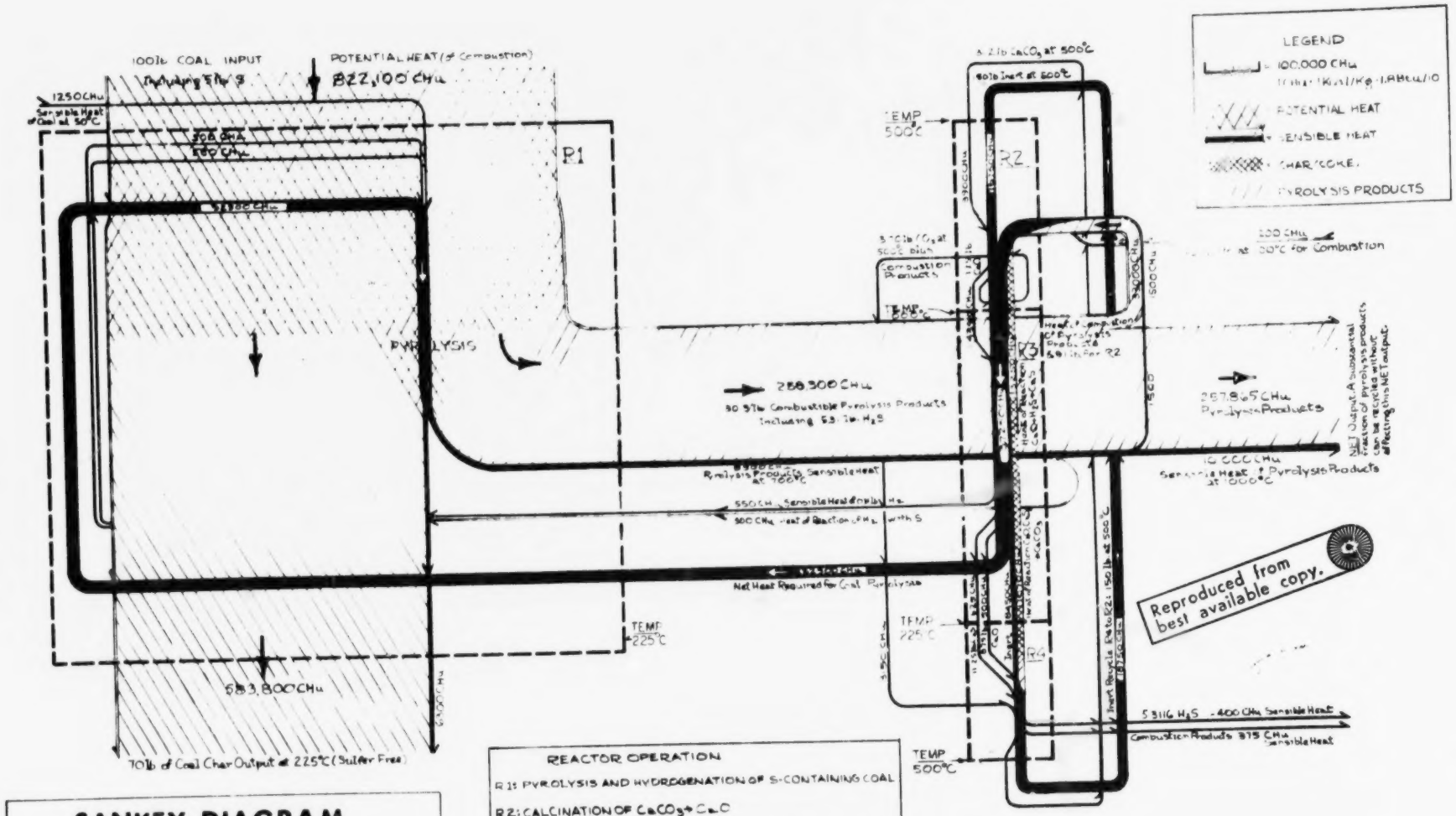

Reproduced from best available copy.

SANKEY DIAGRAM

FOR DESULFURIZATION OF COAL BY COMBINED PYROLYSIS, HYDROGENATION AND H_2S ABSORPTION; WITH H_2S RECOVERY AND ABSORBER REGENERATION.

REACTOR OPERATION

R1: PYROLYSIS AND HYDROGENATION OF S-CONTAINING COAL

R2: CALCINATION OF $CaCO_3 \rightarrow CaO$

R3: H_2S ABSORPTION BY $CaO \rightarrow CaS$ (50% CONVERSION)

R4: $CaO.CaS$ REGENERATION $\rightarrow CaCO_3$

Plate I

Design and Evaluation of a Laboratory Scale-Model Cascade Reactor

A plexiglas model of the proposed dual channel baffled cascade reactor was designed and built to enable laboratory measurements of residence times of solids and of gas flow patterns. The general section is shown in Figure 44 and the complete scale-model is shown in Plate II. Our design of this model enables the experimenter to vary such things as coal feed rate, distance between cascade shelves, slope of shelves and upward gas velocity. The overall height of the reactor is five feet and includes dual feed hoppers at the top, eleven cascade stages, dual solids collector chambers at the bottom and a velocity monitored variable gas feed system. Each cascade stage has multiple gas sampling ports which consist of self-sealing Luer-Lok fittings for gas sampling by fast response mass spectrometry.

Air velocity measurements were made using an Annubar primary flow element which is based on the fundamental Bernoulli flow theorem. An interpolating sample tube is used to sample segment of a 1-1/2" diameter pipe and automatically averaging them using Chebishev. calculus.

Paricle holding times were measured by timing the travel of the leading edge of the particle cloud through the eleven cascade stage system. This procedure results in a slight overestimation of mean velocity but is quite adequate as preliminary data for indicating relative holding effects.

Gas flow patterns were determined by measuring tracer gas distribution (using CO_2) throughout the reactor. Also velocity measurements between channels were made of step inputs of tracer gas. Both of

PLATE II

of these were done by sampling at both sides of each cascade stage using the SRIC MEDSPECT clinical mass spectrometer. The unique ability of this instrument to provide a continuously direct reading of the partial pressure of carbon dioxide instantaneously (60milliseconds) and with no disturbing effect on the pressure and flow at the sampling point makes this a very effective instrument for this purpose. The inlet to the MEDSPECT is designed to measure the partial pressures of CO_2, O_2, and N_2 in an individual human breath. This is done by using a long catheter tube to effect a pressure drop from atmosphere down to an operating pressure of a millitorr thus enabling a rapid transit of the gases into the spectrometer. Because of this, only a small volume (approx. 0.1cc/sec) of sample gas is required and the time constant of the experiment is limited to the reflex response of the experimenter.

Results

The transit times of the solids through the cascade reactor were determined and these times were converted to particle velocities. The results of these experiments are shown in Figure 46; the three curves are for A.S.T.M. 20-40 , 40-60, and 60-100 mesh. In taking transit time measurements, the leading edge of the particle cloud is used. Since this leading edge represents those particles in a distribution of particles which are falling more rapidly than the average, the results in Figure are somewhat overstated; i.e. the average velocity is somewhat lower.

By inspecting Figure 46 it can be seen that the particle velocity drops off with the counter flow gas velocity as would be expected and that the particle velocity for a given counter flow gas velocity decreases with decreasing particle size.

The velocity of the three particle sizes with no gas flow is 1.4 ft./sec. This value compares very well with the value calculated from Equation 47

$$v = 1/2 \sqrt{gd} \qquad (47)$$

where d is the cascade depth and g is the gravitational acceleration. With the plate spacing of two inches, d = 4 in giving v = 1.6 ft/sec.

Visual inspection of the particle stream shows that the particles slide off each plate, in the plate direction, so they impinge on the plate below almost at right angles to it and about half way up. This is a condition envisioned in our previous discussion with the expectation that Equation 47 would still apply. The results support the predicted behavior; namely, that flow through the system is dominated by gravity.

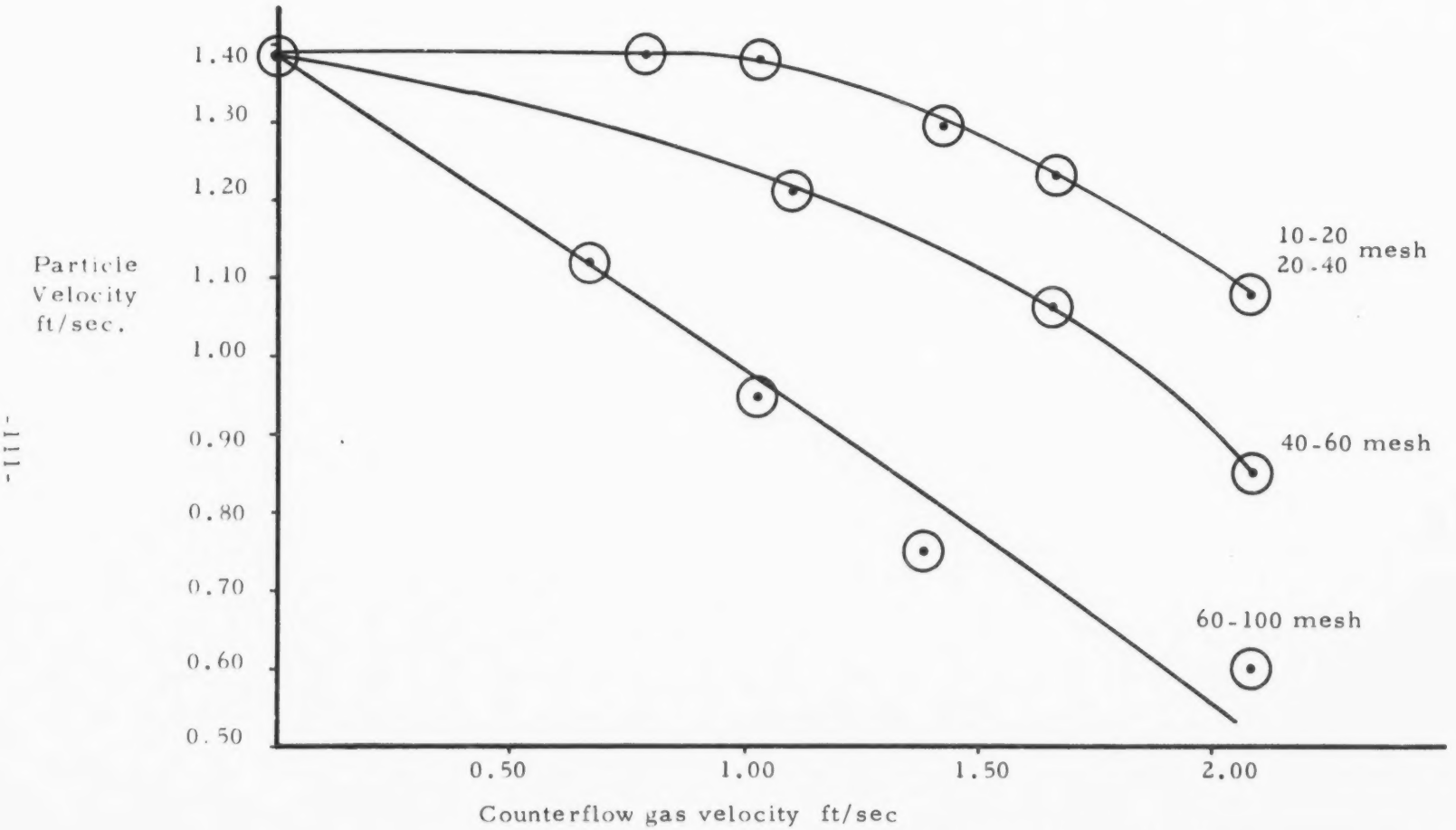

Figure 46. Velocity of Fall Based on Observation of Leading Edge (Batch measurements)

The results of the experiment on rate of gas mixing, using the SRIC MEDSPECT medical mass spectrometer, are shown in Figure 47 The measurement points (bars on the graph) are sampling points located at equal vertical intervals along the reactor. The time is obtained by dividing the distance of the measuring port from the injection point by the counter flow gas velocity. The point at which the gas is injected represents the zero of time on the abscissa. It can be seen that less than a second is required to achieve a uniform gas mixture in the reactor. Curve A shows the decrease in CO_2 concentration, as a function of time, on the side of the dual cascade reactor in which the gas is injected. Curve B shows the increase in CO_2 concentration, as a function of time, on the side of the dual cascade reactor opposite the injection point.

Curve A should represent as exponential decay due to the CO_2 mixing with the carrier gas. This is represented mathematically in Equation 48

$$(C-C_s) = (C_o-C_s)e^{-t/T} \tag{48}$$

where C_o is the initial concentration of CO_2; C_s is the steady state concentration of CO_2; C is the concentration of CO_2 at time t, and T is the mixing half time. Analytically, T may be determined by graphing $2.3 \log (C-C_s)$ vs t. The plot should yield a straight line with slope of $-1/T$. This plot is shown in Figure 48 with symbol o.

Curve B in Figure 46 resembles a (1-e) increase which is represented mathematically as:

$$C' = C_b (1-e^{-t/T'}) \tag{49}$$

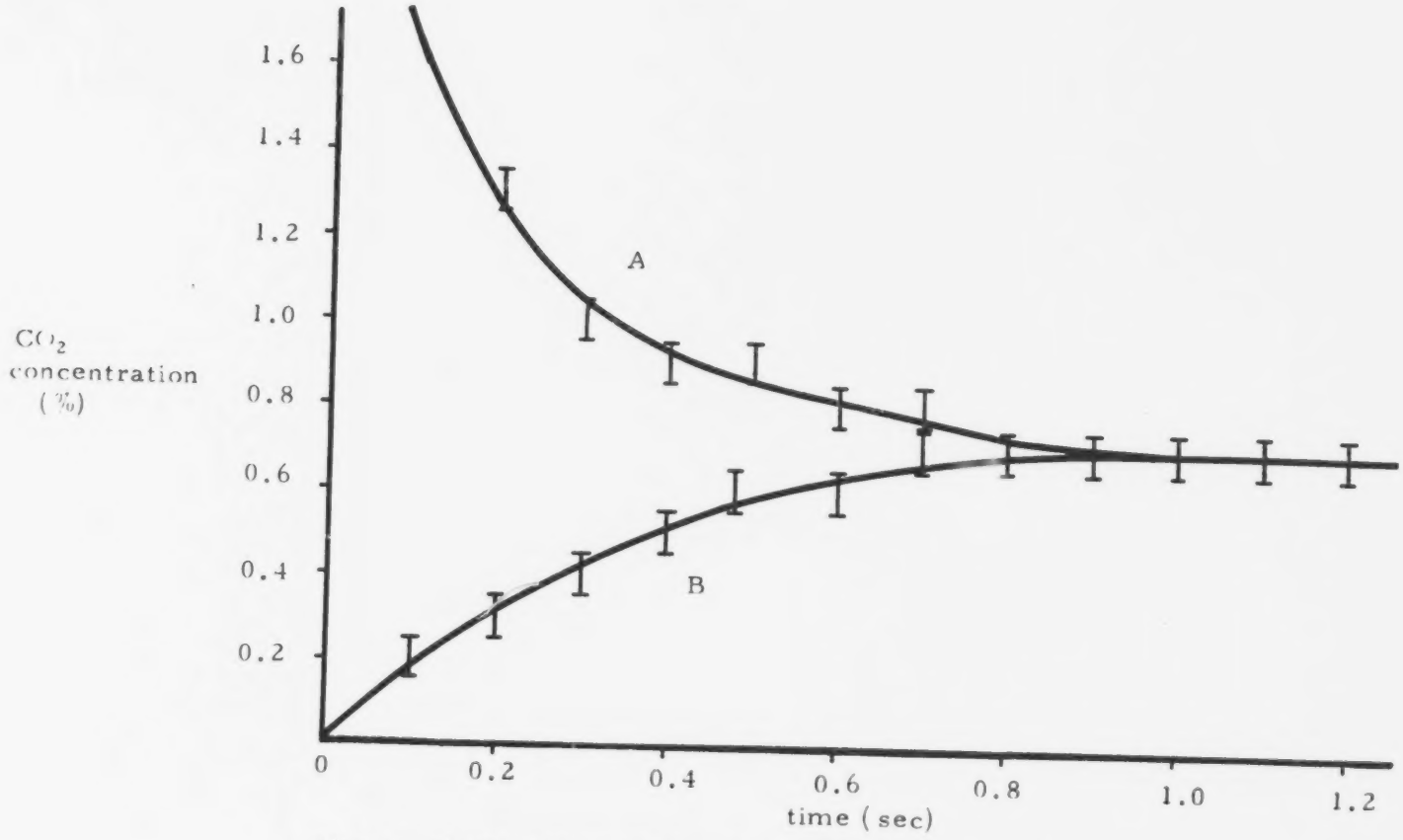

Figure 47. Variation of CO_2 Tracer Concentration Above Injection Point Under Steady State Conditions. Trace is Injected into Channel A and Cross Mixes in Channel B reaching 90% Equilibrium in 0.85 sec.

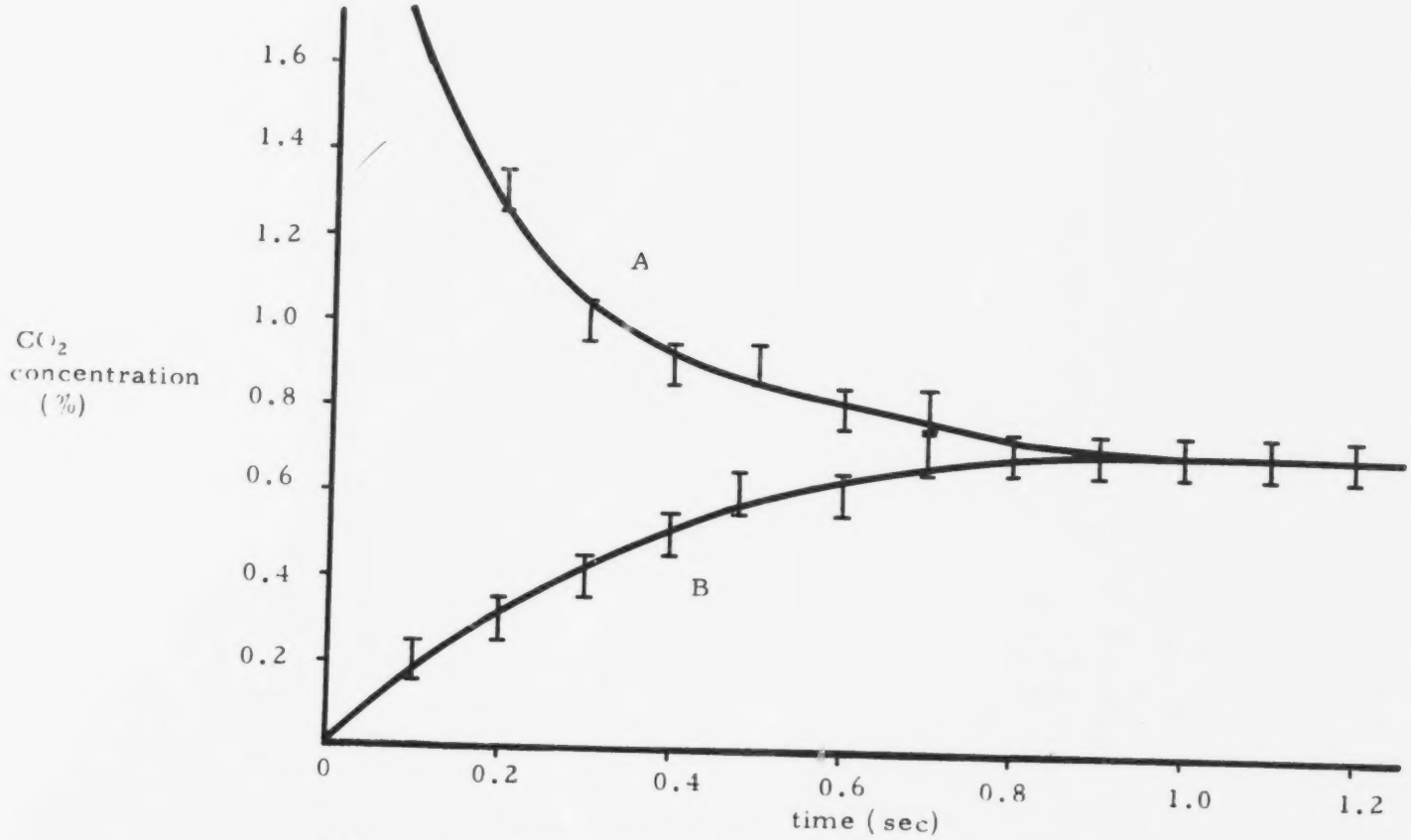

Figure 47. Variation of CO_2 Tracer Concentration Above Injection Point Under Steady State Conditions. Trace is Injected into Channel A and Cross Mixes in Channel B reaching 90% Equilibrium in 0.85 sec.

where C' is the concentration of CO_2 at time t, $C_b = C_s$ = steady state concentration of CO_2 and T' is the mixing half time. To obtain T' analytically, $(1 - C'/C_b)$ is plotted vs t to give a straight line with slope of $1/T'$. This plot is seen in Figure 48 with symbol o.

The value of T and T' ideally should be equal so the two sets of points are plotted together to give a best fit of the points. From the graph of these points (Figure 48) T = 0.27 sec. indicating that 90% of the CO_2 is mixed within 0.9 seconds.

The results of the experiments are very encouraging in that they give good support to our original calculated estimates. By using such a model as has been built, it should be possible to direct the gas flow pattern to obtain even more rapid gas mixing. It appears quite possible that these findings can be used in scaling the model up into an operable pilot reactor.

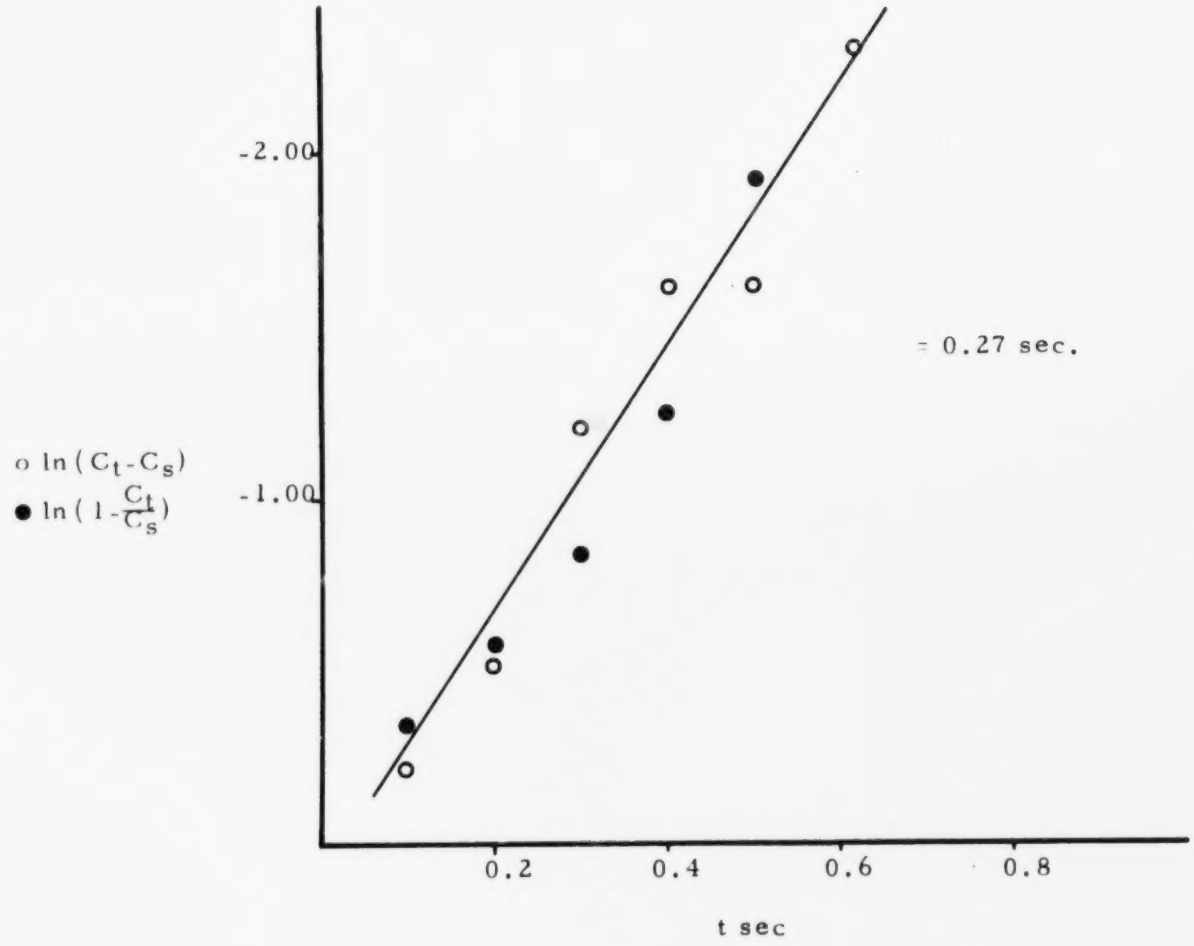

Figure 48. Determination of τ, the Mixing Half Time For the Dual Cascade Reactor

ANALYSIS OF CROSS-MIXING BEHAVIOR OF THE DUAL CHANNEL CASCADE REACTOR

As described in the previous section, the extent of cross-mixing between the channels was investigated using a CO_2 tracer method. At a given air flow up the channels, CO_2 was injected at a steady flow rate into one channel, and the concentration at steady state was measured at every half-stage level above the injection point, in both channels. The concentration of the gas, in the channel, into which the tracer was injected, was found to decay exponentially from an initial value c_o, to a final steady state value c_s. In the other channel the concentration rose from zero at the injection level, in a $1-e^{x}$ manner, to the same steady state value c_s. The exponential fall and rise was determined empirically, and found to have mixing half-times (T) that were the same for both channels. The purpose of this present analysis is to show that the observed exponential behavior can be predicted from reasonable assumptions about the cross-mixing exchange. Valuable results of the analysis include an expression for T as a function of a mixing exchange coefficient and further indications of parameters required for effective scale-up.

Analysis

Figure 49 illustrates the cascade reactor construction, roughly idealized as a set of cubes, of volume ΔW, each containing two cascade plates. Each cube is one cell comprised of two horizontally adjacent cells A and B and is a single stage of the dual channel reactor. The gas exchange by cross-mixing takes place across the vertical dotted line (X-Y) representing the interface between horizontally adjacent cells.

This cross-mixing is represented in Figure 49 by the two horizontal arrows in the two cells below A and B. Cross-mixing between cells must take place as the result of diffusion across the vertical interface X-Y. This follows from consideration of expected flow patterns. From symmetry, we can expect the flow patterns in the two channels to be identical when averaged over a reasonable length of time. This should be true above a certain height even if the initial gas supply is off-axis. Consequently there can be no net flow across the X-Y interface, so any net exchange of a given component or tracer must be due to molecular or turbulent diffusion. As it happens, the Reynolds number for each channel, based on average gas velocities and channel diameters, is close to the critical transition value of 2000 for the experiments so far carried out. However, development of laminar flow will be prevented by the existence of the cascade plates which will keep switching the flow direction. On the other hand, the turbulence intensities are not likely to be particularly high.

Suppose now that the total gas volume flow rate into the cascade reactor is V cc/sec. By symmetry, we can assume that this is equally divided between the two channels, giving a flow rate (V/2) cc/sec in each channel. If the channels each have sides of length a and b, or Area A=ab, the average gas velocity v_g (ignoring the effect of the plates) is

$$v_g = V/2A = V/2ab. \qquad (50)$$

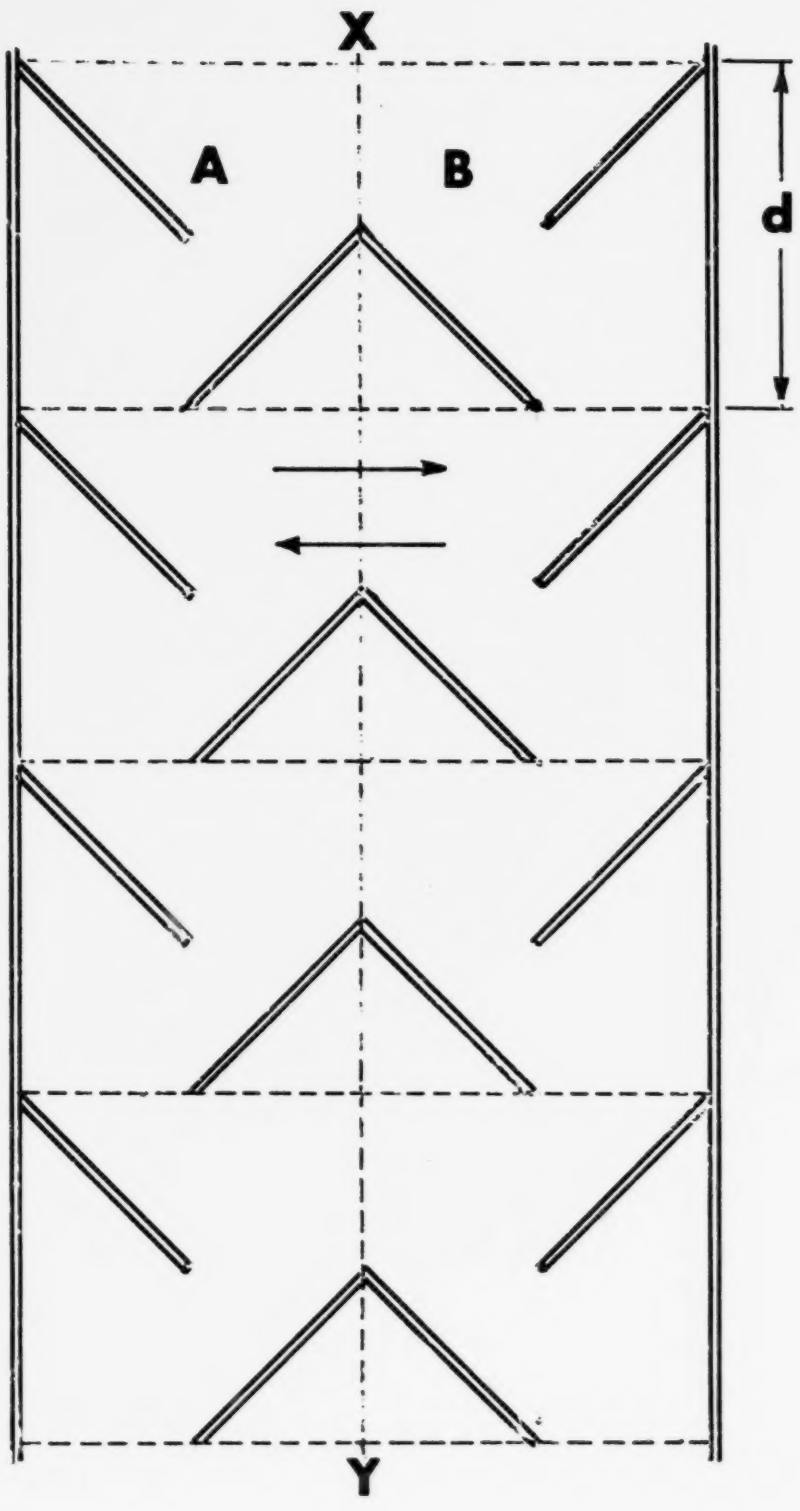

Figure 49 Schematic Diagram of the Dual Channel Cascade Reactor.

Suppose now that the tracer is fed into the left hand channel of the reactor with subsequent cross-mixing into the right hand channel. At some given height L above the injection point the tracer concentration in the left hand channel will be c, and in the right hand channel will be c'. Consider now the left hand cell at height L. The rate at which the tracer is being carried into the cell by the vertical flow is (Vc/2), and the rate of exit is (V/2) (c-∂c). The net rate of entry is (Vc/2)(∂c) and is balanced by the rate of cross-mixing with the horizontally adjacent cell. If we assume an exchange factor β, such that the rate of exchange between adjacent cells is β(c-c') per unit area, then for an interface area between stages of (ad)

$$V/2\ (\partial c) = (ad)\,\beta\,(c-c') \tag{51}$$

Similarly, for the right hand stage

$$-V/2\ (\partial c') = (ad)\beta(c-c') \tag{52}$$

Subtracting Equation 52 from Equation 51 yields

$$\partial c + \partial c' = 0 \tag{53a}$$

or

$$c + c' = c_0 = 2c_s \tag{53b}$$

where c_0 is the initial concentration at the tracer input level in the left hand channel (when $c' = 0$), and $c_s = c = c'$ is the final equilibrium concentration in both channels at some sufficient height (theoretically infinite).

Eliminating c' in Equation 51 using Equation 53b and substituting for V by Equation 50 yields

$$(ab)\, v_g\, (\partial c/d) = 2\, a\beta (c - c_s). \tag{54}$$

The physically real construction of the system is such that the concentration c is probably reasonably uniform throughout each stage, of depth d. Nevertheless, with a sufficient number of stages, or sufficiently small stages, we may treat $(\partial c/d)$ as a differential ratio in the limit. Thus

$$\partial c/d = -dc/dL. \tag{55}$$

Similarly

$$v_g = dL/dt. \tag{56}$$

Consequently, we may write Equation 54 in the form

$$-dc/dt = (2\beta/b)\,(c - c_s). \tag{57}$$

If both numerator and denominator of the right hand side are multiplied by (ad) we find

$$1/b = (ad)/(abd) = A_i/\Delta W = A_W \tag{58}$$

where A_i is the interface area between adjacent stages, ΔW is the volume of each stage, and the symbol A_W is the interface area per unit volume of each stage. Substituting for b in Equation 57 and

integrating yields

$$(c-c_s) = (c_0 - c_s) \exp(-2A_w\beta t). \tag{59}$$

Substituting for c from Equation 53b also yields

$$c' = c_s[1-\exp(-2A_w\beta t)]. \tag{60}$$

Evaluation

Equations 59 and 60 have the form of the Equations for c and c' already established experimentally, with the mixing half times related by

$$\tau = \tau' = 1/2A_w\beta = b/2\beta \tag{61}$$

The mixing can also be represented in terms of height since

$$L=vgt \tag{62}$$

so we may introduce a mixing half length, similarly, as

$$\lambda = v_g/2A_w\beta = V/4a\beta. \tag{63}$$

For fast mixing τ should be as short as possible so that, from Equation 61, A_w and β should be as large as possible. The exchange coefficient β, will probably depend on the velocity (v_g) and possibly on the plate design. For A_w to be large requires the reduction of the cell width b, or the volume of each cell ΔW. This can be done by

filling in dead or stagnant space, or by reducing each cascade plate in width when possible. It means, in effect, that the residence time in each cell is reduced. It also has the potential advantage of increasing the velocity of flow through each cell which, in turn, can be expected to increase β.

If β does not increase with velocity, however, increasing the velocity could be disadvantageous with respect to the overall height required for a given degree of mixing. This is most easily evaluated from Equation 63 which shows that if v_g is increased (by increased flow rate) with other factors remaining constant then the mixing height (λ) increases proportionately. If β increases with velocity, however, we have three possibilities. If $\beta = a\,(V_g)^n$ then:

(a) For $n < 1$, the mixing height increases.

(b) For $n = 1$, the mixing height is unchanged.

(c) For $n > 1$, the mixing height decreases.

Clearly, empirical determination of n will enable designers to decide whether it is desirable on mixing grounds to increase or to decrease the flow velocity.

If the velocity is increased, by infilling dead space to increase A_w, Equation 63 shows that this, fortunately, is a self-cancelling effect at constant V since ($v_g b$) or ($v_g A_w$) remains constant. There can, however, be some benefit if β increases with reduced b (due to increased velocity). It should in fact be advantageous to keep the cell width as small as possible.

The cell depth, or cascade shelf length (a), on the other hand is quite neutral. This parameter appears in Equation 63 in the right hand side. However, if (a) is increased for fixed V, the gas velocity will drop. If the velocity is maintained, then λ is independent of (a). Increasing (a), with proportionately increased V, serves to increase the reactor capacity.

For the cascade unit investigated, some estimate of parameter magnitudes is possible. Experimentally, τ was found to be 0.27 sec with a cascade width (b) of 3.5 in or 8.9 cm, we have

$$\beta = 8.9/2 \times 0.27 = 1.65 \text{ cm/sec.}$$

If flow is laminar, and diffusion is molecular, β the mixing coefficient can be written as $D/\Delta x$, where D is the molecular diffusion coefficient for CO_2 in air and Δx is known. Conversely, if Δx is not known but limits can be established, then D can be calculated, compared with known values, and the probable nature of the flow thus established. Since a cell is almost 10cm wide, the distance between the midpoints of two cells is roughly 10cm, which should constitute an upper limit to Δx. At the other limit, a Δx of 0.1cm (or 1mm) in a flowing system is not impossible, but is thought to be improbable. An intermediate order of magnitude of 1cm or more would seem realistic. These three values of Δx give us, in increasing order, values of D: 0.17cm^2/sec; 1.7cm^2/sec; and 17cm^2/sec. Since measured values of CO_2 in air are about 0.14cm^2/sec, it does not seem possible that the cross-mixing between stages can depend on molecular diffusion. Some form of turbulent diffusion or convective flow must be operative with apparent diffusion coefficients, perhaps as much as an order of magnitude greater than those for molecular diffusion.

Conclusions

From the cross-mixing point of view it would seem to be advantageous to reduce the stage width as much as possible, consistent, of course, with the physical construction and clearances required.

Reactor capacity, on the other hand, is best increased by increasing the cascade depth: this is equivalent to the cascade shelf length.

The effect of increased gas velocity is still undetermined. The mixing half time is either unchanged or reduced: but the mixing half length may be increased. This latter depends on the variation, if any, of cross-mixing coefficient β, with velocity.

The variation of β with velocity is best determined experimentally at this stage of reactor development. The desired variation is an increase that can be represented by $\beta = \alpha (V_g)^n$ with $n \geq 1$. If this is satisfied, the mixing half length remains constant or decreases.

Some increase of v_g with β can be expected since the value obtained for β is higher than could reasonably be expected from molecular diffusion alone (possibly by as much as an order of magnitude). Cross-mixing is evidently by turbulent diffusion or convective flow in spite of the fact that the flow Reynolds number is close to 2000. In low intensity turbulent flow, any increase in velocity can be expected to increase the turbulent diffusion appreciably (with the increase rate falling off as velocity rises).

If β, the mixing coefficient, is measured over a range of gas velocities it is possible that a sudden increase, from a much lower value to the value already reported, may be observed. This would correspond to change from molecular to turbulent diffusion as the flow changes from laminar to turbulent.

It is also evident that design modifications to the symmetry of the cascade plates might also be advantageous, particularly if this increases the convective cross-flow, with the mainstream of the flow swinging from one channel to the other and back again. This could probably be achieved by plate extensions that would increase the flow resistance first on one side and then on the other. This possibility is proposed for experimental verification.

BIBLIOGRAPHY

1. Scientific Research Instruments Corp. Report No. SRIC 68-13 (1968). Also National Technical Information Service Report PB 185882.

2. Scientific Research Instruments Corp. Report No. SRIC 70-14 (1969).

3. F. H. Field, Acc. Chem. Research 1, 42 (1968).

4. D. W. von Krevelen, Coal, D. Van Nostrand Co., New York (1961) p. 259.

5. K. H. von Heek, H. Juntgen and W. Peters, Ber. Bunsen Phys. 71, 113 (1967).

APPENDIX A. SUMMARY OF ANALYSIS OF TEN COALS

SRI No.	Source	% Sulfur Nominal	Moisture	Volatiles	Fixed Carbon	Ash
1	Illinois - Crown Mine - Seam 6 ISGS:1-1	5	8.0	36.2	44.7	11.1
2	Illinois - No.21 Mine - Seam 6 ISGS:5-1	1	5.4	33.8	54.6	6.2
3	Illinois - Northern Illinois - Seam 2 ISGS:25-1	2.5	7.8	33.7	42.5	16.0
4	Illinois - Will Scarlet Mine - Davis Seam ISGS:28-1	5	1.9	37.6	43.2	17.3
5	Illinois - Little Dog Mine - Seam 6 ISGS:32-1-1.60F	4.5	5.1	40.8	44.1	10.0
6	Ohio - Stanley Mine - Pittsburgh #8 Seam USBM: 205	3	1.6	38.1	49.6	10.7
7	Maryland - Royal Mine - Franklin Seam USBM: 106	3	0.6	20.5	62.8	16.1
8	Ohio - Cravat Mine - Pittsburgh #8 Seam USBM: 107	3.5	1.7	37.2	50.4	10.7
9	Pennsylvania - Greenwich #8 Mine - Lower Kittanning(B) Seam USBM: 109	1	0.8	27.9	64.2	7.1
10	Kentucky - Shamrock Mine - Seam 14 USBM: 110	4	1.8	31.3	46.5	20.4
	Anthracite	.67	1.5	9.0	76	13.5
	Lignite	.55	29.3	30.1	33.0	7.6